Gersonde, R., Hodell, D.A., Blum, P., et al., 1999
Proceedings of the Ocean Drilling Program, Initial Reports Volume 177

3. SITE 1088[1]

Shipboard Scientific Party[2]

BACKGROUND AND OBJECTIVES

Site 1088 (proposed site TSO-2B) is located on the Agulhas Ridge, which extends from the northern tip of the Meteor Rise and terminates abruptly at 40°S, 15°E, where it intersects the northern end of an abandoned spreading-ridge axis in the Agulhas Basin (Figs. **F1,** p. 35; **F5,** p. 39; both in the "Leg 177 Summary" chapter). In this region, the Agulhas Ridge is a fairly broad topographic feature with ~2250 m of relief (Figs. **F1,** p. 35; **F5,** p. 39; both in the "Leg 177 Summary" chapter). Piston cores and Parasound echo-sounding profiles across the Agulhas Ridge have demonstrated that this relatively narrow topographic high is draped with sediment consisting of biogenic carbonate oozes, and is not disturbed by turbidites (Figs. **F1, F2**) . A detailed seismic survey was conducted before Leg 177, and Site 1088 was selected in an area of thick (>1000 m) acoustically stratified sediments (Figs. **F3, F4**). Seismic reflectors at Site 1088 can be traced to the north and south where they crop out at the flanks of the Agulhas Ridge (Figs. **F2, F4**). Piston cores taken on the ridge top in 2163 (PS2077-1) and 2254 m (PS2076-3) water depth gave ages of late (Chron 7, ~9.3–10.5 Ma) and middle Miocene (Chron 5, ~11–13.3 Ma), respectively (Fig. **F1**). Extrapolating these depth/age relations to Site 1088, we predicted an age of early Miocene (~12 Ma) at 145 meters below seafloor (mbsf), suggesting that the sedimentary succession was deposited at an average sedimentation rate of 12 m/m.y. Recovery of sediment cores at Site 1088 confirmed that our prediction was basically correct in that the age of the sediment at 200 mbsf in Hole 1088C is ~12 Ma.

Site 1088 represents the northernmost location drilled during Leg 177. The latitude (41°S) places Site 1088 just south of the Subtropical Front (STF), and the water depth (2082 m) places it near the boundary of Circumpolar Deep Water (CDW) and North Atlantic Deep Water (NADW) (Figs. **F1,** p. 35; **F2,** p. 36; both in the "Leg 177 Summary"

F1. Bathymetric profile showing the location of piston cores and Site 1088, **p. 17.**

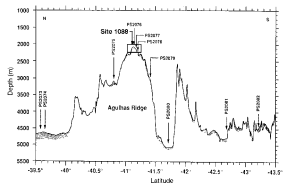

F2. Parasound profile across the Agulhas Ridge, **p. 18.**

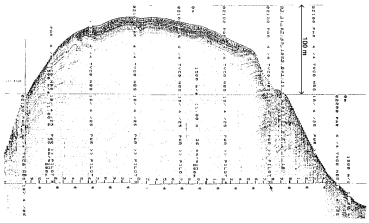

F3. Track line and shotpoints for the site survey of Site 1088, **p. 19.**

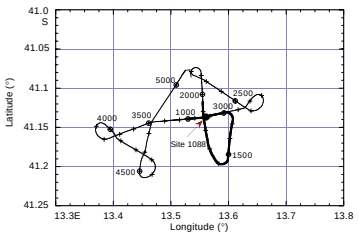

F4. Seismic line showing the location and penetration depth of Site 1088, **p. 20.**

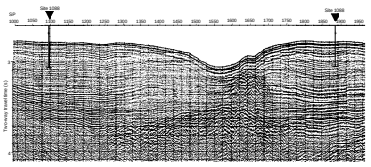

[1]**Examples of how to reference the whole or part of this volume.**
[2]**Shipboard Scientific Party addresses.**

Ms 177IR-103

chapter). Site 1088 represents the shallow end-member of the Agulhas Ridge depth transect, extending from Site 1088 (2082 m), through Site 1090 (3702 m), to Site 1089 (4620 m). The primary objective at Site 1088 was to recover a Cenozoic carbonate record that could be used to study paleoceanographic changes near the STF and to gain information about thermohaline circulation from an upper mid-water-depth site. Specifically, the objectives were to reconstruct long-term changes in (1) surface-water parameters (e.g., sea-surface temperature and seawater chemistry), and the evolution of the STF and its response to southern high-latitude climate variability; (2) biogenic paleoproductivity north of the Polar Front Zone; (3) the mixing ratio between lower upper CDW and upper NADW, and the evolution of these water masses through time; and (4) the subsidence history of the Agulhas Ridge.

Although problems with drilling operations and coring disturbance prevented us from reaching our depth objective of 700 mbsf, we were able to recover a 230-m-thick section comprising a middle Miocene to Pleistocene sedimentary sequence that was deposited at sedimentation rates averaging 25 m/m.y. during the Miocene and decreasing to 8 m/m.y. during the last 6 m.y. Because sedimentation rates are relatively low at this site, our objective was to study paleoceanographic change at a temporal resolution of 10^5 to 10^6 yr. Together with Sites 704 (Ocean Drilling Program [ODP] Leg 114; Wright et al., 1991, 1992) and 1092, located on the Meteor Rise within NADW, the sediments from Site 1088 should provide a history of changes in deep-water circulation, especially during the Miocene. The Neogene sediments at Site 1088 are carbonate rich (ranging from 85 to 95 wt%), have not been deeply buried, and, therefore, should provide reliable stable isotopic stratigraphies that are not compromised by diagenetic alteration.

OPERATIONS

Leg 177 began at 1130 hr on 9 December 1997 with the port call in Cape Town. The traditional joint ODP/ODL (Ocean Drilling Limited) annual holiday celebration was held at the Capetonian Hotel the evening of 10 December. This year's festivities were combined with a retirement party for Captain Ed Oonk.

Replacement and repair work on communications, thruster, waste management, power generation, and lifeboat systems extended the port call to 5 full days.

At 1315 hr on 14 December 1997, the port call ended with the last line ashore, and the vessel headed for Site 1088, which is located about 444 nmi southwest of Cape Town. Because of relatively heavy weather, plans to approach the site along a reference seismic profile were abandoned and the approach was made directly using global positioning system coordinates. The transit was accomplished in 56.5 hr at an average speed of 8.9 kt.

Hole 1088A

A positioning beacon was launched at 2145 hr on 16 December, beginning site operations for the leg. The advanced hydraulic piston corer (APC) coring assembly was deployed and, before spud-in, a temperature measurement was taken a few meters above the seafloor with the APC temperature (APCT) tool in the APC core-catcher (CC) shoe.

Hole 1088A was spudded, with the first APC coring attempt at 0930 hr on 17 December. An anomalous pressure bleedoff indication was noted when the corer was actuated, and the core barrel was recovered full of disturbed sediment. These were indications that the bit had been positioned too deep for the spud attempt and/or that the shearpins had failed before the corer reached the seafloor.

Hole 1088B

The APC was redressed and the drill string was raised 5 m for a second, successful spud-in. A 5.5-m core was recovered, establishing the seafloor depth at 2092 meters below rig floor (mbrf). APC coring continued with azimuthal orientation beginning with Core 4H. APCT measurements were taken every third core. APCT data were adversely affected by vessel heave even though weather conditions had improved somewhat.

After Core 14H at 129 mbsf, the coring line parted at the ropesocket. It was necessary to fish the sinker bars and coring assembly with a second core barrel fitted with a hard-formation CC.

As the corer was being lowered for Core 15H, a ground fault was detected in the top drive. The corer was recovered, and the bit was pulled above the seafloor for the protection of the drill string while troubleshooting was in progress. The electrical problem turned out to be limited to a nick in the insulation of one of the top drive's umbilical cables. Temporary repairs were made to the insulation, and operations resumed after 3 hr of repair time.

Hole 1088C

Hole 1088C was spudded without the position being offset from Hole 1088B. A seafloor depth of 2093.7 mbrf was indicated by the recovered core. The hole was drilled without coring to 124 mbsf, where continuous coring resumed. After four additional APC cores to 162 mbsf, APC coring was abandoned because of excessive overpull and the requirement to drill around the core barrel to free it. Rotary coring then continued with the extended core barrel (XCB) system to 233 mbsf (Core 13X). At that point, coring operations were terminated at the request of the scientific investigators, well short of the originally projected penetration of about 700 m. The drill string was recovered, the positioning beacon was released and retrieved, and the vessel departed at 2230 hr on 18 December.

F5. Lithostratigraphic summary of Site 1088, p. 21.

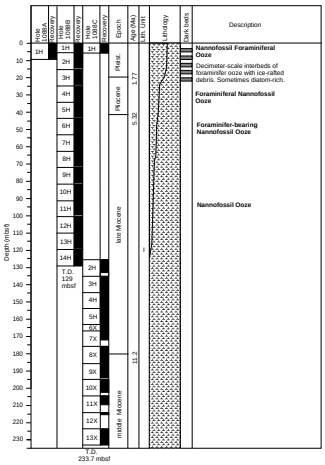

LITHOSTRATIGRAPHY

Overview

Three holes were drilled at Site 1088 to a total depth of 233.7 mbsf, recovering Holocene to middle Miocene calcareous ooze. The dominant lithologies are nannofossil ooze, foraminifer-bearing nannofossil ooze, foraminifer nannofossil ooze, and nannofossil foraminifer ooze. Carbonate contents vary from 85 to 95 wt%. The relative abundance of foraminifers decreases progressively downhole (Fig. F5). Siliceous microfossils are intermittent, mainly as a trace component, although some diatom-bearing nannofossil ooze is present. The sediment color is mainly very pale gray with minor, slightly darker (pale gray) interbed-

ded horizons in the upper 25 m. Faint dark laminations and some pyrized burrows are locally present. Volcanic ash was observed in Sections 177-1088B-7H-CC through 9H-CC.

The lithostratigraphic characteristics of the sediments are defined on the basis of primarily visual core descriptions and sediment smear-slide analyses (Fig. F6; "Site 1088 Smear Slides," p. 29). Additional information was obtained from spectral reflectance measurements, X-ray diffraction (XRD) for quartz, feldspar, clay, and opal abundances (on a carbonate-free basis), and calcium carbonate contents (Fig. F6; Table T1, also in ASCII format in the TABLES directory). One lithostratigraphic unit was identified at this site.

F6. Smear-slide, carbonate, and XRD analyses for Site 1088, p. 22.

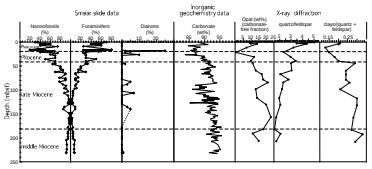

T1. X-ray diffraction data for Site 1088, p. 43.

Description of Lithostratigraphic Unit

Unit I

Intervals: 177-1088A-1H (0–9 mbsf); 177-1088B-1H through 14H (0–129 mbsf); 177-1088C-1H through 13X (0–233.7 mbsf)
Age: Pleistocene to middle Miocene

The upper 20 m of sediment in Hole 1088B consists of very pale gray nannofossil foraminifer ooze with a carbonate content ranging from 85 to 91 wt%. Subordinate, decimeter-scale interbeds of darker, more foraminifer-rich sediment (up to 80% foraminifers) commonly incorporate ice-rafted debris (IRD), rare dropstones, and may also contain diatoms. Analysis of multisensor track (MST) susceptibility and color reflectance data reveals that the darker beds have relatively high susceptibility values that reflect an increased terrigenous sediment content, whereas the pale, pure carbonate intervals have relatively low susceptibility values (Fig. F7). This interval has a lower carbonate content (85–91 wt%). Diatoms were particularly abundant in the darker bed in interval 177-1088B-3H-2, 51–69 cm, where the flora was dominated by *Thalassiothrix* (see "Chronostratigraphy," p. 5). Some of these darker beds appear to have erosional contacts (modified by bioturbation) with the underlying pale nannofossil ooze (Fig. F8).

F7. MST magnetic susceptibility and color reflectance data for Section 177-1088B-2H-3, p. 23.

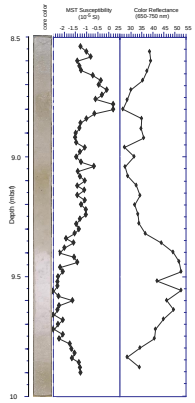

Below 20 mbsf, the proportion of foraminifers in the dominant lithology decreases to about 30% and the darker beds become less distinct. Between 30 and 120 mbsf, the proportion of foraminifers decreases progressively. In the nannofossil ooze between 120 mbsf and the base of Hole 1088C, foraminifers generally comprise less than 10% of the sediment. Carbonate content is relatively high (generally 90–95 wt%) and increases to the base of the hole, with the exception of a lower carbonate interval between 80 and 130 mbsf. The blue reflectance values show close similarity with the carbonate values (Fig. F9; "Geochemistry," p. 12). Below 130 mbsf, smear-slide composition data, carbonate values, and XRD mineralogy (see below) show little change to the base of the hole. Opal in the pre-Quaternary sediments reaches values between 10 and 23 wt%, showing two distinct maxima (~85 and ~156 mbsf) and minima (~98 and 190 mbsf).

F8. Contact between pale foraminifer nannofossil ooze and darker foraminifer nannofossil ooze containing IRD, p. 24.

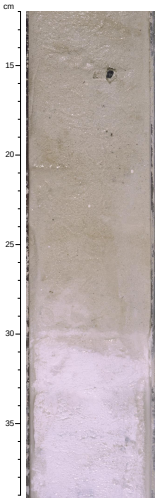

Faint, dark blue-gray laminations are present in the nannofossil ooze and similarly colored rings are present around some burrows. Bioturbation is moderate throughout, where visible, but is difficult to discern in the very pale gray nannofossil ooze, which has little internal color contrast. Pyritized burrows are common and locally form firm concretions. A distinctive chert-replaced burrow is present in interval 177-1088C-

10X-3, 91–100 cm. Abundant *Zoophycos* burrows are present in Core 177-1088B-9H.

X-ray Diffraction Results

XRD measurements were performed on the noncarbonate fraction from selected samples (Fig. F6). The uppermost three samples from Hole 1088B were taken from sediments thought to represent glacial and interglacial intervals of the late Quaternary as inferred from lithology and color changes. The samples probably comprise marine isotope Stages (MISs) 5 (1.43 mbsf), 10 (3.46 mbsf), and 11 (4.00 mbsf). Opal contents of the noncarbonate fractions are 9% for MIS 5, 10% for MIS 10, and 15% for MIS 11. Variations of quartz/feldspar values are in accordance with glacial–interglacial changes, with high values (4.4–5.0) in interglacials and lower values (3.5) in glacial MIS 10. The latter may indicate a higher supply of mineralogically immature terrigenous debris from sources with prevailing mechanical weathering, probably through ice-rafting from Antarctica. An additional possibility is that eolian input changes impact the quartz/feldspar values on glacial–interglacial time scales. The clay mineral/(quartz+feldspar) value shows no distinct variations in the late Quaternary samples.

Below the Pleistocene/Pliocene boundary (~20 mbsf), the clay mineral/(quartz+feldspar) value increases downhole, reaching values of 0.25 to 0.32 toward the base of the hole, and mirrors the quartz/feldspar value, which decreases to its lowest values (<2.0) toward the base of the hole. These compositional changes basically reflect changes in grain-size distributions of terrigenous particles, with decreasing coarse silt abundances downhole, as seen in smear slides of the noncarbonate samples. This suggests that hemipelagic settling of fine-grained material rather than ice-rafting or eolian input of coarse particles probably dominated during the Miocene.

CHRONOSTRATIGRAPHY

Composite Depths

MST data, collected at 2-cm intervals from Holes 1088A through 1088C, and color reflectance data (650–750 nm), collected at 4-cm intervals from Holes 1088A through 1088C, were used to determine depth offsets in the composite section. Gamma-ray attenuation (GRA) bulk density, color reflectance, and magnetic susceptibility measurements were the primary parameters used for the limited hole-to-hole correlation at Site 1088. The three types of data are presented on a composite depth scale in Figures F10, F11, and F12, respectively. The depth offsets are given in Table T2 (also in ASCII format in the TABLES directory).

Only two short depth intervals (0–5.5 and 122–129 meters composite depth [mcd]) were cored multiple times. Thus, continuity of the sedimentary section could not be documented at Site 1088. The composite data show that Holes 1088A and 1088B can be spliced together at intervals 177-1088B-14H-6, 12 cm, and 177-1088C-2H-4, 18 cm (127.12 mcd), to form a single (albeit discontinuous) section down to 230 mcd.

Although the upper 5.5 mbsf was cored in all three holes, no attempt was made to construct a continuous sampling splice over this interval for two reasons. First, Cores 177-1088B-1H and 177-1088C-1H are

F9. Lithologic summary of Site 1088 with blue reflectance and carbonate values, p. 25.

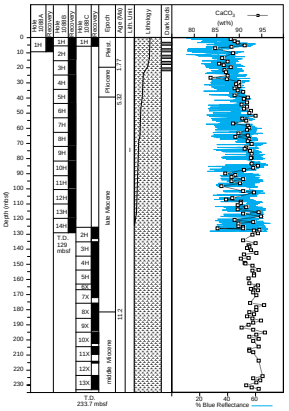

F10. Smoothed GRA bulk density data for Site 1088, p. 26.

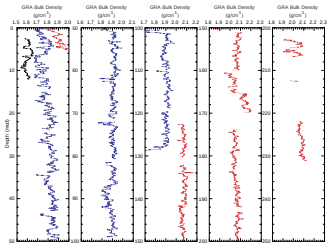

F11. Smoothed color reflectance data for Site 1088, p. 27.

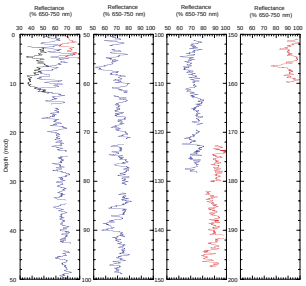

F12. Smoothed magnetic susceptibility data for Site 1088, p. 28.

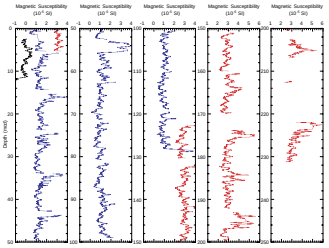

almost the same length (5.5 and 5.8 m, respectively), and the recovered material from these two cores is nearly identical. Second, Core 177-1088A-1H was highly disturbed and its depth relationship to the uppermost cores in the other holes could not be confirmed. Thus, the gap between Cores 177-1088B-1H and 2H could not be spliced with material from either Holes 1088A or 1088C.

T2. Composite depths for Site 1088, p. 44.

Biostratigraphy

Calcareous Nannofossils

Sediments recovered from Site 1088 provide a nearly continuous record for the Pleistocene through middle Miocene. Calcareous nannofossils are abundant or very abundant, with good to medium preservation of assemblages. Overgrowth is a common feature observed in *Discoaster* spp. but, in general, does not prevent identification. One to two samples per section were examined to obtain an accurate age assignment of the cores. The age model used for nannofossil event calibration is mainly derived from tropical and subtropical areas (see "Biostratigraphy," p. 10, in the "Explanatory Notes" chapter), and diachronism can occur. For the same reason, characteristic events included in the Martini (1971) and Okada and Bukry (1980) standard zonations have not been identified (Tables T3, T4, both also in ASCII format in the TABLES directory). The adopted calcareous nannofossil biochronology for the late Neogene, compared to the geomagnetic polarity time scale (GPTS) of Berggren et al. (1995), is included in "Biostratigraphy," p. 10, in the "Explanatory Notes" chapter. Table T5 (also in ASCII format in the TABLES directory) summarizes the calcareous nannofossil biostratigraphic results.

T3. Control points used to calculate sedimentation rates at Site 1088, p. 45.

T4. Biostratigraphic age assignments for Holes 1088B and 1088C, p. 46.

T5. Main calcareous nannofossil species for Holes 1088B and 1088C, p. 48.

Pleistocene

The Pleistocene interval in Hole 1088B is represented from the top to 20.2 mcd, where the first occurrence (FO) of medium-sized *Gephyrocapsa* marks the Pliocene/Pleistocene boundary (Table T5).

The acme and the FO of *Emiliania huxleyi* define the base of Subzones NN21b and NN21a at 1.10 and 2.65 mcd, respectively. The top of the *Gephyrocapsa caribbeanica* acme is contemporaneous with the FO of *E. huxleyi* and represents a good alternative event for identifying the base of Subzone NN21a, especially when dissolution occurs. The last occurrence (LO) of *Pseudoemiliania lacunosa* is observed around 4.40 mcd and defines the base of Zone NN20. The top and the base of the small *Gephyrocapsa* acme (see "Biostratigraphy," p. 10, in the "Explanatory Notes" chapter) are not clearly recognized; closer sampling and quantitative analyses will be necessary to define these events. However, an obvious dominance of the "very small *Gephyrocapsa*" complex is observed between 8.0 and 15.0 mcd. The LO and FO of *Reticulofenestra asanoi* are recognized at 11.80 and 15.07 mcd, respectively. The re- entrance of medium *Gephyrocapsa* is found at 11.8 mcd. The LO of large *Gephyrocapsa* (>5.5 µm) is present at 15.07 mcd, and its FO is present at 16.80 mcd (Tables T3, T5). The LO of *Calcidiscus macintyrei* is observed at 18.30 mcd.

Pliocene

Typical Pliocene biostratigraphic markers, such as taxa of the genera *Discoaster* and *Amaurolithus,* were found only at low abundance. Nevertheless, a semiquantitative analysis conducted on the upper Pliocene

assemblages allowed the recognition of the LOs of *Discoaster brouweri* (Zone NN19), *Discoaster pentaradiatus* (Zone NN18), *Discoaster surculus* (Zone NN17), and *Discoaster tamalis* (top of Zone NN16) at around 21.30, 22.8, 23.89, and 25.55 mcd, respectively. A hiatus of about 0.5 m.y. may occur between 20.95 and 22.80 mcd (Table **T5;** Fig. **F13**). Assemblages characterized by *Sphenolithus* spp. (*S. abies/neoabies*) and *Reticulofenestra pseudoumbilicus* were assigned an early Pliocene age. The LO of *Sphenolithus* spp. is present between 31.90 and 32.70 mcd, whereas the LO of *R. pseudoumbilicus* falls between 33.40 and 33.90 mcd. The top of the small *Gephyrocapsa* acme is recognized close to the LO of *Sphenolithus* spp. (32.30 mcd); the base of this acme is less clear than the top, but it seems to begin close to 40.0 mcd. This acme was defined by Marino (1994) from the Mediterranean area. Events defined by ceratoliths and related forms, such as *Triquetrorhabdulus rugosus,* have not been identified because of the extremely low abundance or absence of these taxa (Tables **T3, T5**).

F13. Age-depth plot of calcareous nannofossil and diatom datum events at Site 1088, **p. 29.**

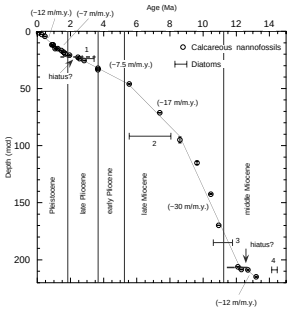

Miocene

The Miocene interval is represented in both Holes 1088B (late Miocene) and 1088C (middle–late Miocene). The upper Miocene assemblages are characterized by few to rare specimens of *Discoaster* spp. and *Amaurolithus* spp. Nevertheless, some events are tentatively recognized. In Hole 1088B, the LO of *Discoaster quinqueramus,* the FO of *Amaurolithus* s.l., the FO of *D. quinqueramus,* and the LO of *Discoaster hamatus* are placed at around 46.05, 71.29, 97.30, and 115.2 mcd, respectively (Table **T5**). Rare specimens of *Amaurolithus amplificus* are observed in Sample 177-1088B-7H-3, 140 cm, but it is not possible to establish the range of distribution. The above cited events allow us to identify Zones NN10 through NN12 for the latest Miocene. Rio et al. (1990) referred to a late Miocene interval of absence of *R. pseudoumbilicus* <7 µm (paracme). This characteristic feature is not observed at Site 1088 for the corresponding interval (Zones NN10 and NN11).

In Hole 1088C (Table **T6,** also in ASCII format in the **TABLES** directory), the FO of *D. hamatus* between 142.14 and 142.84 mcd defines the base of Zone NN9. The LO of *Coccolithus miopelagicus* is clearly identified between 169.71 and 169.97 mcd, approximately defining Zone NN8. This last event is the most useful for identifying the upper/middle Miocene boundary (Raffi and Flores, 1995). Unfortunately, it is not possible to recognize the zones of the middle Miocene because standard markers such as *Sphenolithus heteromorphus, Discoaster kugleri,* and *Catinaster coalitus* are absent. The LO of *Coronocyclus nitescens,* FO of *Calcidiscus macintyrei,* LO of *Calcidiscus premacintyrei,* and last common occurrence (LCO) of *Cyclicargolithus floridanus* are observed between 205.80 and 215.37 mcd, and can be considered indicative of the base of Zone NN6 (Tables **T3, T5**). The identification of these events suggests the possibility of a hiatus at ~207.0 mcd. (Figs. **F13, F14**). No characteristic markers from Zone NN5 have been observed at the bottom of Site 1088, which is tentatively assigned to this interval of time (<13.2 Ma) (Tables **T3, T5**).

T6. Main components of the planktic foraminifer assemblage in Hole 1088B, **p. 52.**

F14. Biostratigraphic correlations and age designations for Site 1088, **p. 30.**

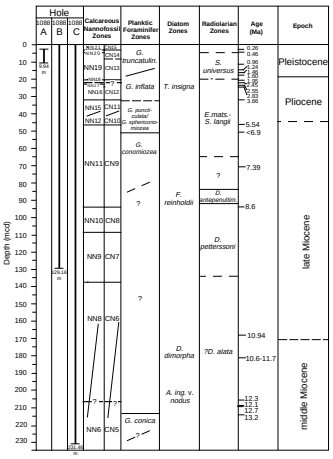

Planktic Foraminifers

Planktic foraminifers are abundant in the >63-µm fraction throughout the cores examined from Holes 1088B and 1088C (Table **T6**). Samples from Sections 177-1088B-1H-CC through 14H-CC and 177-1088C-1H-CC through 13X-CC were studied. The ages of the sections range

from Quaternary to middle Miocene. The Pliocene/Pleistocene boundary can be defined in Hole 1088B between Samples 177-1088B-2H-CC, 12–19 cm (14.44 mcd), and 3H-CC, 14–19 cm (23.97 mcd), on the basis of the FO of *Globorotalia truncatulinoides* in Sample 2H-CC, 12–19 cm, which indicates an age of less than ~2 Ma (Berggren et al., 1995). In Hole 1088C, only Sample 177-1088C-1H-CC, 12–17 cm, contains *G. truncatunlinoides,* suggesting a Quaternary age (Table **T6**). The absence or low abundance of several important marker species makes it difficult to subdivide the studied sections into the subantarctic zonal scheme of Jenkins and Srinivasan (1986) (see **"Biostratigraphy,"** p. 10, in the "Explanatory Notes" chapter). In addition, absolute ages are currently only available for a few subantarctic and transitional foraminifer datums (Berggren et al., 1995). However, the presence of ventroconical forms of *Globorotalia miotumida* (=*Globorotalia conomiozea* according to Kennett and Srinivasan, 1983) in Sample 177-1088B-6H-CC, 13–18 cm indicates an age <6.9 Ma (Berggren et al., 1995) (Table **T6**). The FO of this form was difficult to determine because of the gradation between different forms within the *G. miotumida* complex.

The Pliocene–Pleistocene assemblages of Site 1088 are dominated by *Globigerina bulloides, Neogloboquadrina pachyderma* (sinistral), *Globorotalia crassula, G. crassaformis, G. inflata,* and *G. puncticuloides*. The Miocene assemblages of Site 1088 are dominated by *G. miotumida, G. panda,* and *G. mayeri*. *Globorotalia quinqueloba* and *Globigerinita glutinata* are present throughout the studied cores. In addition, abundant to rare occurrences of *Globigerinoides sacculifer, G. obliquus, Globigerina falconensis, Globigerinita uvula, Globigerinella aequilateralis, Neogloboquadrina humerosa,* and *Globoquadrina dehiscens* were recorded at Site 1088.

Preservation

Planktic foraminifers are generally well preserved in Sections 177-1088B-1H-CC through 5H-CC. Pliocene and Miocene assemblages are moderately preserved in both Holes 1088B and 1088C. Preservation changes were easily detected in the studied sections as an increase in the ratio of *Globorotalia* vs. *Globigerina* in the less well-preserved samples.

Benthic Foraminifers

Benthic foraminifers were present in all the CC samples from this site, generally constituting less than 5% of the total foraminifer fauna from the >63-µm fraction studied. Quantitative estimates of relative species abundance were made with counts of as many as 190 specimens per sample. Diversity is variable, with a maximum of 39 taxa recorded in Sample 177-1088B-8H-CC, 10–15 cm, and a minimum of less than 20 taxa in Samples 177-1088B-1H-CC, 7–12 cm, and 177-1088C-1H-CC, 12–17 cm. Preservation is generally good throughout, showing some deterioration downhole, particularly below ~120 mcd. Absolute foraminifer abundances, while variable, exhibit a clear trend toward higher values uphole, reaching a maximum of 246 specimens/cm^3 in Sample 177-1088B-5H-CC, 12–18 cm. These changes in foraminifer abundance appear to reflect the general pattern of sedimentation at Site 1088, from nannofossil ooze (low abundance) during the middle and late Miocene to nannofossil foraminifer ooze (higher abundance) during the Pliocene–Pleistocene.

Biostratigraphic differentiation of Site 1088 is limited to the LO of *Stilostomella lepidula* in Section 177-1088B-2H-CC, which supports a

late Pleistocene age above 14.44 mcd (e.g., Thomas, 1987). Interesting assemblage changes are evident in the transition from middle to upper Miocene, characterized by increased relative abundances of the genus *Uvigerina*, notably *U. hispidicostata*. In addition, *Cibicidoides mundulus, C. wuellerstorfi, Epistominella exigua, Gyroidinoides soldanii,* and *Bolivina* spp. all tend to be more common downhole (Table T7, also in ASCII format in the TABLES directory).

T7. Benthic foraminifers at Site 1088, p. 53.

Diatoms

Diatom identification was conducted on smear slides. Because of the high carbonate content, ranging between 85 and 95 wt%, of the total sediment throughout the entire recovered section at Site 1088 (Fig. F6), selected samples were acid cleaned for the study of the noncarbonate biosiliceous residue (Table T8, also in ASCII format in the TABLES directory).

T8. Diatom, silicoflagellate, ebridian, *Actiniscus*, sponge spicule, and phytolith occurrence, Site 1088, p. 55.

In general, uncleaned smear slides contain only low concentrations of diatoms, silicoflagellates, ebridians, and *Actiniscus,* and some samples have been identified as barren of these microfossils. However, sponge spicules are recorded in all investigated samples at varying abundances. Only one interval (177-1088B-3H-2, 60 cm) contains abundant and well-preserved diatoms, with an assemblage dominated by taxa of the *Thalassiothrix antarctica-longissima* group.

In the noncarbonate residue slides, moderately preserved diatom assemblages were recovered in five other sediment intervals representing the time between ~14 and 3 Ma. The uppermost interval (177-1088B-3H-CC, 14–19 cm) represents the late Pliocene *Thalassiosira insigna/T. vulnifica* Zone and, thus, places the *Thalassiothrix*-rich interval encountered in the same core in the same time interval (Fig. F14; Table T4). Interval 1088B-10H-CC, 10–15 cm, has a diatom assemblage marked by the common occurrence of *Actinocyclus ingens* var. *ovalis,* a zonal marker that ranges in age between 8.7 and 6.3 Ma. The co-occurrence of *Nitzschia cylindrica* places this interval in the early *F. reinholdii* Zone on the basis of the FO of *N. cylindrica* at 7.6 Ma (Barron, 1992). However, the calcareous nannofossil age assignment of this interval (see "Calcareous Nannofossils," p. 6) indicates an age ranging in the lower portion of the *F. reinholdii* Zone (~8 Ma). Interval 1088B-13H-CC, 11–16 cm, contains an assemblage dominated by *Coscinodisus marginatus* and the *Thalassiothrix antarctica-longissima* group. Age-indicative taxa were not encountered. The co-occurrence of *Actinocyclus ingens* and *Denticulopsis dimorpha* places interval 177-1088C-8X-5, 10–12 cm, in the middle–late Miocene *D. dimorpha* Zone. The oldest interval containing significant diatoms in the acid-cleaned residue is 177-1088C-11X-2, 48–50 cm, and it is assigned to the middle Miocene *A. ingens* var. *nodus* Zone.

Evidence for eolian transport of diatoms is present in intervals 177-1088B-5H-CC, 12–18 cm, and 10H-CC, 10–15 cm, where the freshwater diatom *Aulacoseira granulata* and opaline phytoliths were identified, respectively.

In general, diatoms do not contribute significantly to the establishment of an age-depth model at Site 1088 (Table T4; Fig. F14). However, their occurrences indicate the potential of sediment intervals that are rich in biosiliceous components at the northernmost site of the Leg 177 transect. These biosiliceous intervals might be related to short-term paleoceanographic changes leading to increased paleoproductivity at Site 1088.

Radiolarians

Radiolarians are present in all the CC samples from Holes 1088A, 1088B, and 1088C. In general, the radiolarian preservation is excellent to moderate, and abundance varies from abundant to moderate, except for Sample 177-1088C-13X-CC in which only a few specimens were present in a strewn slide (Table T9, also in ASCII format in the TABLES directory).

T9. Main components of the radiolarian assemblage in Holes 1088B and 1088C, p. 57.

The radiolarian fauna of Site 1088 indicates a Quaternary to middle Miocene age and is characterized by the dominant occurrence of low- to mid-latitude species. Typical Antarctic species, such as *Antarctissa denticulata,* occur only in the upper part of Hole 1088B (Samples 177-1088B-1H-CC through 3H-CC).

The Quaternary/Pliocene boundary is placed between Samples 177-1088B-2H-CC (14.44 mcd) and 8H-CC (71.37 mcd). This interval can be assigned to the Pleistocene *Eucyrtidium matsuyamai* to Pliocene *Sphaeropyle langii* Zones on the basis of the common occurrence of *Lamprocyrtis heteroporos* in Samples 1088B-3H-CC through 7H-CC (Fig. F14; Table T4).

A distinctive late Miocene assemblage containing *Diartus hughesi* is first recognized in Sample 177-1088B-10H-CC, which is correlative with the *Didymocyrtis antepenultima* Zone. Therefore, the interval from Sample 1088B-7H-CC through 10H-CC, which contains *Stichocorys peregrina,* spans the Pliocene to upper Miocene.

Samples 177-1088B-11H-CC through 14H-CC and 177-1088C-2H-CC, 99.16 to 130.47 mcd, are assigned to the middle Miocene *Diartus petterssoni* Zone on the basis of the sporadic presence of the nominal species and persistent occurrence of *Didymocyrtis laticonus.*

Didymocyrtis mammifera, ranging in age from early to middle Miocene, was identified in Samples 177-1088C-3H-CC, 9X-CC, 10X-CC, and 13X-CC. On the basis of the previously known range of *D. mammifera,* an interval from Sample 177-1088C-3H-CC to 13X-CC, 141.49 to 233.27 mcd, may be correlative with the *Dorcadospyris alata* Zone, although the nominal species is absent. Further investigation is necessary to make precise correlation. Below Sample 177-1088C-4H-CC, 150.54 mcd, radiolarian assemblages are particularly monotonous. *Cyrtocapsella japonica* predominates in Samples 1088C-4H-CC through 8X-CC, whereas the assemblages below Sample 1088C-9X-CC are characterized by the presence of *C. tetrapera*. This type of radiolarian assemblage is very similar to that in the mid-latitude northwestern Pacific region and is considered to be middle Miocene in age. The LO of *Cyrtocapsella japonica*, which is placed between Samples 177-1088C-3H-CC and 4H-CC, is dated at 8.9 Ma in the northwest Pacific (Motoyama, 1996).

Paleomagnetism

Archive halves of all APC cores recovered at Site 1088 were measured using the shipboard pass-through magnetometer. Measurements were made at 5-cm intervals. For Cores 177-1088A-1H through 10H, six measurement steps were conducted after alternating-field demagnetization at peak fields of 0, 5, 10, 15, 20, and 25 mT. For Cores 177-1088A-11H through 14H, and all APC cores from Hole 1088C, three measurement steps were conducted after 0-, 10-, and 25-mT peak-field demagnetization.

Natural remanent magnetic moments were about 10^{-4} Am^2 throughout the core, approximately two orders of magnitude above the noise level of the magnetometer. Inclinations show a tendency to steepen during progressive demagnetization. Throughout the demagnetization sequence, however, inclinations remain less than those expected (60°) for the site location (Fig. F15) and declinations are highly scattered. This suggests a low-inclination (possibly radial) remagnetization of the core. The perceived drill-string remagnetization may have been exacerbated by physical disturbance of the poorly consolidated nannofossil/foraminifer oozes.

F15. Inclination values measured after 25-mT demagnetization, Holes 1088A–1088C, p. 31.

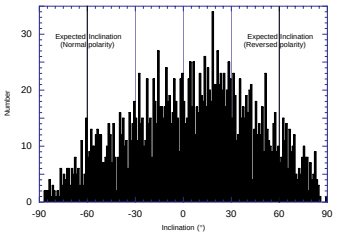

Stratigraphic Summary

A 233.4-m-thick sedimentary section spanning the interval from the Pleistocene through the middle Miocene was recovered at Site 1088. The basal age was estimated to be ~13–14 Ma. Holes 1088A, 1088B, and 1088C were cored with the APC to 9.5, 129.0, and 162.3 mbsf, respectively. Drilling in Hole 1088C continued with the XCB to a total depth of 233.4 mbsf. A continuous sedimentary section could not be documented at Site 1088. Furthermore, a magnetostratigraphy was not obtained at Site 1088 because of core-barrel-induced magnetization problems.

Age assignment and calculation of sedimentation rates for Site 1088 are based primarily on calcareous nannofossil biostratigraphy. Calcareous nannofossil Zones NN6 through NN21 and CN5 through CN15, respectively, were identified on the basis of examination of CC and additional samples, indicating rather continuous sedimentation. Planktic foraminifers and diatoms provided only a few datum levels. Radiolarian assemblages, which were encountered at excellent to moderate preservation in all CC samples, contain only few age-indicative taxa that allow the identification of long-range zones that are not well tied to the GPTS (Fig. F14; Table T4). On the basis of combined biostratigraphic results, 25 age-depth control points were selected. The control points represent mean depths (mbsf and mcd) of samples below and above the biostratigraphic datums (Table T3). The depth uncertainty associated with the calcareous nannofossil datums is about ±0.7 m, corresponding to a resolution of one-half core section.

The resulting age-depth interpretation shows a rather continuous sedimentation. Low sedimentation rates, which might be indicative of a hiatus or condensed sections, are found only between 1.95 and 2.45 Ma (20.95–22.8 mcd) and from 12.3 to 12.7 Ma (206.1–207.0 mcd; Fig. F13). These discontinuities, however, may be an artifact of age uncertainties associated with the calcareous nannofossil datums. On the basis of the age model derived from the biostratigraphic control points, the Pliocene/Pleistocene boundary can be placed at 19.61 mbsf (19.61 mcd), the Miocene/Pliocene boundary at 43.90 mbsf (43.90 mcd), and the middle/late Miocene boundary at 183.31 mbsf (181.45 mcd).

Calculated sedimentation rates average 12 m/m.y. in the Pleistocene and 7 m/m.y. in the Pliocene (Fig. F13; Table T3). Late Miocene sedimentation rates average 28 m/m.y., twice those of the younger Pliocene–Pleistocene section. Before 12.3 Ma, sedimentation rates drop, reaching values of <1 m/m.y.

GEOCHEMISTRY

Volatile Hydrocarbons

As part of the shipboard safety and pollution program, volatile hydrocarbons (methane, ethane, and propane) were measured in the sediments of Site 1088 from every core using the standard ODP headspace sampling technique. Results are presented in Table T10 and Figure F16. Headspace methane concentrations were generally low (4–11 parts per million by volume [ppmv]) throughout the sedimentary sequence at Site 1088, except for the uppermost sediments, which showed slightly higher values of 39 ppmv. Traces of ethane and propane were detected in the uppermost sediments (Sample 177-1088B-1H-4, 0–5 cm). Higher molecular weight hydrocarbon gases were not observed.

Interstitial Water Chemistry

Shipboard chemical analyses of interstitial water in the sediments from Site 1088 included measurements of salinity, pH, alkalinity, chlorinity, calcium, magnesium, sulfate, silica, phosphate, ammonium, strontium, and lithium (see "Geochemistry," p. 18, in the "Explanatory Notes" chapter for details on methods). The results from the shipboard analyses are presented in Table T11 and Figure F17. The results represent 35 interstitial water samples taken from Hole 1088B to a depth of 116 mbsf and seven samples taken from Hole 1088C from 129 to 230 mbsf; the total of 42 samples is considered to represent a single continuous profile.

Chlorinity increases downhole, with a slight local maximum at ~40 mbsf. This pattern may result from the downward diffusion of higher salinity water associated with the last glacial maximum (McDuff, 1985). The reason an increase is not also observed in Na^+ is probably because Na^+ concentrations are determined by charge balance calculations and thus Na^+ concentrations include the errors associated with measurement of all major cations and anions.

The sediments from this low–sedimentation-rate site are rich in carbonate throughout the length of the profile, and carbonate recrystallization processes apparently dictate some of the interstitial chemistry. For example, the increases in Ca^{+2} and Sr^{+2} are consistent with biogenic carbonate dissolution.

The sediments are only mildly reducing as indicated by a decrease in sulfate from bottom-water values of 29 to ~20 mM at 230 mbsf. Sulfate depletion with depth is accompanied by corresponding increases in NH_4^+, with a high degree of inverse correlation between sulfate and NH_4^+ (Fig. F18). The mildly reducing character of these sediments and generally slow rates of organic matter diagenesis are also indicated by the near constant alkalinity with depth.

Dissolved silica increases to a nearly constant value of ~900 µM, close to saturation for opal. There is a local maximum at ~25–30 mbsf that may be associated with diatom-rich layers, supported by diatom abundances observed in smear slides from this site (see "Lithostratigraphy," p. 3). The small local minimum in dissolved silica just below the maximum is likely the result of some sediment constituent, perhaps aluminum, exerting control over silica solubility (see van Beusekom et al., 1997, and references therein). Without some local control over silica

T10. Concentrations of methane, ethane, and propane at Site 1088, p. 58.

F16. Concentration of methane vs. depth at Site 1088, p. 32.

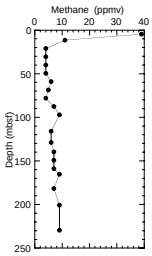

T11. Interstitial water chemistry at Site 1088, p. 59.

F17. Interstitial water chemistry profiles vs. depth at Site 1088, p. 33.

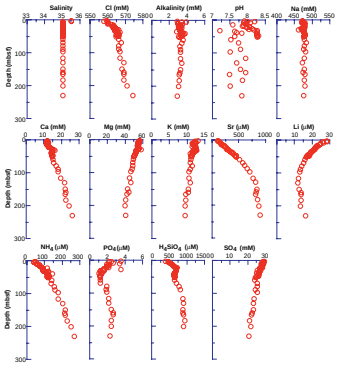

F18. Interstitial water ammonium vs. sulfate at Site 1088, p. 34.

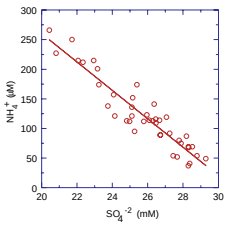

solubility, the local minimum in dissolved silica would probably have been smoothed out by diffusional processes.

Phosphate concentrations in the interstitial waters of Site 1088 are low throughout the profile, likely as a consequence of elevated Ca^{+2} and formation of an authigenic phosphorus-bearing phase like carbonate fluorapatite (Filippelli and Delaney, 1996).

Solid Phase Analysis

A total of 140 sediment samples were analyzed for inorganic carbon by coulometric titration at Site 1088. Calcium carbonate ($CaCO_3$) contents vary between 83.6 and 95.7 wt%, with an average value of 91.4 wt% (Table **T12;** Fig. **F19**). In the upper 30 m, which corresponds to the lithofacies of nannofossil foraminifer ooze with IRD (see **"Lithostratigraphy,"** p. 3), $CaCO_3$ contents are slightly lower than deeper in the section. $CaCO_3$ contents are also slightly lower in the sediments from 90 to 127 mbsf.

PHYSICAL PROPERTIES

GRA bulk density, magnetic susceptibility, natural gamma-ray (NGR) emission, and *P*-wave velocity were measured with the MST on most whole-core sections recovered from Site 1088 (Table **T13**). Color reflectance and resistivity were measured on the working half of all split APC cores using the Oregon State University Split Core Analysis Track (OSU-SCAT) (see **"Lithostratigraphy,"** p. 5, in the "Explanatory Notes" chapter). Other physical properties measurements conducted on discrete 10-cm^3 samples included moisture, density, and *P*-wave velocity (Table **T13**). Samples for moisture and density determination were taken at an average of two per section. Measured parameters were initial wet bulk mass (M_b), dry mass (M_d), and dry volume (V_d). Velocity was measured on split-core sections using the *P*-wave velocity sensor 3 (PWS3). Comparisons between the whole-core MST data and physical properties measured on discrete samples are shown in Figure **F20.**

Multisensor Track

P-wave velocity, GRA bulk density, magnetic susceptibility, and NGR were determined every 2 cm for all cores from each hole. Sampling time was 4 s at every point for each sensor. Data were reduced with a 10-point running average for presentation in this report (Fig. **F20**). *P*-wave velocities were not measured for the XCB cores from Hole 1088C. Magnetic susceptibility shows characteristic downhole fluctuations, although the intensity was very low with only small variations. NGR values generally correspond to the variations of magnetic susceptibility (Fig. **F20**).

P-wave Velocity

Velocity data gathered by the MST *P*-wave logger (PWL) were of poor quality. This was partly the result of coarse-grained foraminifer ooze in the upper part of the holes that resulted in high signal attenuation. In cores from the lower parts of the holes, there was insufficient contact between the sediment and the core liner, resulting in poor signal transmission. This can cause, for example, the second rather than first wave-

T12. Concentrations of IC and $CaCO_3$ at Site 1088, **p. 61.**

F19. Calcium carbonate vs. depth at Site 1088, **p. 35.**

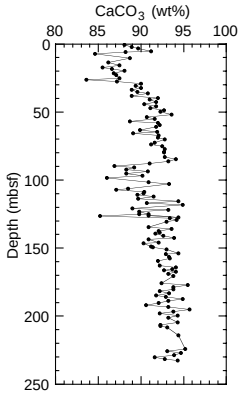

T13. Physical properties measurements at Site 1088, **p. 64.**

F20. Site 1088 moisture and density data compared with MST, OSU-SCAT, and NGR data, **p. 36.**

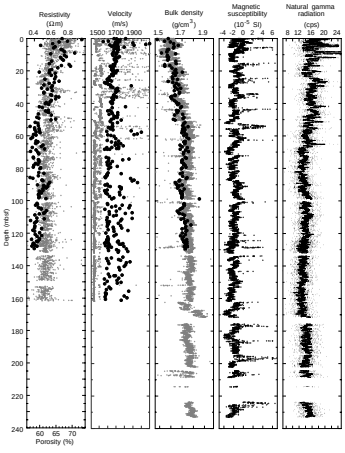

let to be auto-picked by the PWL, which may result in the bimodal velocity distribution (80 m/s difference) seen in Figure F20. Average velocities were around 1500 m/s. *P*-wave velocities measured with the PWS3 velocimeter were consistently greater than those logged by the PWL. Shallow cores had average velocities around 1700 m/s. Scatter in the data increases downhole because of anomalously high velocities (~1900 m/s) in the center of some core sections. The density data show a smooth increase downhole (Fig. F20). In both the PWL and PWS3 data sets the overall trend in velocity was a decrease downhole.

Moisture and Density

Moisture content and density were determined on two samples per core section in Hole 1088B and in the APC cores from Hole 1088C. The results are shown in Figure F20. The overall trend of the wet bulk density profile is a downhole increase caused by compaction. There is good agreement in this trend with GRA densities, although GRA densities are consistently ~0.05 g/cm³ greater (Fig. F21). Grain density increased gradually downhole, coincident with increasing carbonate concentrations (Fig. F22).

Resistivity and Porosity

Resistivity measurements at Site 1088 show greatest values at the top of the cored interval and gradually decrease downhole. Resistivity values range from 0.35 to ~0.8 Ωm, with discrete spikes exceeding 1.0 Ωm. In general, resistivity is inversely proportional to sediment interstitial water content for a given lithology and is, therefore, expected to increase with depth as porosity decreases because of compaction. The resistivity profile at Site 1088 is atypical in that resistivity actually decreases downhole, whereas porosity measured on discrete samples decreases (Fig. F20). This may be an artifact resulting from failure of the thermistors on the landing board of the OSU-SCAT, giving unreliable core temperatures. Figure F20 was produced using an assumed core temperature of 20°C. Calibrated thermistors were installed for later sites and this atypical relationship between resistivity and porosity was not observed at Site 1089. An alternative explanation could be the decreasing grain size of the terrigenous and carbonate fraction with depth (see "Lithostratigraphy," p. 3) at Site 1088. Greater total grain surface area with ionic clouds around the grains may lead to greater "surface" conductivity than normal interstitial water.

Diffuse Spectral Reflectance

Diffuse spectral reflectance variations in four 100-nm bands correlate well with each other at Site 1088, and the overall trend is a downward increase (Figs. F23, F24). A long-term trend toward higher reflectance that begins at the top of Hole 1088B and continues through ~60 mbsf is apparent in each of the 100-nm color bands. Values in the red band range from lows of ~30% to highs of ~70%. Superimposed on the long-term trend is cyclic behavior with a depth scale of ~1 m. At depths below ~60 mbsf, reflectance exhibits relatively constant mean values. This pattern is also observed in the GRA density measurements (Fig. F24) and the carbonate measurements from Site 1088 (see "Geochemistry," p. 12). The positive correlation between high reflectivity and high density, and low reflectivity and low density sediments, suggests that

F21. Relationship between GRA and MAD bulk density at Site 1088, p. 37.

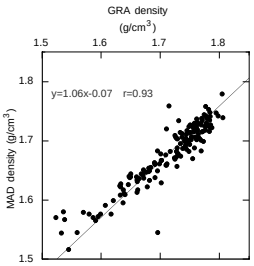

F22. Downhole increases in grain density and carbonate content at Site 1088, p. 38.

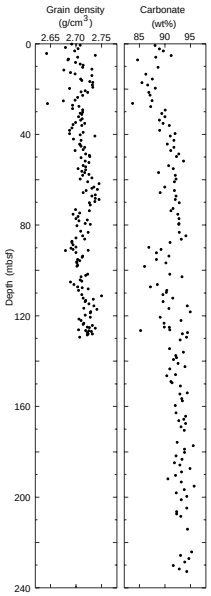

F23. OSU-SCAT spectral reflectance compared to GRA density at Site 1088, p. 39.

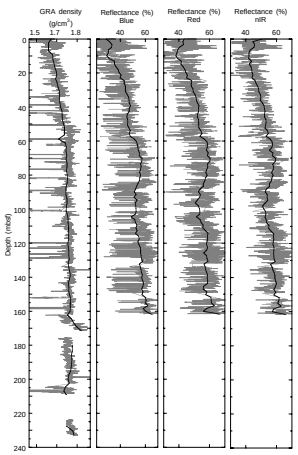

color and density variations at Site 1088 are largely driven by variations in sediment carbonate content.

Heat Flow

A total of 23 thermal conductivity measurements conducted on core sections gave values ranging from 0.83 to 1.21 W/(m·K) (Fig. F25; Table T14, also in ASCII format in the TABLES directory).

Five downhole temperature measurement attempts were made at Site 1088: one in bottom water about 20 m above the seafloor, and four in sediment with Cores 177-1088-4H, 7H, 11H, and 14H (Table T15). Four measurements yielded very noisy data which could not be used to estimate the temperature (Fig. F26). This is probably the result of considerable ship heave, which created random frictional heat. One attempt had an electronic failure and did not collect any data. A meaningful determination of the heat flow was therefore impossible at Site 1088.

F24. Diffuse spectral reflectance variations at Hole 1088A, p. 40.

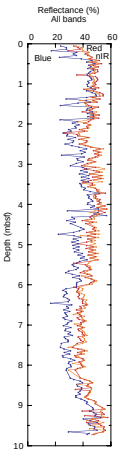

F25. Thermal conductivity measurements at Site 1088, p. 41.

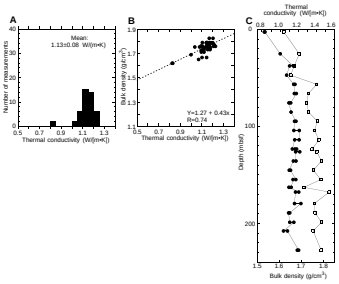

T14. Thermal conductivity measurements at Site 1088, p. 65.

T15. Temperature measurement attempts at Site 1088, p. 66.

F26. Downhole temperature measurements at Site 1088, p. 42.

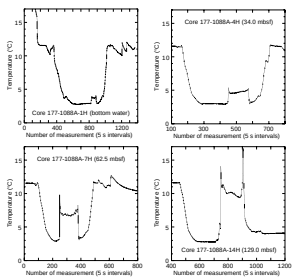

REFERENCES

Barron, J.A., 1992. Neogene diatom datum levels in the equatorial and North Pacific. *In* Ishizaki, K., and Saito, T. (Eds.), *The Centenary of Japanese Micropaleontology:* Tokyo (Terra Sci. Publ.), 413–425.

Berggren, W.A., Kent, D.V., Swisher, C.C., III, and Aubry, M.-P., 1995. A revised Cenozoic geochronology and chronostratigraphy. *In* Berggren, W.A., Kent, D.V., Aubry, M.-P., and Hardenbol, J. (Eds.), *Geochronology, Time Scales and Global Stratigraphic Correlation*. Spec. Publ.—Soc. Econ. Paleontol. Mineral. (Soc. Sediment. Geol.), 54:129–212.

Filippelli, G.M., and Delaney, M.L., 1996. Phosphorus geochemistry of equatorial Pacific sediments. *Geochim. Cosmochim. Acta*, 60:1479–1495.

Jenkins, D.G., and Srinivasan, M.S., 1986. Cenozoic planktonic foraminifers from the equator to the sub-antarctic of the southwest Pacific. *In* Kennett, J.P., von der Borch, C.C., et al., *Init. Repts. DSDP,* 90: Washington (U.S. Govt. Printing Office), 795–834.

Kennett, J.P., and Srinivasan, M.S., 1983. *Neogene Planktonic Foraminifera: A Phylogenetic Atlas:* Stroudsburg, PA (Hutchinson Ross).

Marino, M., 1994. Biostratigrafia integrata a nannofosili calcari e foraminiferi planctonici di alcune succesioni terrigene pliocenico-superiori del Bacino di Sant' Arcangelo (Appennino meridionale). *Boll. Soc. Geol. Ital.,* 113:329–354.

Martini, E., 1971. Standard Tertiary and Quaternary calcareous nannoplankton zonation. *In* Farinacci, A. (Ed.), *Proc. 2nd Int. Conf. Planktonic Microfossils Roma:* Rome (Ed. Tecnosci.), 2:739–785.

McDuff, R.E., 1985. The chemistry of interstitial waters, Deep Sea Drilling Project Leg 86. *In* Heath, G.R., Burckle, L.H., et al., *Init. Repts. DSDP,* 86: Washington (U.S. Govt. Printing Office), 675–687.

Motoyama, I., 1996. Late Neogene radiolarian biostratigraphy in the subarctic Northwest Pacific. *Micropaleontology,* 42:221–260.

Okada, H., and Bukry, D., 1980. Supplementary modification and introduction of code numbers to the low-latitude coccolith biostratigraphic zonation (Bukry, 1973; 1975). *Mar. Micropaleontol.,* 5:321–325.

Raffi, I., and Flores, J.-A., 1995. Pleistocene through Miocene calcareous nannofossils from eastern equatorial Pacific Ocean (Leg 138). *In* Pisias, N.G., Mayer, L.A., Janecek, T.R., Palmer-Julson, A., and van Andel, T.H. (Eds.), *Proc. ODP, Sci. Results,* 138: College Station, TX (Ocean Drilling Program), 233–286.

Rio, D., Fornaciari, E., and Raffi, I., 1990. Late Oligocene through early Pleistocene calcareous nannofossils from western equatorial Indian Ocean (Leg 115). *In* Duncan, R.A., Backman, J., Peterson, L.C., et al., *Proc. ODP, Sci. Results,* 115: College Station, TX (Ocean Drilling Program), 175–235.

Thomas, E., 1987. Late Oligocene to Recent foraminifers from Deep Sea Drilling Project Sites 608 and 610, northeastern North Atlantic. *In* Ruddimann, W.F., Kidd, R.B., Thomas, E., et al., *Init. Repts. DSDP,* 94: Washington (U.S. Govt. Printing Office), 997–1031.

van Beusekom, J.E.E., van Bennekom, A.J., Tréguer, P., and Morvan, J., 1997. Aluminum and silicic acid in water and sediments of the Enderby and Crozet Basins. *Deep-Sea Res.*, 44:987–1003.

Wright, J.D., Miller, K.G., and Fairbanks, R.G., 1991. Evolution of modern deepwater circulation: evidence from the late Miocene Southern Ocean. *Paleoceanography,* 6:275–290.

————, 1992. Early and middle Miocene stable isotopes: implications for deepwater circulation and climate. *Paleoceanography,* 7:357–389.

Figure F1. North-south bathymetric profile across the Agulhas Ridge, obtained during *Polarstern* Cruise ANT-IX/4, showing the location of piston cores and Site 1088. Box at the crest of the Agulhas Ridge delimits the area depicted in Figure F2, p. 18.

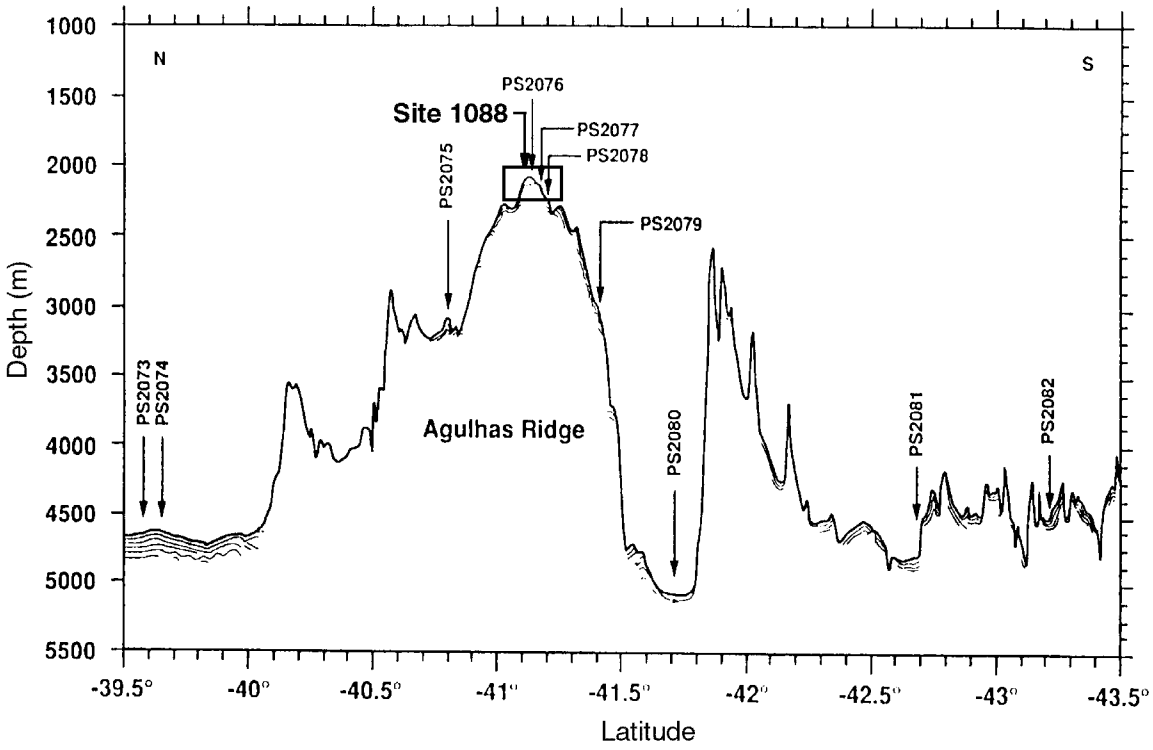

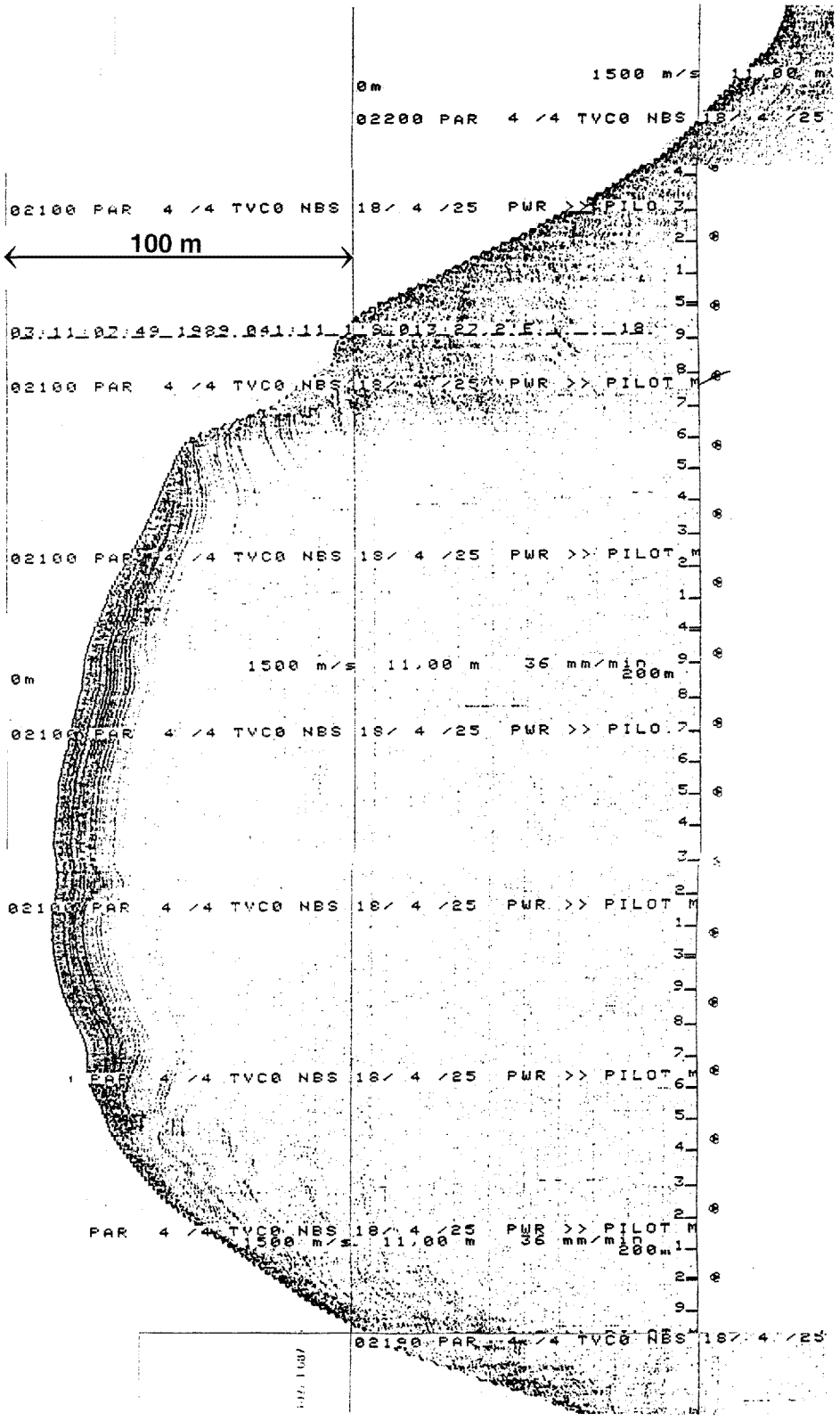

Figure F2. Parasound profile across the Agulhas Ridge collected during *Polarstern* Cruise ANT-IX/4. See Figure F1, p. 17, for location.

Figure F3. Track line and shotpoints for the site survey of Site 1088 conducted during *Thompson* Cruise TTN057. The bold portion of the track line corresponds to the segment of the seismic profile displayed in Figure **F4,** p. 20.

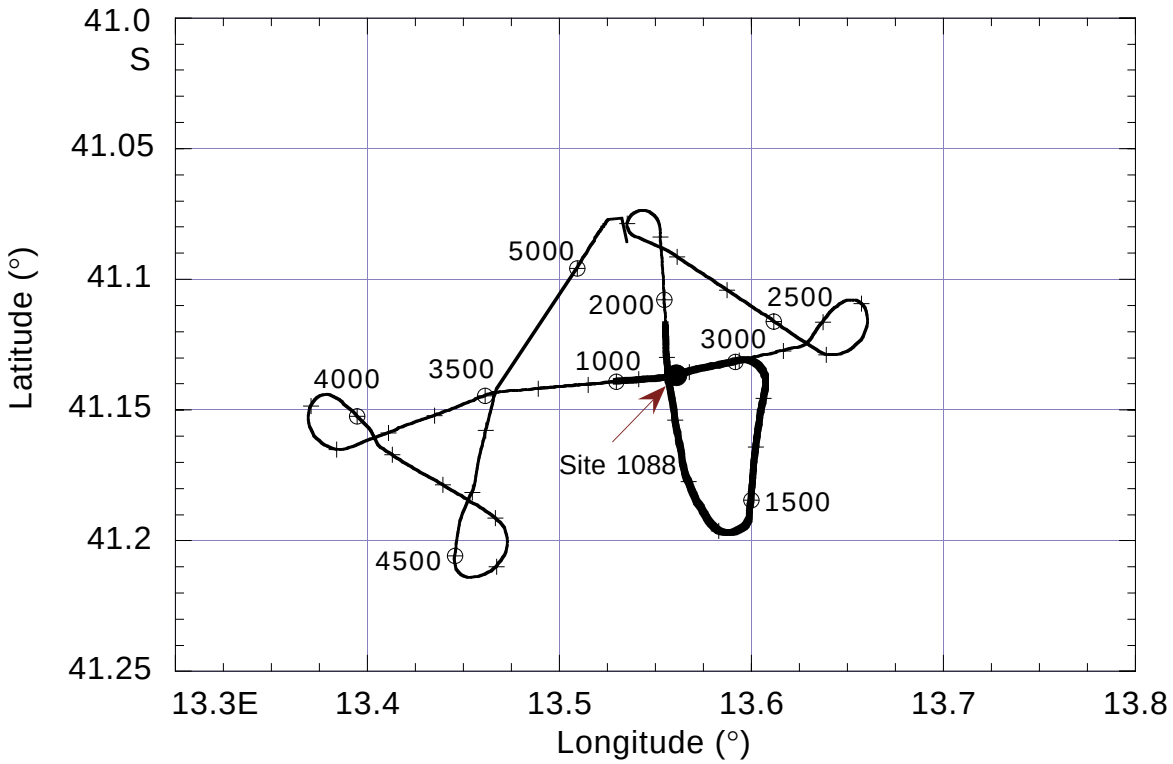

Figure F4. Single-channel seismic line collected during site-survey *Thompson* Cruise TTN057, showing the location and penetration depth of Site 1088. SP = shotpoint.

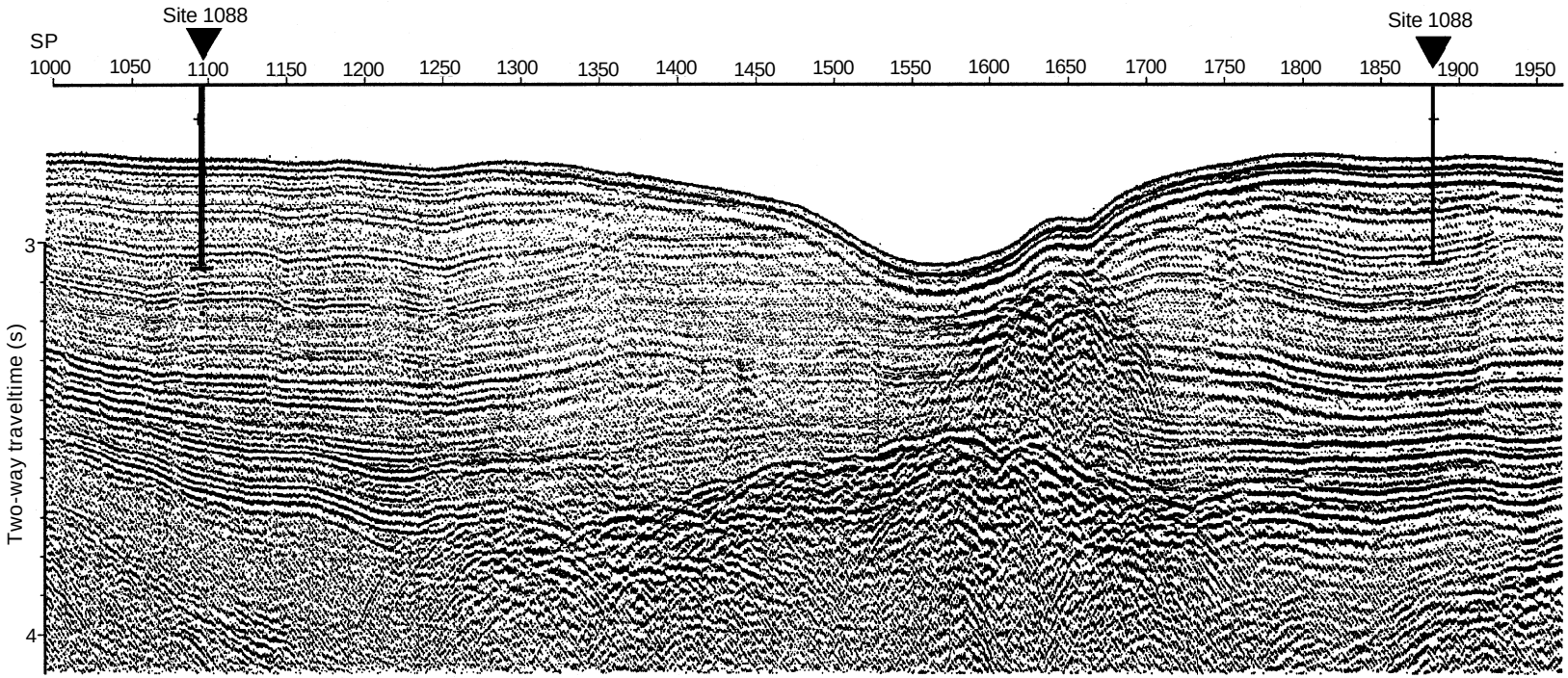

Figure F5. Lithostratigraphic summary of Site 1088 showing principal lithologies and schematic core recovery. T.D. = total depth.

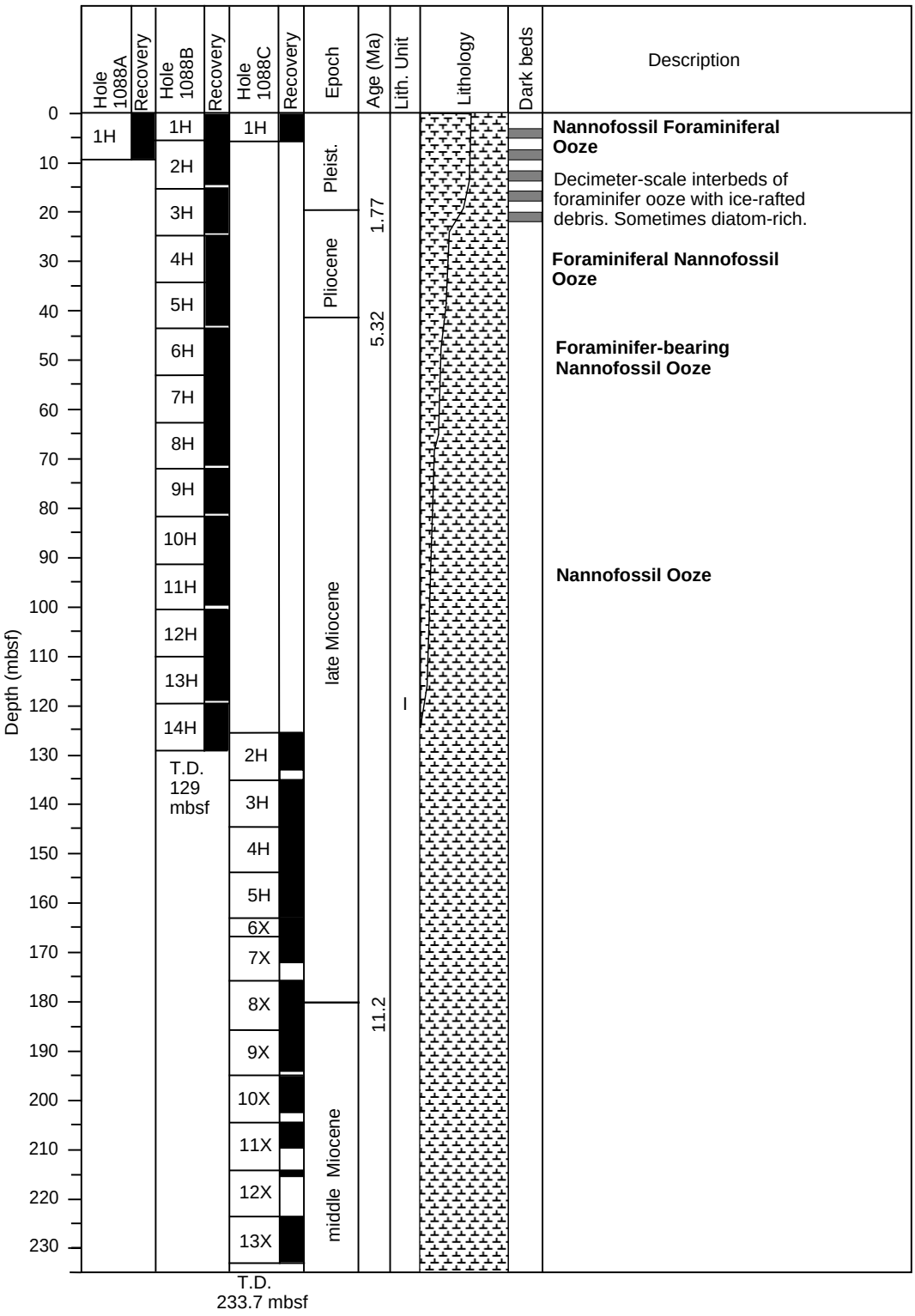

Figure F6. Smear-slide analysis of major sedimentary components and results of carbonate and XRD analyses for Site 1088.

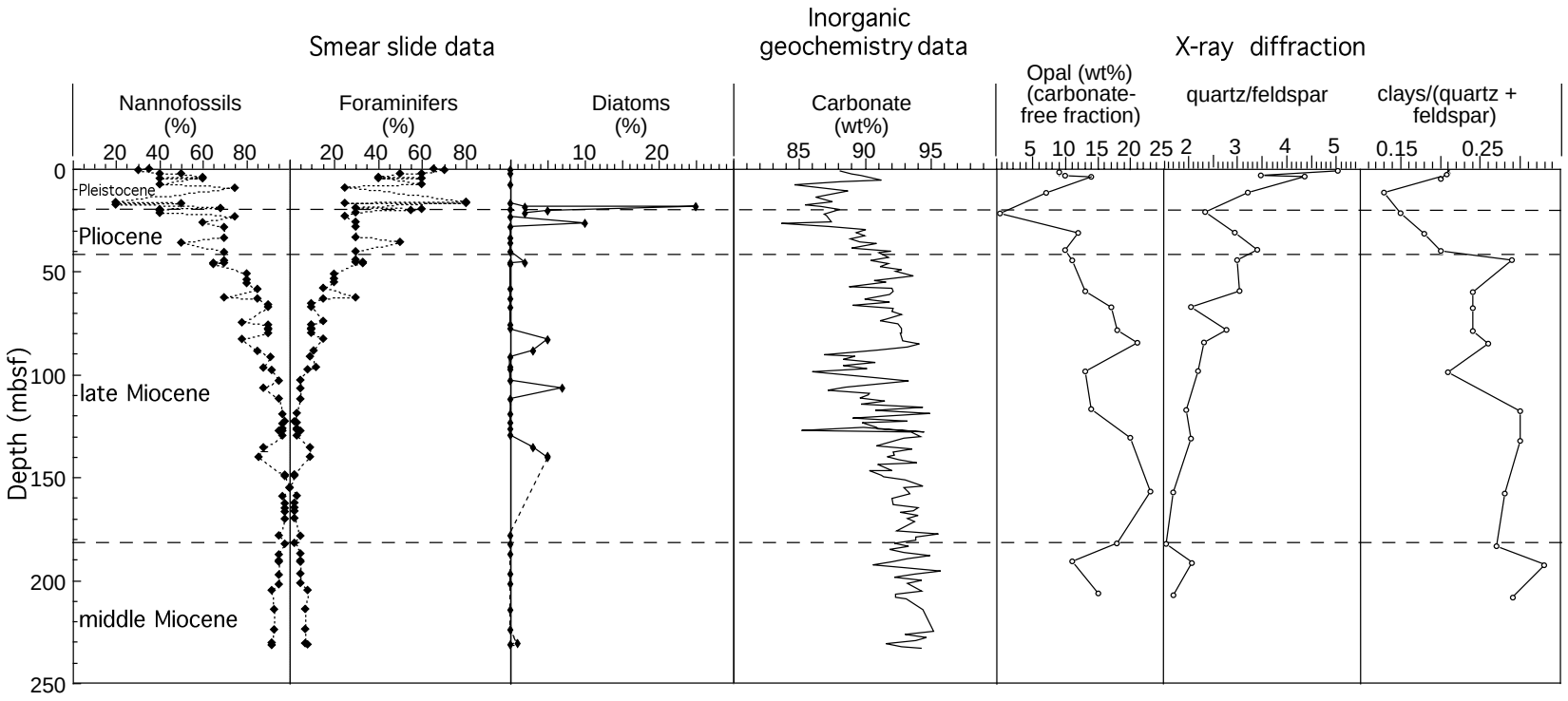

Figure F7. MST magnetic susceptibility and color reflectance data for Section 177-1088B-2H-3, showing the occurrence of darker intervals coincident with increased susceptibility values (terrigenous sediment content).

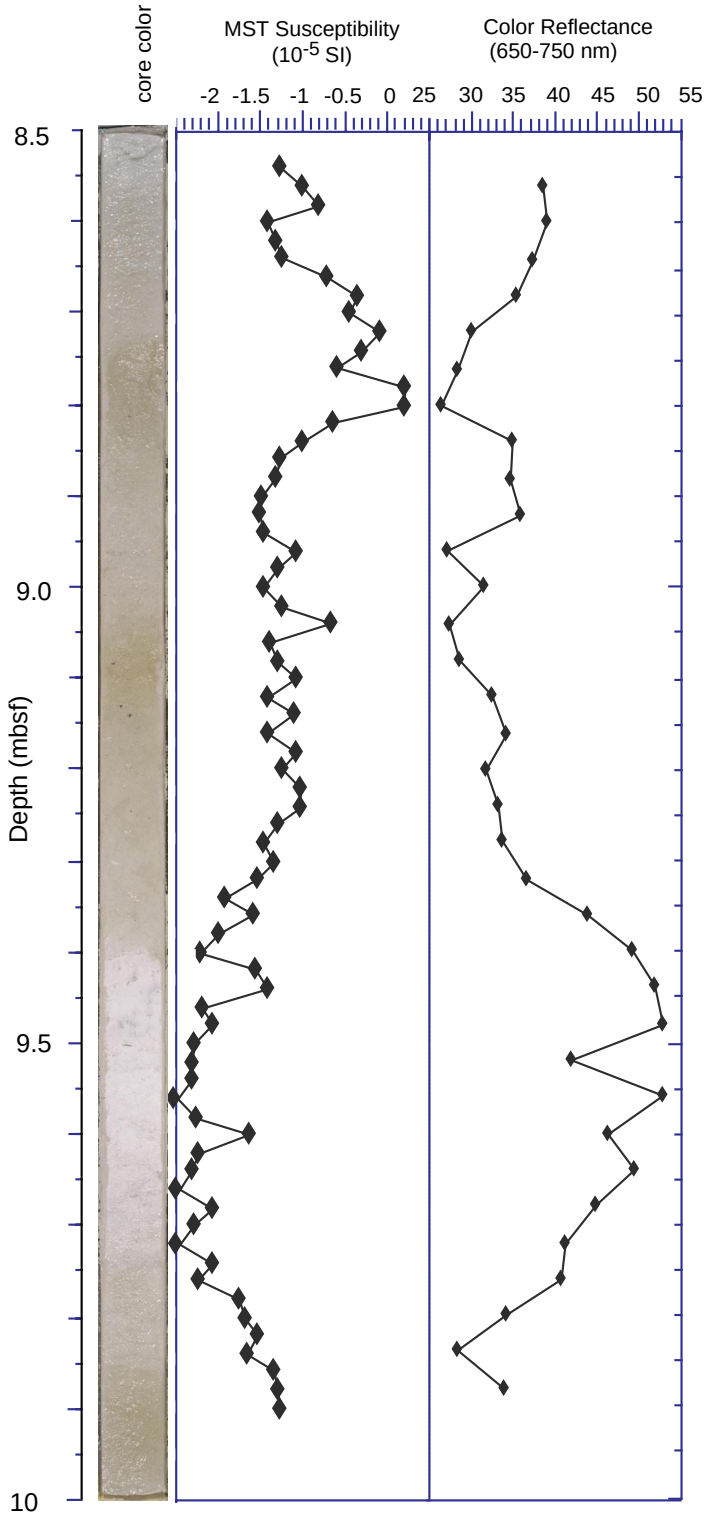

Figure F8. Core photograph of interval 177-1088B-1H-4, 12–39 cm, showing the possible erosional contact (modified by bioturbation) between pale foraminifer nannofossil ooze and the overlying darker bed of foraminifer nannofossil ooze containing ice-rafted debris (30–31 cm).

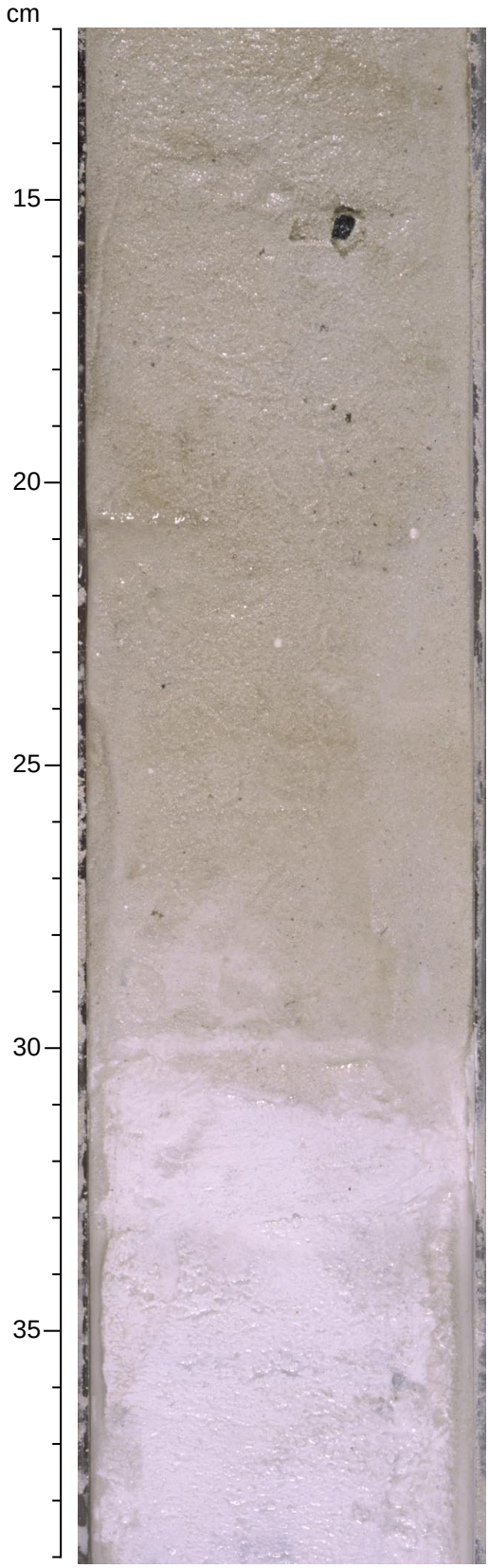

Figure F9. Lithologic summary diagram of Site 1088 with blue reflectance and carbonate values. T.D. = total depth.

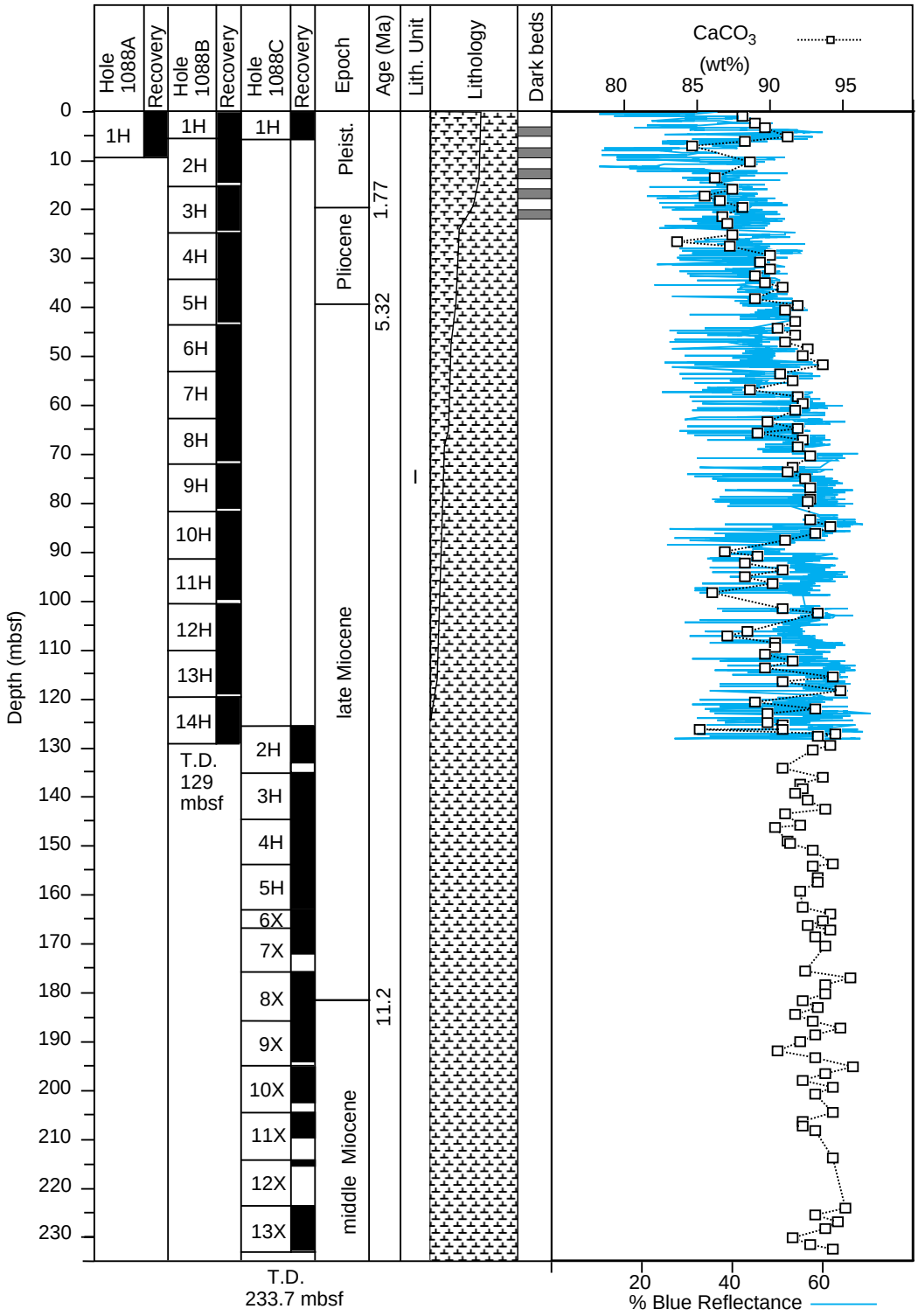

Figure F10. Smoothed (5-point average) GRA bulk density data for Site 1088. Holes 1088A (left curve), 1088B (middle curve), and 1088C (right curve) are horizontally offset from each other by a constant (0.15 g/cm³). Data from the top 5 cm of each core have been removed, as well as bulk density values <1 g/cm³ and >2.8 g/cm³.

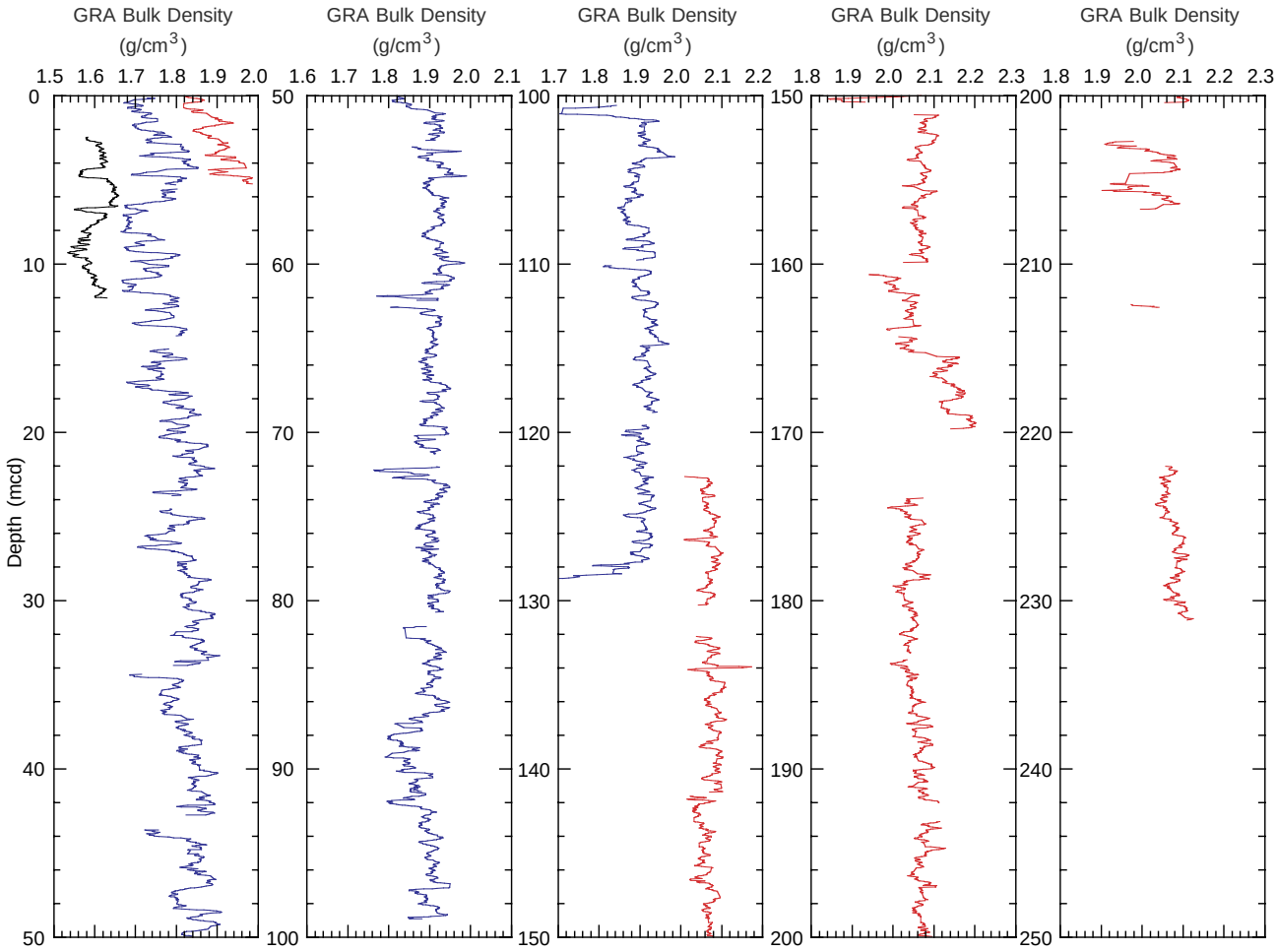

Figure F11. Smoothed (5-point average) color reflectance data (650–750 nm) for Site 1088. Holes 1088A (left curve), 1088B (middle curve), and 1088C (right curve) are horizontally offset from each other by a constant (15%). Data from the top 5 cm of each core have been removed.

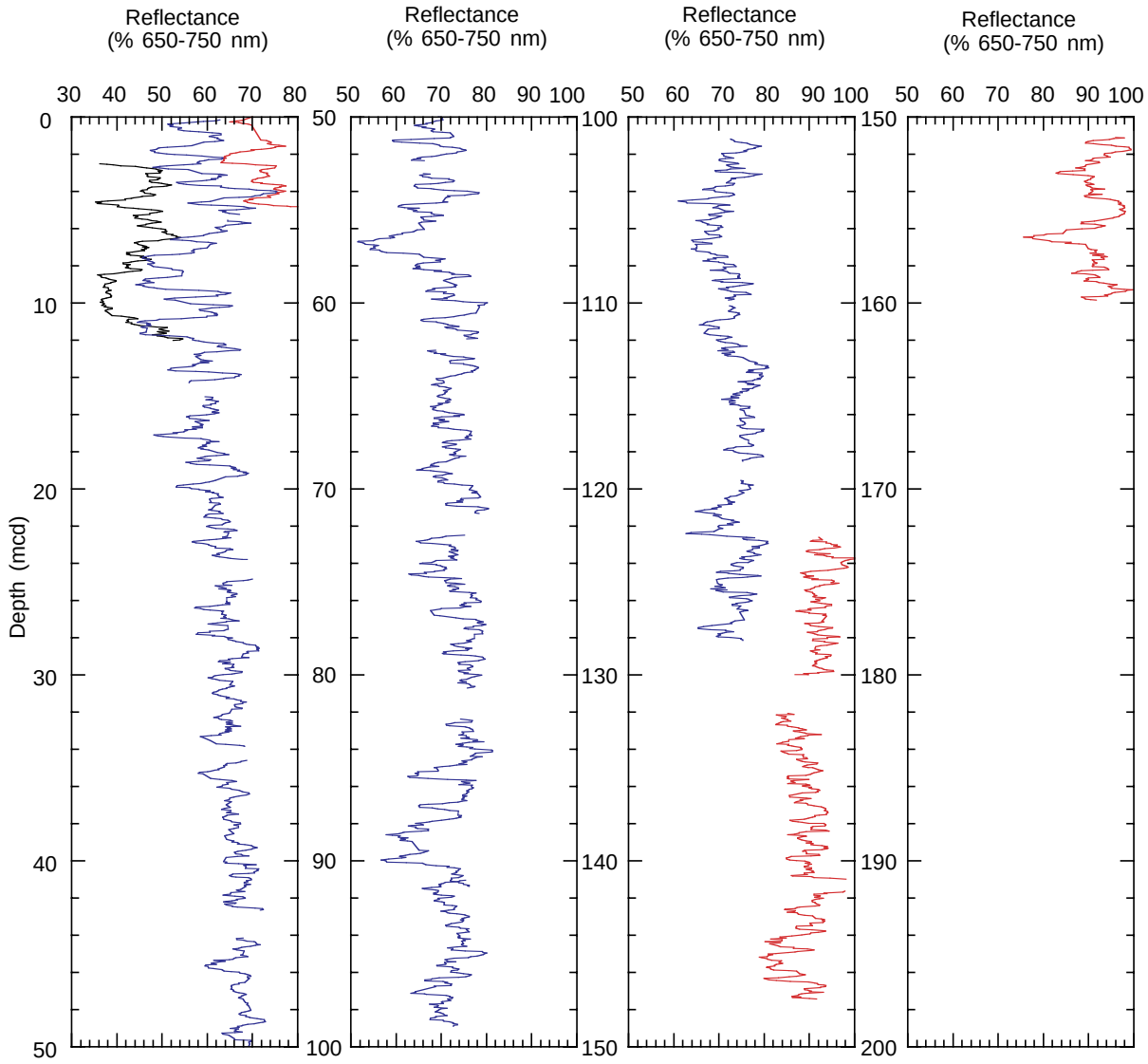

Figure F12. Smoothed (5-point average) magnetic susceptibility data for Site 1088. Holes 1088A (left curve), 1088B (middle curve), and 1088C (right curve) are horizontally offset from each other by a constant (2.0 × 10^{-5} SI units). Data from the top 5 cm of each section, as well as magnetic susceptibility values <–6.3 and >1.9 (× 10^{-5} relative SI units), have been removed. This culling process resulted in the removal of magnetic susceptibility data for Section 177-1088B-1H-2.

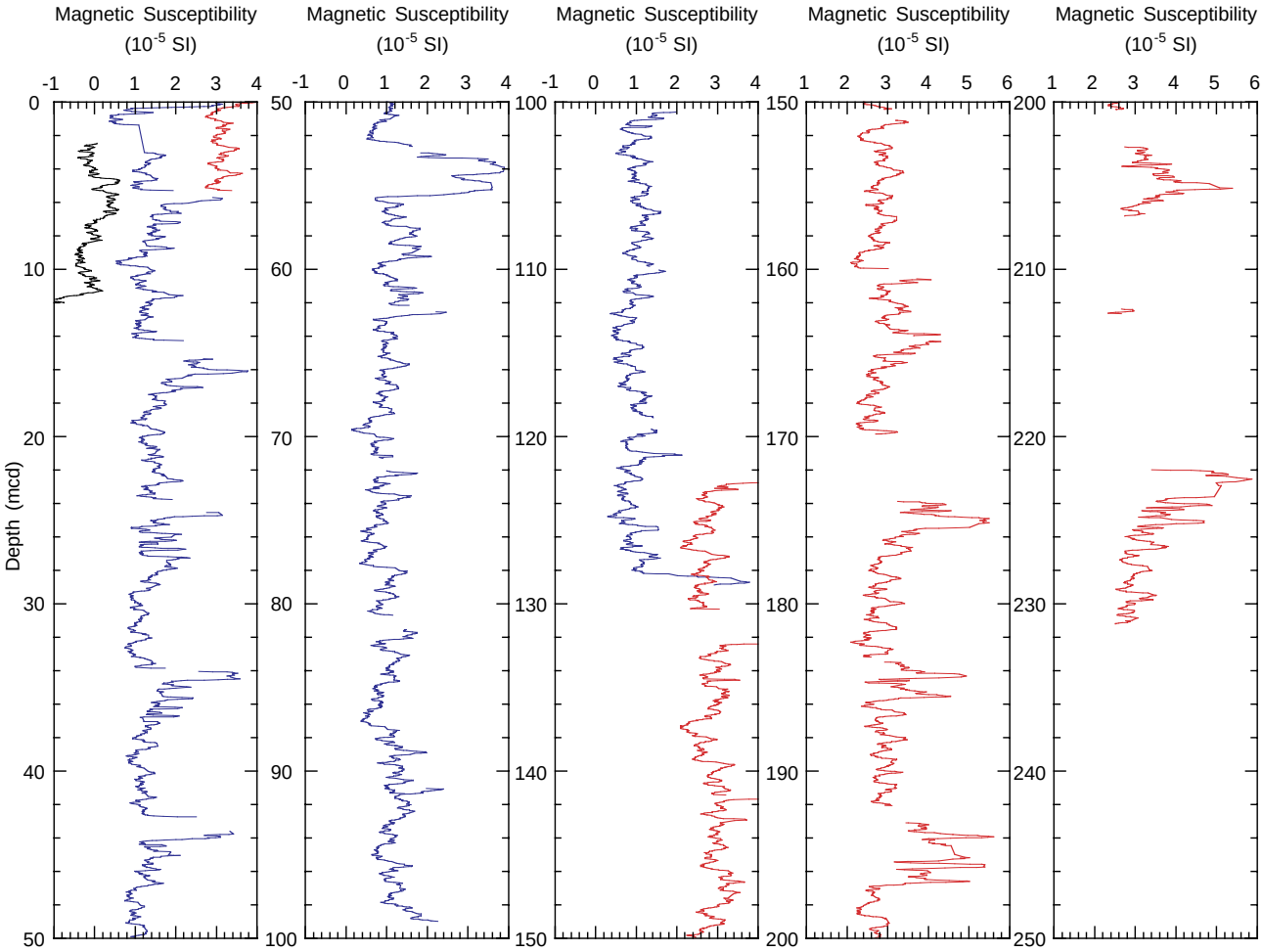

Figure F13. Age-depth plot of calcareous nannofossil and diatom datum events at Site 1088, using data from Holes 1088B and 1088C. Age-depth control points are based on 24 calcareous nannofossil datums and one diatom datum (Table T3, p. 45). The horizontal bars indicate the range of the diatom zones. Numbers refer to the following diatom zones: 1 = *T. insigna*, 2 = *F. reinholdii*, 3 = *D. dimorpha,* and 4 = *A. ingens* var. *nodus*. The solid lines indicate a visual best fit through the age-depth control points. Corresponding sedimentation rate averages are given in parentheses.

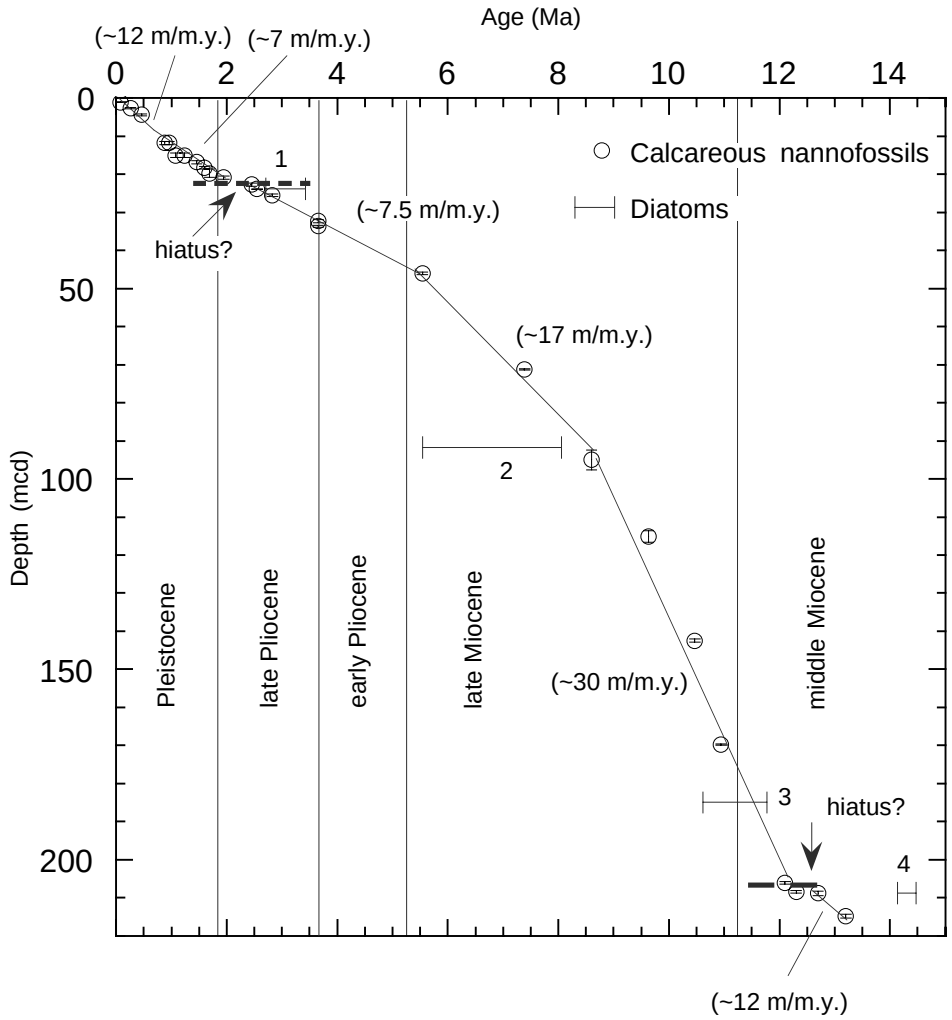

Figure F14. Biostratigraphic correlation chart and selected age designations for Site 1088.

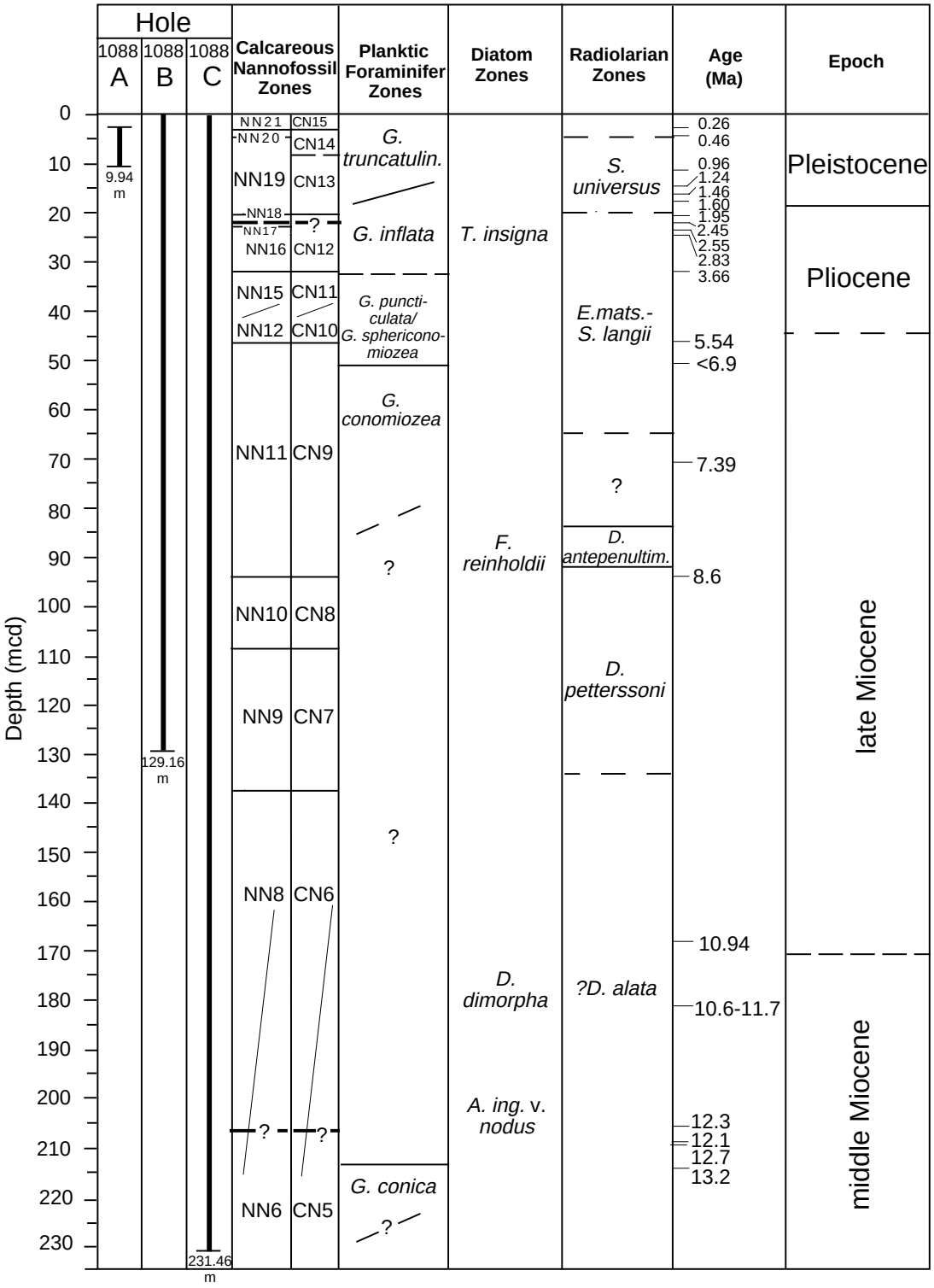

Figure F15. Histogram showing distribution of inclination values measured after demagnetization at peak fields of 25 mT, Holes 1088A–1088C.

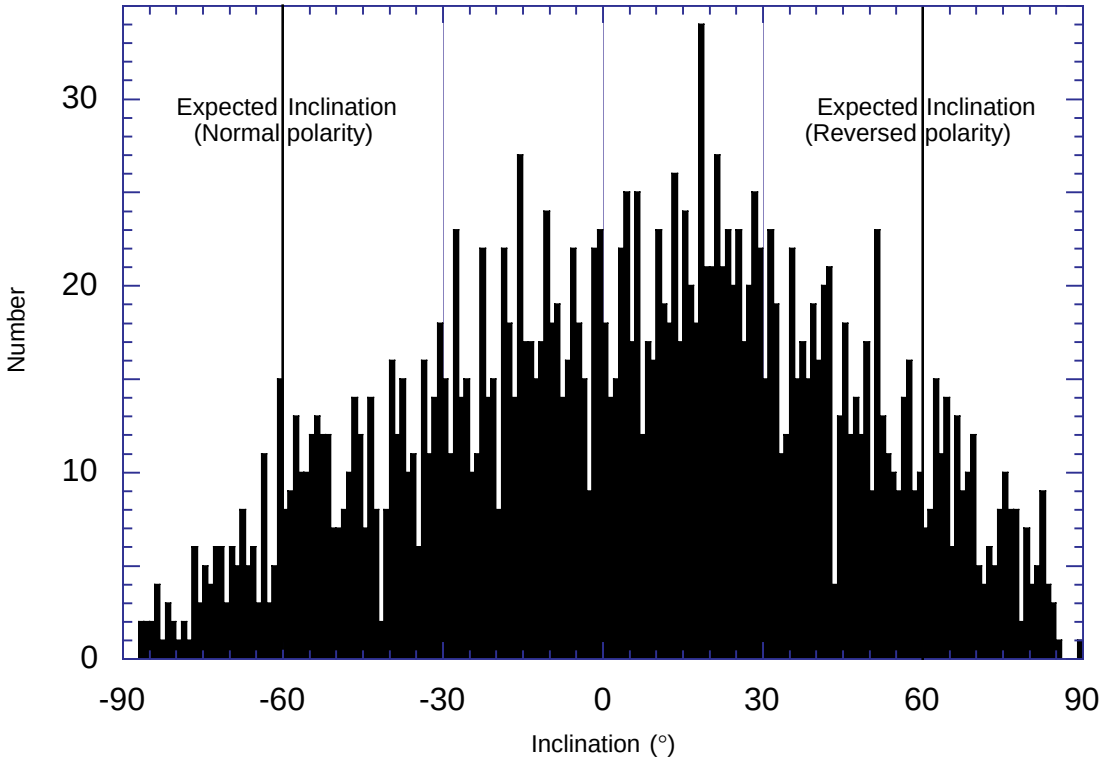

Figure F16. Concentration of methane vs. depth at Site 1088 obtained using the headspace technique. Data are reported in Table T10, p. 58.

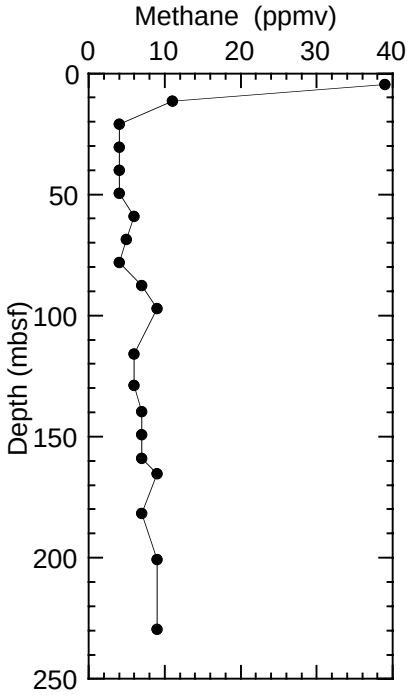

Figure F17. Interstitial water chemistry profiles vs. depth for salinity, chlorinity, alkalinity, pH, sodium, calcium, magnesium, potassium, strontium, lithium, ammonium, phosphate, silica, and sulfate at Site 1088. Data are reported in Table T11, p. 59.

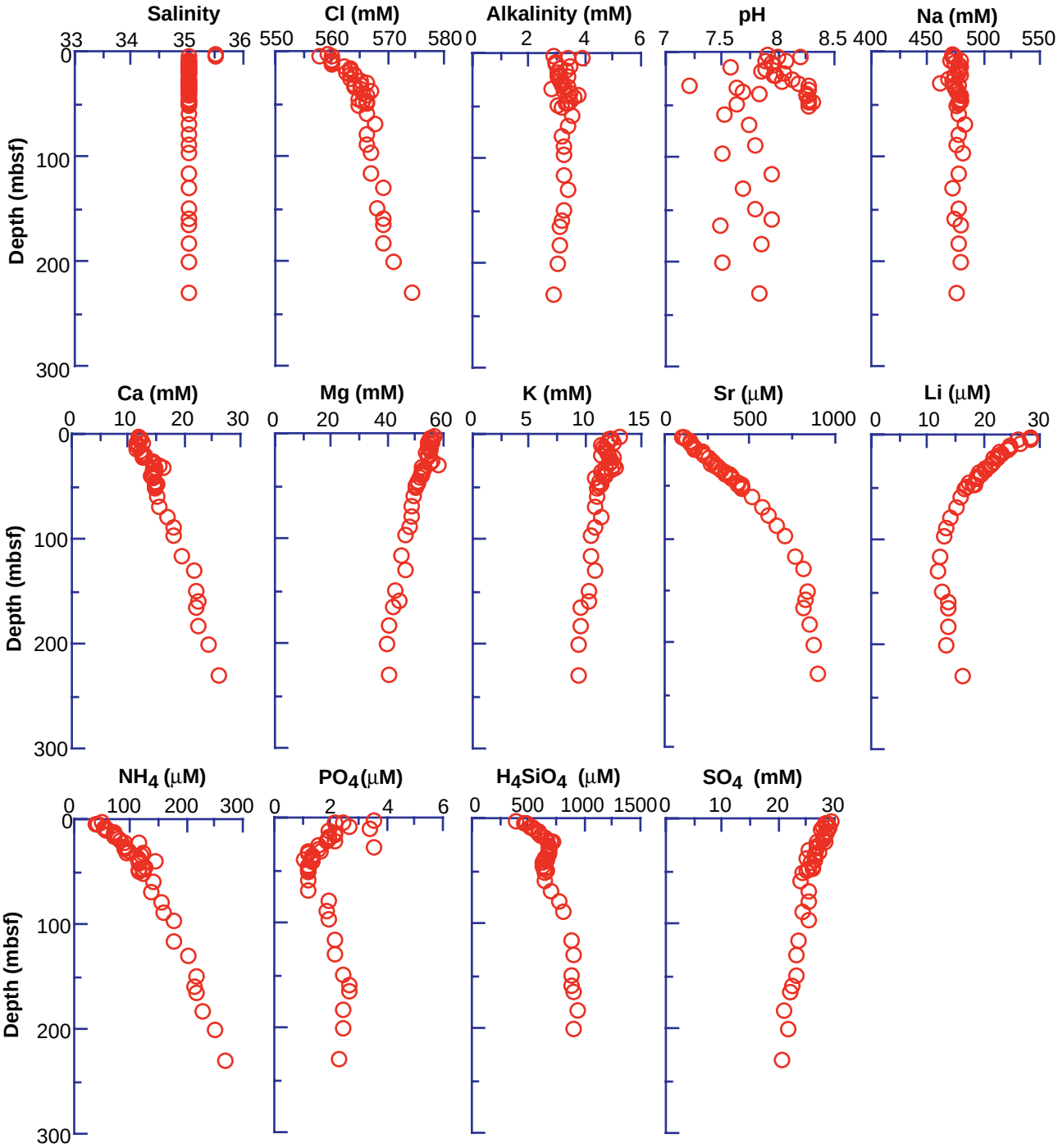

Figure F18. Interstitial water ammonium vs. sulfate at Site 1088 showing strong inverse correlation as a result of de-ammonification reactions during organic matter diagenesis via sulfate reduction; the correlation coefficient r = –0.94.

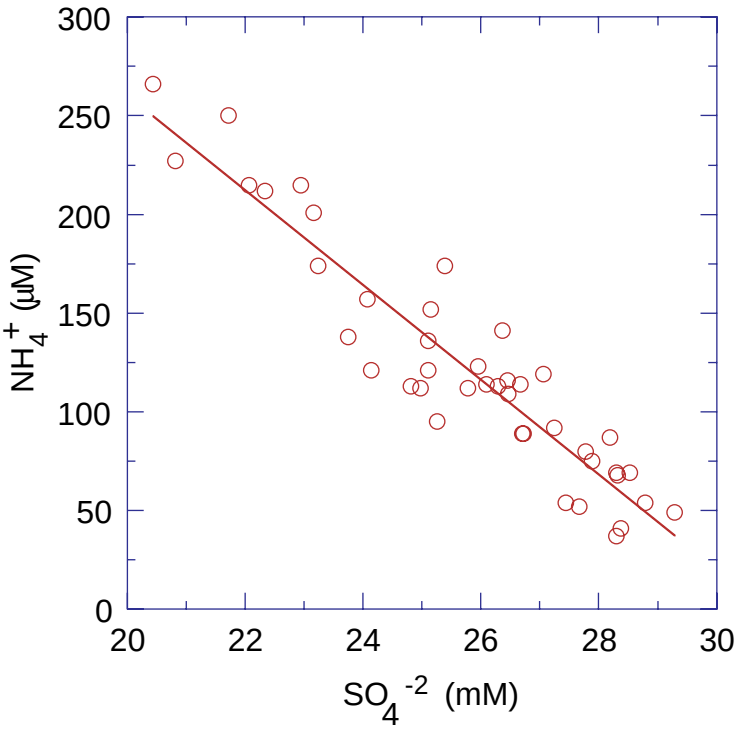

Figure F19. Concentration of calcium carbonate vs. depth at Site 1088. Data are reported in Table T12, p. 61.

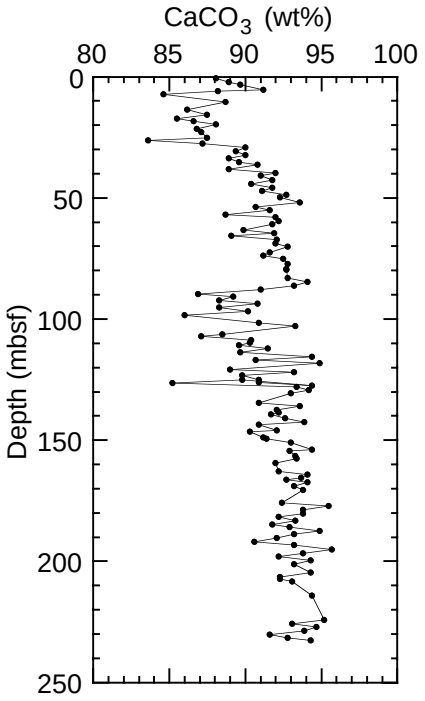

Figure F20. Site 1088 downhole variations of porosity (solid circles = MAD method) and OSU-SCAT resistivity (dots), *P*-wave velocities (dots = PWL; solid circles = PWS3), GRA bulk density (dots) and MAD bulk density (solid circles), volume-specific magnetic susceptibility, and NGR (line = data smoothed with a 10-point running average).

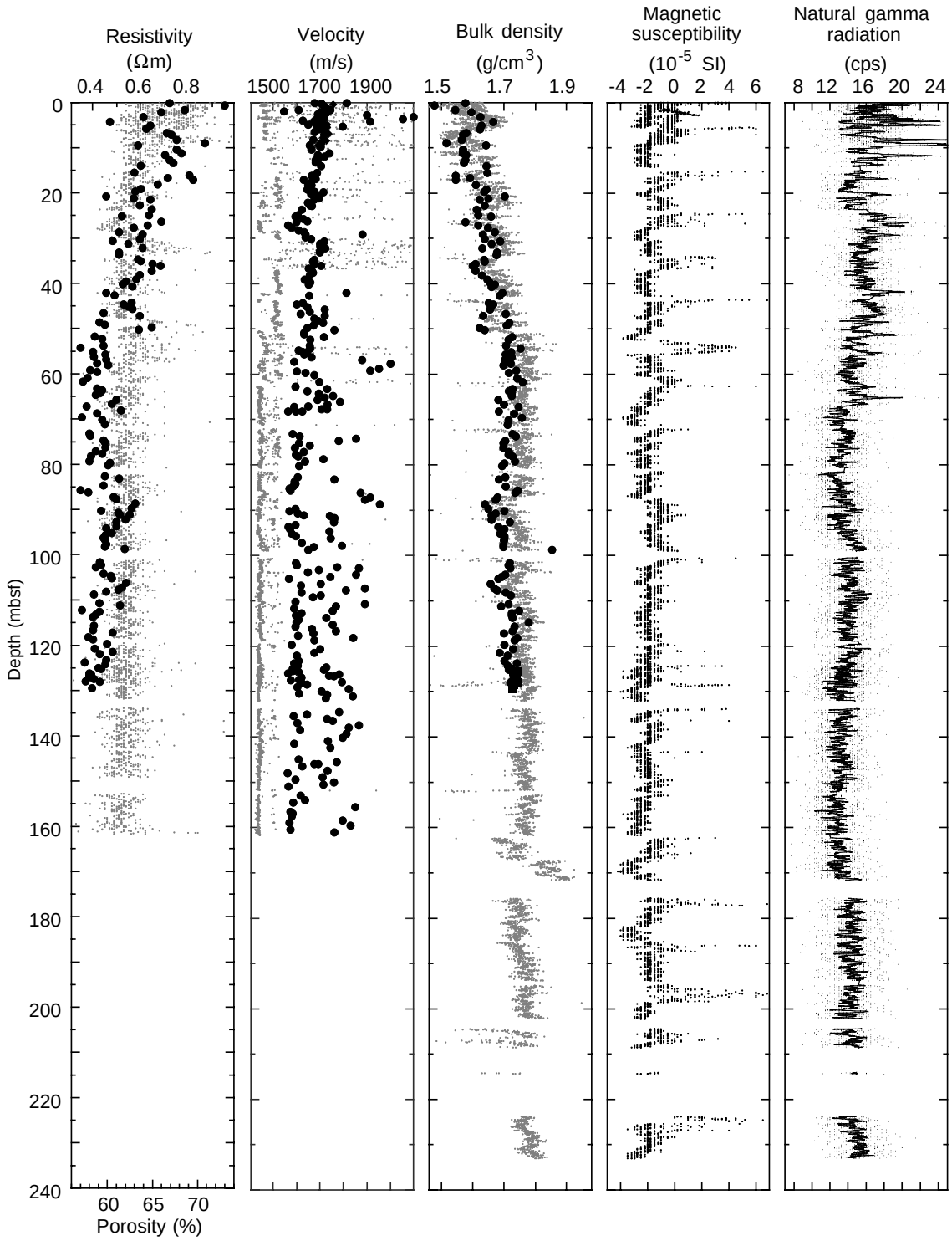

Figure F21. Relationship between GRA bulk density and MAD bulk density at Site 1088.

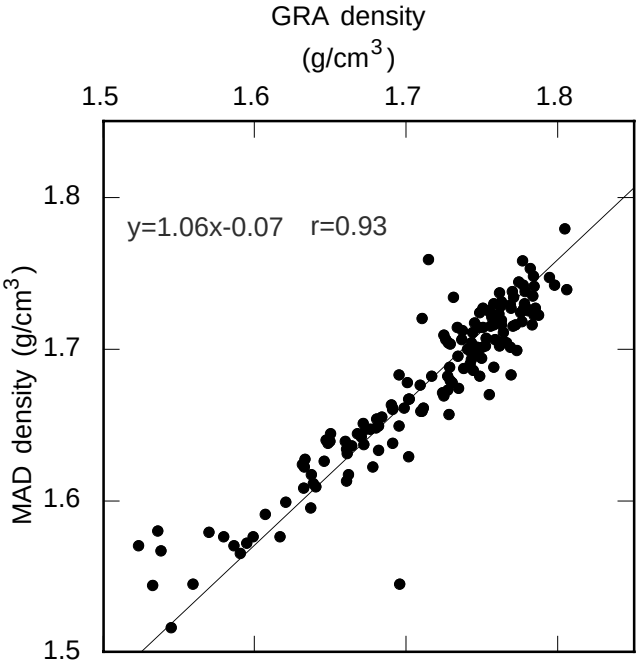

Figure F22. Comparison of downhole increases in grain density and carbonate content at Site 1088.

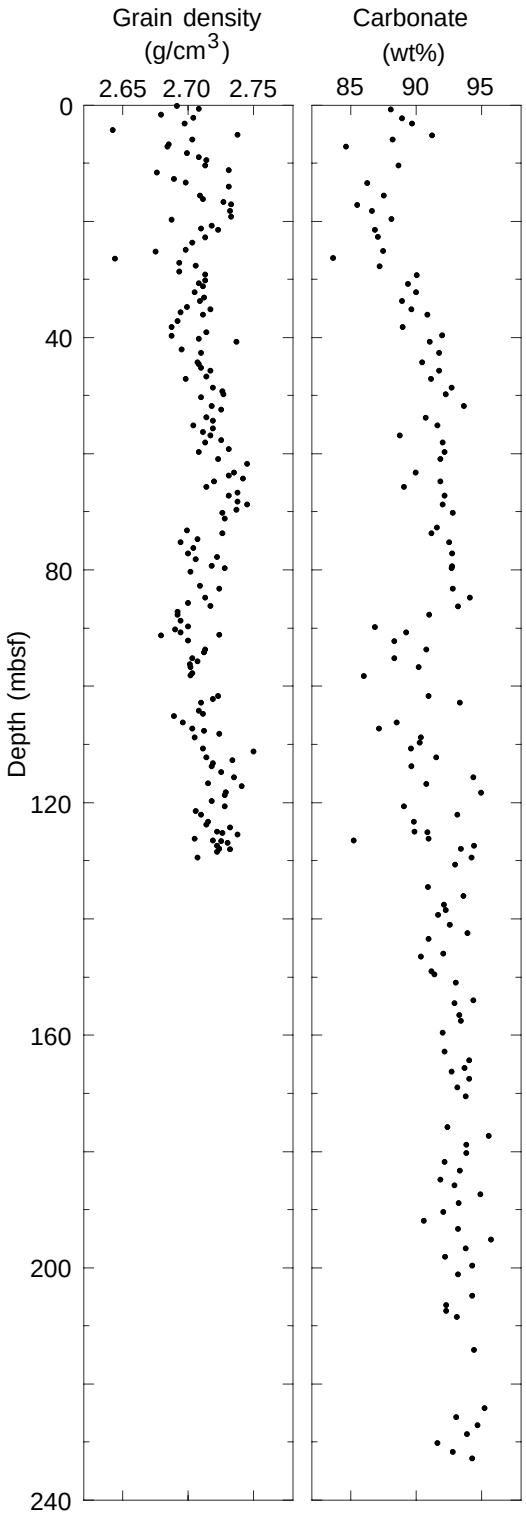

Figure F23. OSU-SCAT diffuse spectral reflectance compared to GRA density at Site 1088. Both GRA density and reflectance increase downhole in Holes 1088B and 1088C. Heavy lines = data smoothed with a 10-point running average; nIR = near infrared.

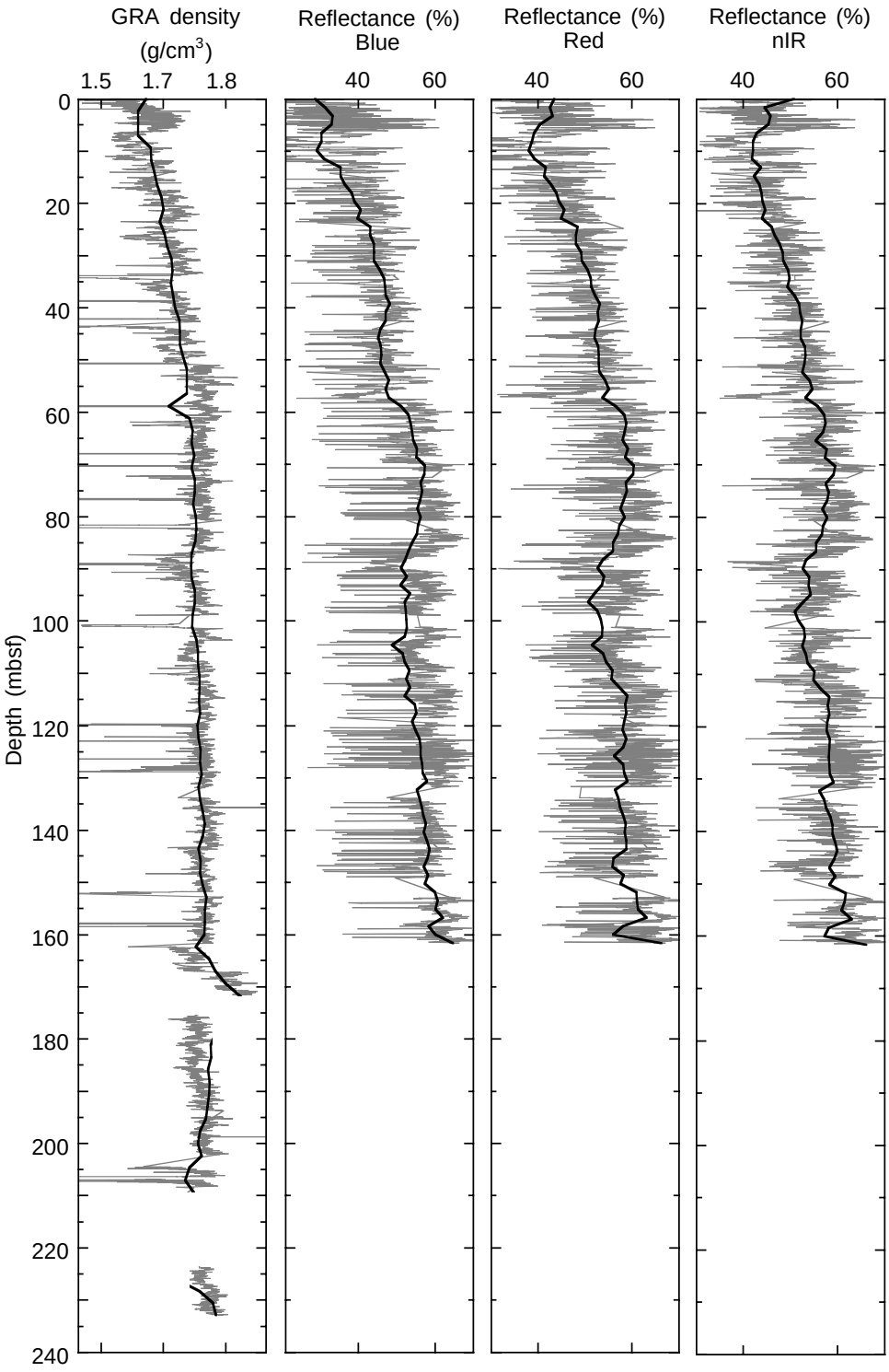

Figure F24. Diffuse spectral reflectance variations in the three 100-nm bands measured correlate well at Hole 1088A. nIR = near infrared.

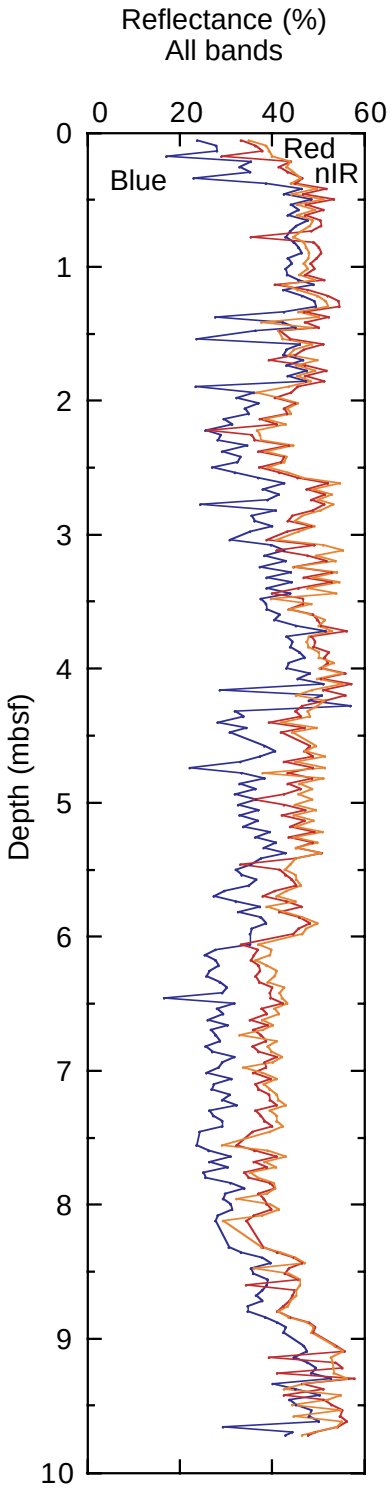

Figure F25. Thermal conductivity measurements of sediment cores at Site 1088. **A.** Frequency distribution of measured values. **B.** Correlation of measured values with interpolated GRA bulk density values. **C.** Thermal conductivity (solid circles) compared to interpolated GRA bulk density (open squares).

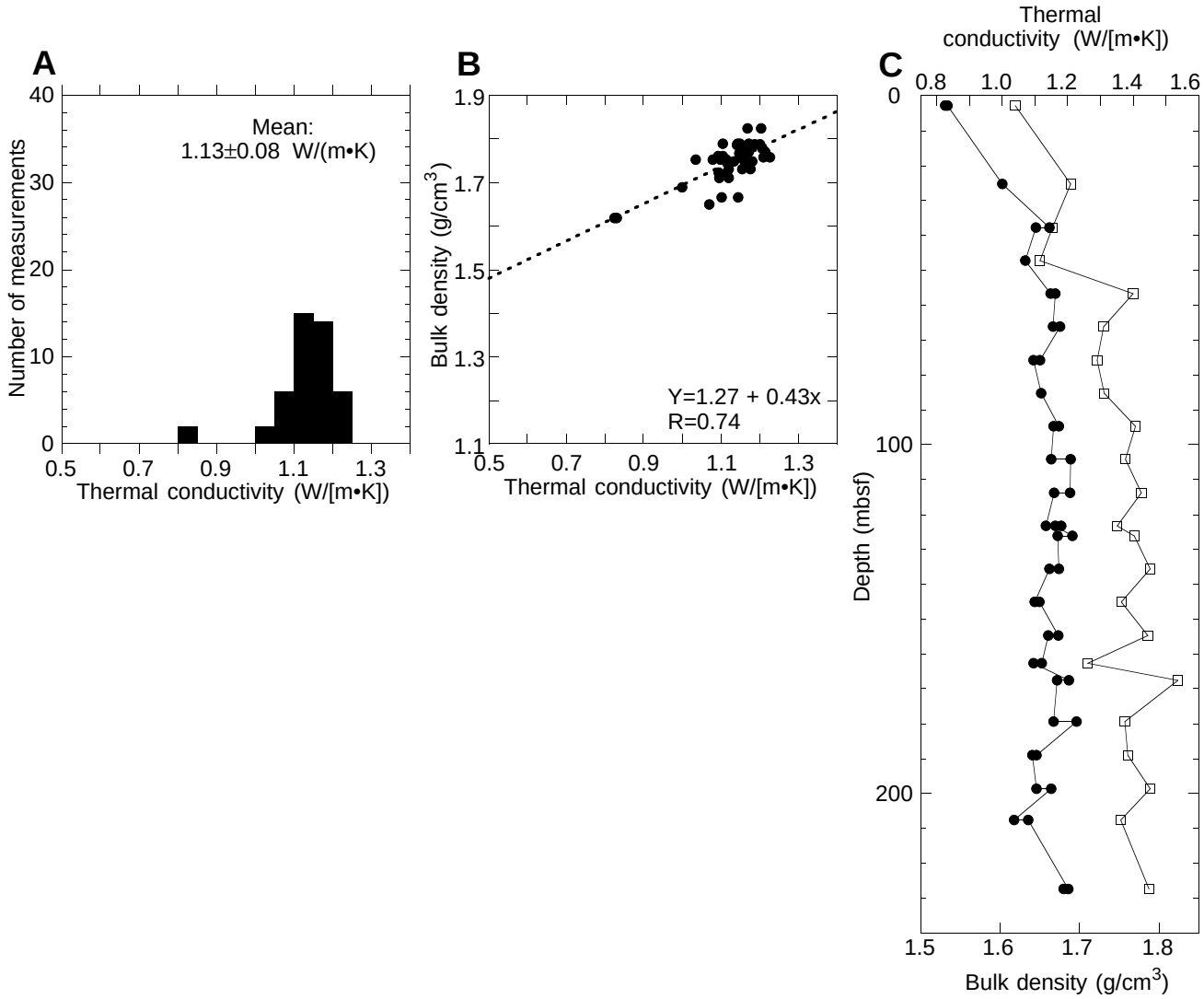

Figure F26. Downhole temperature measurements at Site 1088. The time-temperature record shown in each panel is ~1 hr. A bottom-water measurement was taken with the barrel of Core 177-1088A-1H before the core was shot. Sediment measurements were taken after the corresponding cores were shot.

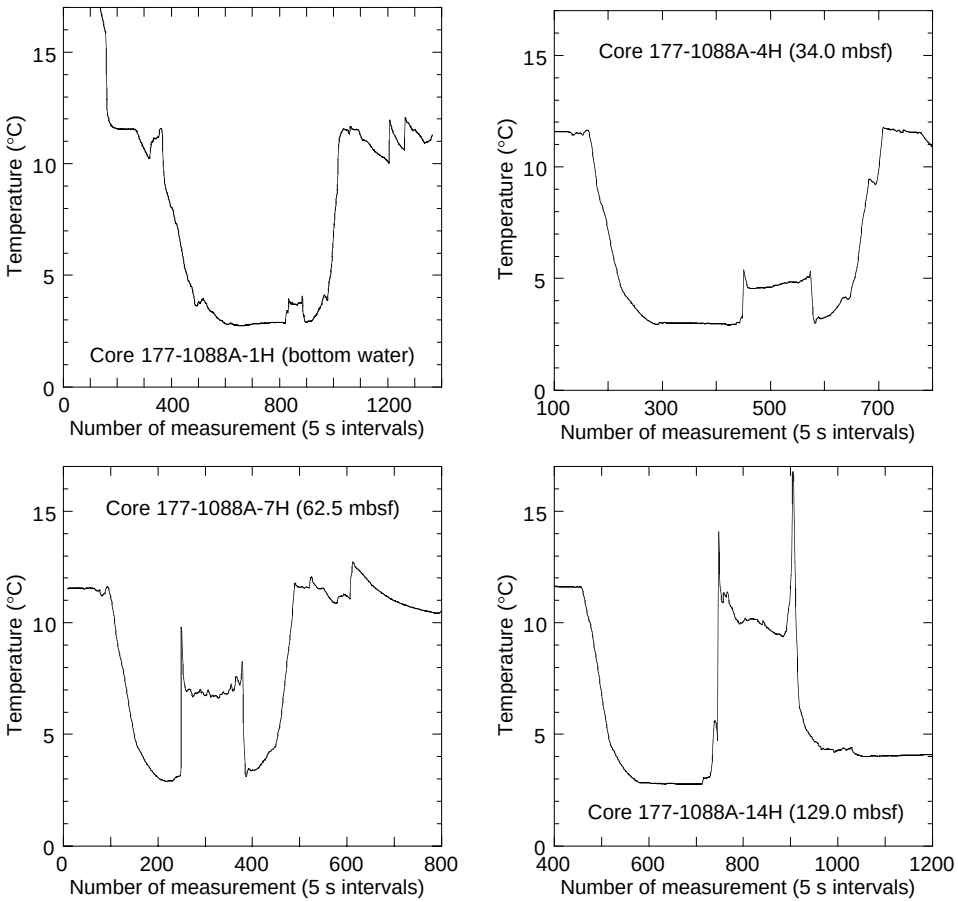

Table T1. X-ray diffraction data for Site 1088.

Core, section, interval (cm)	Depth (mbsf)	Depth (mcd)	Quartz/feldspar (XRD peak area ratio)	Clay/(quartz + feldspar) (XRD peak area ratio)	Opal carbonate-free fraction (wt%; XRD intensity)
177-1088B-					
1H-1, 142-144	1.43	1.43	5.04	0.21	9
1H-3, 44-47	3.46	3.455	3.48	0.21	10
1H-3, 99-101	4.00	4.00	4.37	0.20	14
2H-5, 15-17	11.66	11.66	3.21	0.13	7
3H-5, 45-47	21.46	21.46	2.34	0.15	0
4H-5, 77-79	31.28	31.28	2.96	0.18	12
5H-4, 98-100	39.49	39.49	3.41	0.20	10
6H-1, 73-75	44.24	44.24	3.00	0.29	11
7H-5, 62-64	59.63	59.63	3.04	0.24	13
8H-4, 22-24	67.23	67.23	2.07	0.24	17
9H-5, 23-25	78.24	78.24	2.79	0.24	18
10H-2, 123-125	84.24	84.24	2.33	0.26	21
11H-5, 115-117	98.16	98.16	2.20	0.21	13
13H-5, 76-78	116.72	116.72	1.96	0.30	14
177-1088C-					
2H-5, 46-48	128.91	128.91	2.05	0.30	20
5H-3, 72-74	154.67	154.67	1.69	0.28	23
8X-5, 10-12	181.71	181.71	1.55	0.27	18
9X-4, 70-72	190.41	190.41	2.08	0.33	11
11X-2, 48-50	206.39	206.39	1.69	0.29	15

Note: XRD = X-ray diffraction. This table is also available in ASCII format in the **TABLES** directory.

Table T2. Composite depths for Site 1088.

Core, section	Depth (mbsf)	Offset (m)	Depth (mcd)
177-1088A-			
1H-1	0.00	2.38	2.38
177-1088B-			
1H-1	0.00	0	0.00
2H-1	5.50	0	5.50
3H-1	15.00	0	15.00
3H-1	15.00	0	15.00
4H-1	24.50	0	24.50
5H-1	34.00	0	34.00
6H-1	43.50	0	43.50
7H-1	53.00	0	53.00
8H-1	62.50	0	62.50
9H-1	72.00	0	72.00
10H-1	81.50	0	81.50
11H-1	91.00	0	91.00
12H-1	100.50	0	100.50
13H-1	110.00	0	110.00
14H-1	119.50	0	119.50
177-1088C-			
1H-1	0.00	-0.3	-0.30
2H-1	124.30	-1.86	122.44
3H-1	133.80	-1.86	131.94
4H-1	143.30	-1.86	141.44
5H-1	152.80	-1.86	150.94
6X-1	162.30	-1.86	160.44
7X-1	166.00	-1.86	164.14
8X-1	175.60	-1.86	173.74
9X-1	185.20	-1.86	183.34
10X-1	194.80	-1.86	192.94
11X-1	204.40	-1.86	202.54
12X-1	214.10	-1.86	212.24
13X-1	223.70	-1.86	221.84

Note: This table is also available in ASCII format in the **TABLES** directory.

Table T3. Control points used to calculate sedimentation rates at Site 1088.

Code	Event/zone	Depth range of stratigraphic datums: Top Core, section, interval (cm)	Top Depth (mbsf)	Top Depth (mcd)	Base Core, section, interval (cm)	Base Depth (mbsf)	Base Depth (mcd)	Mean Depth (mbsf)	Mean Depth (mcd)	Age (Ma)	Sedimentation rate (m/m.y.)
		177-			177-						
CN	acme *E. huxleyi*	1088B-1H-1, 110-110	1.10	1.10	1088B-1H-1, 120-120	1.20	1.20	1.15	1.15	0.085	
CN	FO *E. huxleyi*	1088B-1H-2, 100-100	2.50	2.50	1088B-1H-2, 130-130	2.80	2.80	2.65	2.65	0.26	
CN	LO *lacunosa*	1088B-1H-3, 120-120	4.20	4.20	1088B-1H-4, 10-10	4.60	4.60	4.40	4.40	0.46	~12
CN	LO *R. asanoi*	1088B-2H-4, 140-140	11.40	11.40	1088B-2H-5, 70-70	12.20	12.20	11.80	11.80	0.88	
CN	RE *Gephyrocapsa* medium (4-5.5 µm)	1088B-2H-4, 140-140	11.40	11.40	1088B-2H-5, 70-70	12.20	12.20	11.80	11.80	0.96	
CN	FO *R. asanoi*	1088B-2H-CC, 12-19	14.44	14.44	1088B-3H-1, 70-70	15.70	15.70	15.07	15.07	1.08	
CN	FO *Gephyrocapsa* large (>5.5 µm)	1088B-2H-CC, 12-19	14.44	14.44	1088B-3H-1, 70-70	15.70	15.70	15.07	15.07	1.24	
CN	FO *Gephyrocapsa* large (>5.5 µm)	1088B-3H-1, 140-140	16.40	16.40	1088B-3H-2, 70-70	17.20	17.20	16.80	16.80	1.46	~7
CN	LO *C. macintyrei*	1088B-3H-2, 140-140	17.90	17.90	1088B-3H-3, 70-70	18.70	18.70	18.30	18.30	1.60	
CN	FO *Gephyrocapsa* medium (4-5.5 µm)	1088B-3H-3, 70-70	18.70	18.70	1088B-3H-4, 140-140	20.90	20.90	19.80	19.80	1.69	
CN	LO *D. brouweri*	1088B-3H-4, 70-70	20.20	20.20	1088B-3H-5, 70-70	21.70	21.70	20.95	20.95	1.95	
CN	LO *D. pentaradiatus*	1088B-3H-5, 140-140	22.40	22.40	1088B-3H-6, 70-70	23.20	23.20	22.80	22.80	2.45	
CN	LO *D. surculus*	1088B-3H-6, 130-130	23.80	23.80	1088B-3H-CC, 14-19	23.97	23.97	23.89	23.89	2.55	~8
DIAT	RAN *T. insigna* zonal range	1088B-3H-CC, 14-19	23.97	23.97	1088B-3H-CC, 14-19	23.97	23.97	23.97	23.97	2.6-3.3	
CN	LO *D. tamalis*	1088B-4H-1, 70-70	25.20	25.20	1088B-4H-1, 140-140	25.90	25.90	25.55	25.55	2.83	
CN	LO *Sphenolithus* spp.	1088B-4H-5, 140-140	31.90	31.90	1088B-4H-6, 70-70	32.70	32.70	32.30	32.30	3.66	
CN	LO *R. pseudoumbilicus*	1088B-4H-6, 140-140	33.40	33.40	1088B-4H-7, 40-40	33.90	33.90	33.65	33.65	3.66	
CN	LO *D. quinqueramus*	1088B-6H-2, 70-70	45.70	45.70	1088B-6H-2, 139-139	46.39	46.39	46.05	46.05	5.54	~17
CN	FO *Amaurolithus* spp.	1088B-8H-6, 130-130	71.20	71.20	1088B-8H-CC, 10-15	71.37	71.37	71.29	71.29	7.39	
DIAT	RAN *F. reinholdii* zonal range	1088B-10H-CC, 10-15	91.50	91.50	1088B-10H-CC, 10-15	91.50	91.50	91.50	91.50	5.6-8.1	
CN	FO *D. quinqueramus*	1088B-11H-4, 140-140	96.90	96.90	1088B-11H-5, 70-70	97.70	97.70	97.30	97.30	8.60	
CN	LO *D. hamatus*	1088B-13H-3, 70-70	113.70	113.70	1088B-13H-5, 70-70	116.70	116.70	115.20	115.20	9.63	~30
CN	FO *D. hamatus*	1088C-4H-1, 70-70	144.00	142.14	1088C-4H-1, 140-140	144.70	142.84	144.35	142.49	10.47	
CN	LO *C. miopelagicus*	1088C-7X-4, 140-140	171.57	169.71	1088C-7X-CC, 16-21	171.83	169.97	171.70	169.84	10.94	
DIAT	RAN *D. dimorpha* zonal range	1088C-8X-CC, 20-25	185.22	185.22	1088C-8X-CC, 20-25	185.22	185.22	185.22	185.22	10.6-11.7	~30
CN	LO *C. nitescens*	1088C-11X-1, 140-140	205.80	205.80	1088C-11X-2, 60-60	206.50	206.50	206.15	206.15	12.10	
CN	FO *C.macintyrei*	1088C-11X-3, 140-140	208.80	208.27	1088C-11X-CC, 72-77	209.37	209.37	209.09	208.82	12.30	
CN	LO *C. premacintyrei*	1088C-11X-3, 140-140	208.80	208.27	1088C-11X-CC, 72-77	209.37	209.37	209.09	208.82	12.70	
CN	LCO *C. floridanus*	1088C-12X-1, 20-20	214.30	214.30	1088C-12X-CC, 89-94	215.37	215.37	214.84	214.84	13.20	~12
DIAT	RAN *A. ing.* var. *nodus* zonal range	1088C-11X-CC, 72-77	209.37	209.37	1088C-11X-CC, 72-77	209.37	209.37	209.37	209.37	14.2-14.4	

Notes: Code abbreviations: CN = calcareous nannofossils, DIAT = diatom. Event abbreviations: FO = first occurrence, LO = last occurrence, RE = reentrance, RAN = total range. This table is also available in ASCII format in the **TABLES** directory.

Table T4. Summary of biostratigraphic age assignments for Holes 1088B and 1088C. (See table note. Continued on next page.)

Core, section, interval (cm)	Depth (mbsf)	Depth (mcd)	Calcareous nannofossil zone	Calcareous nannofossil age (Ma)	Diatom zone	Diatom age (Ma)	Radiolaria zones	Radiolaria age (Ma)	Planktic foraminifer zone	Planktic foraminifer age (Ma)
177-1088A-										
1H-CC, 15-20	9.89	12.27	NN19	<0.88						
177-1088B-										
1H-1, 110-110	1.10	1.10	NN21b	<0.085						
1H-1, 120-120	2.50	2.50	NN21a	>0.085						
1H-2, 100-100	2.50	2.50	NN21a	<0.26						
1H-2, 130-130	2.80	2.80	NN20	>0.26						
1H-3, 120-120	4.20	4.20	NN20	<0.46						
1H-4, 10-10	4.60	4.60	NN19	>0.46						
1H-CC, 7-12	5.41	5.41	NN19	0.46-0.88			*S. universus*	0.46-2.61		
2H-4, 140-140	11.40	11.40	NN19	<0.88						
2H-5, 70-70	12.20	12.20	NN19	>0.96						
2H-CC, 12-19	14.44	14.44	NN19	<1.08				<2.61	*G. truncatulinoides*	<2.0
3H-1, 70-70	15.70	15.70	NN19	>1.24						
3H-1, 140-140	16.40	16.40	NN19	<1.46						
3H-2, 70-70	17.20	17.20	NN19	>1.46						
3H-2, 140-140	17.91	17.91	NN19	<1.60						
3H-4, 70-70	20.20	20.20	NN19	<1.69						
3H-4, 140-140	20.90	20.90	NN19	>1.69						
3H-4, 140-140	20.90	20.90	NN19	<1.95						
3H-5, 70-70	21.70	21.70	NN18	>1.95						
3H-5, 140-140	22.40	22.40	NN18	<2.45						
3H-6, 70-70	23.20	23.20	NN17	>2.45						
3H-6, 130-130	23.80	23.80	NN17	<2.55						
3H-CC, 14-19	23.97	23.97	NN16	>2.55	*T. insigna*	2.6-3.3	*E. mats.-S. langii*	<6.79	*G. inflata*	
4H-1, 70-70	25.20	25.20	NN16	<2.83						
4H-1, 140-140	25.90	25.90	NN16	>2.83						
4H-5, 140-140	31.90	31.90	NN16	<3.66						
4H-6, 140-140	33.90	33.90		>3.66						
4H-CC, 13-18	34.08	34.08	Not identified	3.66-5.6			*E. mats.-S. langii*	<6.79	*G. inflata*	
5H-CC, 12-18	42.92	42.92		3.66-5.6			*E. mats.-S. langii*	<6.79		
6H-2, 70-70	45.70	45.70	NN12	<5.54						
6H-2, 139-139	46.40	46.40	NN11	>5.54						
6H-CC, 13-18	52.86	52.86	NN11	5.54-739			*E. mats.-S. langii*	<6.79	*G. conomiozea*	<6.9
7H-CC, 23-28	62.47	62.47	NN11	5.54-739			*E. mats.-S. langii*	<6.79		
8H-6, 130-130	71.30	71.30	NN11	<7.39						
8H-CC, 10-15	71.47	71.47	NN11	>7.39						
9H-CC, 9-14	80.83	80.83	NN11	7.39-8.6						
10H-CC, 10-15	91.50	91.50	NN11	7.39-8.6	*F. reinholdii*	5.6-8.1	*D. antepenultima*	7.7-11.53		
11H-4, 140-140	96.90	96.90	NN11	<8.6						
11H-5, 70-70	97.70	97.70	NN10	>8.6						
11H-CC, 9-14	99.16	99.16	NN10	8.6-9.63			*D. petterssoni*	10.8-12.5		
12H-CC, 9-14	110.05	110.01	NN10	8.6-9.63			*D. petterssoni*	10.8-12.5		

Table T4 (continued).

Core, section, interval (cm)	Depth (mbsf)	Depth (mcd)	Calcareous nannofossil zone	Calcareous nannofossil age (Ma)	Diatom zone	Diatom age (Ma)	Radiolaria zones	Radiolaria age (Ma)	Planktic foraminifer zone	Planktic foraminifer age (Ma)
13H-3, 70-70	113.70	113.70	NN10	<9.63						
13H-5, 70-70	116.70	116.70	NN9	>9.63						
13H-CC, 11-16	119.05	119.05	NN9	>9.63			*D. petterssoni*	10.8-12.5		
14H-CC, 12-17	129.11	129.11	NN9	>9.63			*D. petterssoni*	10.8-12.5		
177-1088C-										
1H-CC, 12-17	5.76	5.46	NN9	9.63-10.47					*G. truncatulinoides*	
2H-CC, 19-24	132.33	130.47	NN9	9.63-10.47			*D. petterssoni*	10.8-12.5		
3H-CC, 10-15	143.35	141.49	NN9	<10.47			? *D. alata*	? 12.5-15.25		
4H-1, 70-70	144.00	142.14	NN9	<10.47						
4H-1, 140-140	144.70	142.84	NN8?	>10.47						
4H-CC, 12-17	152.40	150.54	NN8?	10.47-10.94			? *D. alata*	? 12.5-15.25		
5H-CC, 12-17	162.13	160.27	NN7	10.47-10.94			? *D. alata*	? 12.5-15.25		
6X-CC, 11-16	165.94	164.08	NN7	10.94-12.1			? *D. alata*	? 12.5-15.25		
7X-4, 140-140	171.57	169.71	NN7	<10.94						
7X-CC, 16-21	171.83	169.97	NN7	>10.94			? *D. alata*	? 12.5-15.25		
7X-CC, 16-21	171.83	169.97	NN7	>10.94			? *D. alata*	? 12.5-15.25		
8X-CC, 20-25	185.22	185.22	NN7	10.94-12.1	*D. dimorpha*	10.6-11.7	? *D. alata*	? 12.5-15.25		
9X-CC, 15-20	194.06	194.06	NN7	10.94-12.1			? *D. alata*	? 12.5-15.25		
10X-CC, 18-23	202.48	202.48	NN7	10.94-12.1			? *D. alata*	? 12.5-15.25		
11X-1, 140-140	205.80	205.80	NN7	<12.1						
11X-2, 60-60	206.50	206.50	NN7?	>12.1						
11X-3, 140-140	208.27	208.27	NN6	<12.3						
11X-CC, 72-77	209.37	209.37	NN6	>12.7	*A. ing.* v. *nodus*	14.4-14.2	? *D. alata*	? 12.5-15.25		
12X-1, 20-20	214.30	214.30	NN6	<13.2						
12X-CC, 89-94	215.37	215.37	NN6	>13.2			? *D. alata*	? 12.5-15.25	*G. conica*	
13X-CC, 17-22	233.27	233.27	NN6	>13.2			? *D. alata*	? 12.5-15.25	*G. conica*	

Note: This table is also available in ASCII format in the **TABLES** directory.

Table T5. Distribution of main calcareous nannofossil species in Holes 1088B and 1088C. (**See table note.** Continued on next three pages.)

Core, section, interval (cm)	Depth (mbsf)	Depth (mcd)	Abundance	Preservation	*Coccolithus miopelagicus*	*Cyclicargolithus floridanus*	*Calcidiscus premacintyrei*	*Coronocyclus nitescens*	*Reticulofenstra pseudoumbilicus*	*Discoaster hamatus*	*Discoaster neohamatus*	*Calcidiscus macintyrei*	*Reticulofenstra pseudoumbilicus*	*Discoaster hamatus*	*Discoaster neohamatus*	*Discoaster bellus*	*Discoaster brouweri*	*Discoaster pentaradiatus*	*Discoaster quinqueramus*	*Discoaster tamalis*	*Gephyrocapsa small*	*Calcidiscus macintyrei*	*Gephyrocapsa caribbeanica*	*Pseudoemiliania lacunosa*	*Gephyrocapsa* medium (4-5.5 µm)	*Gephyrocapsa* large (>5.5 µm)	*Gephyrocapsa* sp. 3	*Reticulofenestra asanoi*	*Emiliania huxleyi*
177-1088B-																													
1H-1, 110-110	1.10	1.10	A	M																									D
1H-1, 120-120	1.20	1.20	A	M																									C
1H-2, 20-20	1.70	1.70	A	M																									C
1H-2, 60-60	2.10	2.10	A	M																									C
1H-2, 100-100	2.50	2.50	A	M																									C
1H-2, 130-130	2.80	2.80	A	M																			A						
1H-2, 140-140	2.90	2.90	A	M																			A						
1H-3, 120-120	4.20	4.20	A	M																			A						
1H-4, 10-10	4.60	4.60	A	M																			A	F					
1H-4, 25-25	4.75	4.75	A	M																			A	F					
1H-4, 40-40	4.90	4.90	A	M																			D	F					
1H-4, 70-70	5.20	5.20	A	M																			D	A					
1H-CC, 7-12	5.41	5.41	A	M																			A	C	C		C		
2H-1, 70-70	6.20	6.20	A	M																			D	C	C				
2H-1, 140-140	6.90	6.90	A	M																			F	C	C				
2H-2, 70-70	7.70	7.70	A	M																			F	C	C		C		
2H-2, 140-140	8.40	8.40	A	M																	D			C			C		
2H-3, 70-70	9.20	9.20	A	M																	D			C			C		
2H-3, 140-140	9.90	9.90	A	M																	A			C			C		
2H-4, 70-70	10.70	10.70	A	M																	D			C	C		F		
2H-4, 140-140	11.40	11.40	A	M																	F			C	F		F		
2H-5, 70-70	12.20	12.20	A	M																	A			F	F			F	
2H-5, 140-140	12.90	12.90	A	M																	D			C	F			A	
2H-6, 70-70	13.70	13.70	A	M																				C				F	
2H-CC, 12-19	14.44	14.44	A	M																	D			C				A	
3H-1, 70-70	15.70	15.70	A	M																				C		C			
3H-1, 140-140	16.40	16.40	A	M																				C		C			
3H-2, 70-70	17.20	17.20	A	M																				C					
3H-2, 140-140	17.90	17.90	A	M																		R		C	C				
3H-3, 70-70	18.70	18.70	A	M																		F		C	C				
3H-3, 140-140	19.40	19.40	A	M																		F			C				
3H-4, 70-70	20.20	20.20	A	M																		F		C	F				
3H-4, 140-140	20.90	20.90	A	M																		F		C					
3H-5, 70-70	21.70	21.70	A	M													C					R		C					
3H-5, 140-140	22.40	22.40	A	M													C					R		C					
3H-6, 70-70	23.20	23.20	A	M													F	F				F		C					
3H-6, 130-130	23.80	23.80	A	M													F	F				R		C					
3H-CC, 14-19	23.97	23.97	A	M													R	F				F		C					
4H-1, 70-70	25.20	25.20	A	G													R	C				R		C					
4H-1, 140-140	25.90	25.90	A	G													R	F		R		R							
4H-2, 70-70	26.70	26.70	A	G													F	F		R		R		C					
4H-2, 140-140	27.40	27.40	A	M													R	F		R		F		C					
4H-3, 70-70	28.20	28.20	A	G													R	F				F		F					
4H-3, 140-140	28.90	28.90	A	M														R		R		R		C					
4H-4, 70-70	29.70	29.70	A	G													F	C		R		F		C					
4H-4, 140-140	30.40	30.40	A	G													C	C		R		F		C					
4H-5, 70-70	31.20	31.20	A	M													F	C		R		R		C					
4H-5, 140-140	31.90	31.90	A	M													F	F		R		R		F					
4H-6, 70-70	32.70	32.70	A	G													F	F		R	D	F		C					
4H-6, 140-140	33.40	33.40	A	M													C	C		R	D			F					

Table T5 (continued).

Core, section, interval (cm)	Depth (mbsf)	Depth (mcd)	Abundance	Preservation	*Coccolithus miopelagicus*	*Cyclicargolithus floridanus*	*Calcidiscus premacintyrei*	*Coronocyclus nitescens*	*Reticulofenstra pseudoumbilicus*	*Discoaster hamatus*	*Discoaster neohamatus*	*Calcidiscus macintyrei*	*Reticulofenstra pseudoumbilicus*	*Discoaster hamatus*	*Discoaster neohamatus*	*Discoaster bellus*	*Discoaster brouweri*	*Discoaster pentaradiatus*	*Discoaster quinqueramus*	*Discoaster tamalis*	*Gephyrocapsa small*	*Calcidiscus macintyrei*	*Gephyrocapsa caribbeanica*	*Pseudoemiliania lacunosa*	*Gephyrocapsa* medium (4-5.5 µm)	*Gephyrocapsa* large (>5.5 µm)	*Gephyrocapsa* sp. 3	*Reticulofenestra asanoi*	*Emiliania huxleyi*
4H-7, 40-40	33.90	33.90	A	M									C				F	F		F	D	R		C					
4H-CC, 13-18	34.08	34.08	A	M									C				R	R		R	D			C					
5H-1, 70-70	34.70	34.70	A	G									C				R	R			D	F		F					
5H-1, 139-139	35.39	35.39	A	G									C				F	F		R	A	R		F					
5H-2, 70-70	36.20	36.20	A	M									C				R	F		R	A			C					
5H-2, 139-139	36.89	36.89	A	M									C				R	F			C	R		C					
5H-3, 70-70	37.70	37.70	A	M									F				R	F			C			R					
5H-3, 139-139	38.39	38.39	A	G									C				F	C			C	R		R					
5H-4, 70-70	39.20	39.20	A	M									A				R	R			A	F		R					
5H-4, 140-140	39.90	39.90	A	G									C				R	R											
5H-5, 68-68	40.68	40.68	A	M									C				R	R				R							
5H-5, 140-140	41.40	41.40	A	M									C				R	R											
5H-6, 70-70	42.20	42.20	A	M									F					R				F							
5H-CC, 12-18	42.92	42.92	A	G									C				R	R				C							
6H-2, 70-70	45.70	45.70	A	M									C				R	F				F							
6H-2, 139-139	46.39	46.39	A	M									A				R	R	R										
6H-3, 70-70	47.20	47.20	A	M									A									F							
6H-3, 139-139	47.89	47.89	A	M									C				R	C	R			R							
6H-4, 70-70	48.70	48.70	A	M									C					R											
6H-CC, 13-18	52.86	52.86	A	G									A					R				R							
7H-1, 140-140	54.40	54.40	A	M									A					R	R										
7H-2, 70-70	55.20	55.20	A	M									C				R	R	F			R							
7H-2, 140-140	55.90	55.90	A	M									C				R	R	R										
7H-3, 70-70	56.70	56.70	A	M									A				R	R	R			R							
7H-3, 140-140	57.40	57.40	A	M									A					R	R										
7H-4, 70-70	58.20	58.20	A	M									C				R	R	R			R							
7H-4, 137-137	58.87	58.87	A	M									A						R			F							
7H-5, 70-70	59.70	59.70	A	M									C			cf.			R										
7H-6, 70-70	61.20	61.20	A	M									C						R			F							
7H-7, 7-7	62.07	62.07	A	M									A						R			F							
7H-CC, 23-28	62.47	62.47	A	M									A					R	R										
8H-1, 140-140	63.90	63.90	A	M									C						R			F							
8H-3, 140-140	66.90	66.90	A	M									C				R												
8H-5, 140-140	69.90	69.90	A	M									C						R										
8H-6, 130-130	71.20	71.20	A	M									A									F							
8H-CC, 10-15	71.37	71.37	A	M									F						R			R							
9H-1, 140-140	73.40	73.40	A	M									C						R										
9H-4, 140-140	77.90	77.90	A	M									C						R			R							
9H-6, 120-120	80.70	80.70	A	M									C						R										
9H-CC, 9-14	80.83	80.83	A	G									C						R			R							
10H-3, 70-70	85.20	85.20	A	M									C						R										
10H-6, 70-70	89.70	89.70	A	M									C						R										
10H-CC, 10-15	91.50	91.50	A	M									C			R		R	R			R							
11H-1, 140-140	92.40	92.40	A	M									C			cf.			R			F							
11H-2, 70-70	93.20	93.20	A	M									C						R			F							
11H-2, 140-140	93.90	93.90	A	M									C						R										
11H-3, 70-70	94.70	94.70	A	M									C						R			F							
11H-4, 70-70	96.20	96.20	A	M									C		cf.		R		R										
11H-4, 140-140	96.90	96.90	A	M												R			R										
11H-5, 70-70	97.70	97.70	A	M									C									F							

Table T5 (continued).

Core, section, interval (cm)	Depth (mbsf)	Depth (mcd)	Abundance	Preservation	*Coccolithus miopelagicus*	*Cyclicargolithus floridanus*	*Calcidiscus premacintyrei*	*Coronocyclus nitescens*	*Reticulofenstra pseudoumbilicus*	*Discoaster hamatus*	*Discoaster neohamatus*	*Calcidiscus macintyrei*	*Reticulofenstra pseudoumbilicus*	*Discoaster hamatus*	*Discoaster neohamatus*	*Discoaster bellus*	*Discoaster brouweri*	*Discoaster pentaradiatus*	*Discoaster quinqueramus*	*Discoaster tamalis*	*Gephyrocapsa small*	*Calcidiscus macintyrei*	*Gephyrocapsa caribbeanica*	*Pseudoemiliania lacunosa*	*Gephyrocapsa* medium (4-5.5 µm)	*Gephyrocapsa* large (>5.5 µm)	*Gephyrocapsa* sp. 3	*Reticulofenestra asanoi*	*Emiliania huxleyi*
11H-6, 50-50	99.00	99.00	A	M									C				R	R				F							
11H-CC, 9-14	99.16	99.16	A	P									C		R			R				R							
12H-1, 70-70	101.20	101.20	A	M									C		cf.	R	R												
12H-2, 70-70	102.70	102.70	A	M									C				R					R							
12H-3, 70-70	104.20	104.20	A	M									C		R		R												
12H-3, 140-140	104.90	104.90	A	M									C									R							
12H-4, 70-70	105.70	105.70	A	M									A		R														
12H-7, 10-10	109.60	109.60	A	M										cf.		R						R							
12H-CC, 9-14	110.01	110.01	A	P									C		R	R													
13H-1, 70-70	110.70	110.70	A	M									C		R	R						R							
13H-3, 70-70	113.70	113.70	A	M									C		R														
13H-5, 70-70	116.70	116.70	A	M									C	F	R							F							
13H-4, 130-130	115.80	115.80	A	M									C	R	R							F							
13H-5, 140-140	117.40	117.40	A	M									C		R	cf.						F							
13H-6, 70-70	118.20	118.20	A	M									C	R															
13H-6, 140-140	118.90	118.90	A	M									C	R								F							
13H-CC, 11-16	119.05	119.05	A	M									F	R		cf.						R							
14H-1, 140-140	120.90	120.90	A	M									C	R															
14H-3, 70-70	123.20	123.20	A	M									F	R	R							F							
14H-4, 140-140	125.40	125.40	A	M									F	R								R							
14H-5, 140-140	126.90	126.90	A	M									F	R								F							
14H-6, 129-129	128.29	128.29	A	M									C	R															
14H-7, 65-65	128.95	128.95	A	M										R								R							
14H-CC, 12-17	129.11	129.11	A	M									C									R							
177-1088C-																													
2H-1, 40-40	124.70	122.84	A	M					F	F		F																	
2H-1, 70-70	125.00	123.14	A	M					R	R		F																	
2H-1, 140-140	125.70	123.84	A	M					C	R		F																	
2H-2, 70-70	126.50	124.64	A	M					C			R																	
2H-2, 140-140	127.20	125.34	A	M					F	F		F																	
2H-3, 70-70	128.00	126.14	A	M					C	R	R	R																	
2H-4, 140-140	130.20	128.34	A	M					C	R		C																	
2H-5, 70-70	131.00	129.14	A	M					F	R		F																	
2H-5, 140-140	131.70	129.84	A	M					C			C																	
2H-6, 15-15	131.95	130.09	A	M					F	R																			
2H-CC, 19-24	132.33	130.47	A	M					D	R	R	F																	
3H-CC, 10-15	143.35	141.49	A	M					D	R		C																	
4H-1, 70-70	144.00	142.14	A	M					D	R		R																	
4H-1, 140-140	144.70	142.84	A	M					C			F																	
4H-2, 70-70	145.50	143.64	A	M					A			R																	
4H-3, 70-70	147.00	145.14	A	M					C			C																	
4H-5, 70-70	150.00	148.14	A	M					A			R																	
4H-6, 140-140	152.20	150.34	A	M					C			R																	
4H-CC, 12-17	152.40	150.54	A	M					A			C																	
5H-2, 140-140	155.70	153.84	A	M					F			F																	
5H-3, 140-140	157.20	155.34	A	M					R			C																	
5H-CC, 12-17	162.13	160.27	A	M					C			R																	
6X-3, 10-10	165.40	163.54	A	M					C			F																	
6X-CC, 11-16	165.94	164.08	A	M					C			F																	
7X-2, 70-70	167.87	166.01	A	M					A			C																	

Table T5 (continued).

Core, section, interval (cm)	Depth (mbsf)	Depth (mcd)	Abundance	Preservation	*Coccolithus miopelagicus*	*Cyclicargolithus floridanus*	*Calcidiscus premacintyrei*	*Coronocyclus nitescens*	*Reticulofenstra pseudoumbilicus*	*Discoaster hamatus*	*Discoaster neohamatus*	*Calcidiscus macintyrei*	*Reticulofenstra pseudoumbilicus*	*Discoaster hamatus*	*Discoaster neohamatus*	*Discoaster bellus*	*Discoaster brouweri*	*Discoaster pentaradiatus*	*Discoaster quinqueramus*	*Discoaster tamalis*	*Gephyrocapsa small*	*Calcidiscus macintyrei*	*Gephyrocapsa caribbeanica*	*Pseudoemiliania lacunosa*	*Gephyrocapsa* medium (4-5.5 µm)	*Gephyrocapsa* large (>5.5 µm)	*Gephyrocapsa* sp. 3	*Reticulofenestra asanoi*	*Emiliania huxleyi*
7X-2, 140-140	168.57	166.71	A	M					A			R																	
7X-3, 70-70	169.37	167.51	A	M	R				F			R																	
7X-3, 140-140	170.07	168.21	A	M	R				R			F																	
7X-4, 70-70	170.87	169.01	A	M	R				F			R																	
7X-4, 140-140	171.57	169.71	A	M					C																				
7X-CC, 16-21	171.83	169.97	A	M	F				A			F																	
8X-1, 70-70	176.30	176.30	A	M	C				F			R																	
8X-1, 140-140	177.00	177.00	A	M	C				C																				
8X-2, 70-70	177.80	177.80	A	M	F				A			R																	
8X-2, 140-140	178.50	178.50	A	M	C				A			F																	
8X-3, 70-70	179.30	179.30	A	M	F				C			F																	
8X-6, 140-140	184.50	184.50	A	M	F				C																				
8X-CC, 20-25	185.22	185.22	A	M	F				C			F																	
9X-2, 140-140	188.10	188.10	A	M	F				C			R																	
9X-5, 140-140	192.60	192.60	A	M	F				C			R																	
9X-CC, 15-20	194.06	194.06	A	M	R				C			C																	
10X-1, 70-70	195.50	195.50	A	M	F				F			F																	
10X-2, 140-140	197.70	197.70	A	M	C				A			F																	
10X-4, 70-70	200.00	200.00	A	M	F				C			R																	
10X-5, 140-140	202.20	202.20	A	M	F				R			F																	
10X-CC, 18-23	202.48	202.48	A	M	R				A			F																	
11X-1, 140-140	205.80	205.80	A	M	F				C			R																	
11X-2, 60-60	206.50	206.50	A	M	F	R		C	C			R																	
11X-3, 70-70	207.57	207.57	A	M	R			F	F			R																	
11X-3, 140-140	208.27	208.27	A	M	F			F	F			R																	
11X-CC, 72-77	209.37	209.37	A	G	R		F		F																				
12X-1, 20-20	214.30	214.30	A	M	R		F	C	C																				
12X-CC, 89-94	215.37	215.37	A	G	R	C	C	C	F																				
13X-1, 70-70	224.40	224.40	A	M	F	C	C		A																				
13X-2, 70-70	225.90	225.90	A	M	R	F	A	C	A																				
13X-4, 70-70	228.90	228.90	A	M	F	C	A	C	A																				
13X-5, 70-70	230.40	230.40	A	M	F	F	A	C	A																				
13X-6, 70-70	231.90	231.90	A	M	C	C	F	C	C																				
13X-7, 20-20	232.90	232.90	A	M	F	F	F	F	C																				
13X-CC, 17-22	233.27	233.27	A	G	R	A	A	A																					

Notes: Abundance abbreviations: D = dominant, A = abundant, C = common, F = few, R = rare. Preservation abbreviations: G = good, M = moderate, P = poor. For more specific definitions, refer to **"Biostratigraphy,"** p. 10, in the "Explanatory Notes" chapter. This table is also available in ASCII format in the **TABLES** directory.

Table T6. Distribution of the main components of the planktic foraminifer assemblage in Holes 1088B and 1088C.

Core, section, interval (cm)	Depth (mbsf)	Depth (mcd)	Abundance	Preservation	*Dentoglobigerina altispira*	*Globigerina apertura*	*Globigerina bulloides*	*Globigerina decoraperta*	*Globigerina falconensis*	*Globigerina praebulloides*	*Globigerina quinqueloba*	*Globigerina woodi*	*Globigerinella aequilateralis*	*Globigerinella calida*	*Globigerinita glutinata*	*Globigerinita uvula*	*Globigerinoides conglobatus*	*Globigerinoides immaturus*	*Globigerinoides obliquus*	*Globigerinoides quadrilobatus*	*Globigerinoides ruber*	*Globigerinoides sacculifer*	*Globoquadrina dehiscens*	*Globorotalia conica*	*Globorotalia crassaformis*	*Globorotalia crassula*	*Globorotalia inflata*	*Globorotalia mayeri*	*Globorotalia menardii*	*Globorotalia miotumida*	*Globorotalia panda*	*Globorotalia puncticulata*	*Globorotalia puncticuloides*	*Globorotalia scitula*	*Globorotalia truncatulinoides*	*Neogloboquadrina acostaensis*	*Neogloboquadrina continuosa*	*Neogloboquadrina humerosa*	*Neogloboquadrina mayeri*	*Neogloboquadrina pachyderma* (sinistral)	*Neogloboquadrina pachyderma* (dextral)	*Orbulina bilobata*	*Orbulina universa*	*Sphaeroidinellopsis seminulina*
177-1088B-																																											
1H-CC, 7-12	5.41	5.41	A	G			D				F				A										A	A	A						R	F			F			F		R		
2H-CC, 12-19	14.44	14.44	A	M			D				A				A										A	A	A					A		F									
3H-CC, 14-19	23.97	23.97	A	M			A							F	A							R			A	A	A					A							D			R	
4H-CC, 13-18	34.08	34.08	A	G			D				D			R	A		R	R							A	F	F		R		A	A	R						C	A		R	
5H-CC, 12-18	42.92	42.92	A	G			D		R		A				A	F			R			R				A	F			R		A	A	F		F				A			F	
6H-CC, 13-18	52.86	52.86	A	M		F	D	F			A	A			A					R					A	A				A			A	A		F				A			F	
7H-CC, 23-28	62.47	62.47	A	M		F	D				F	A														F				A				A		F				A			R	
8H-CC, 10-15	71.47	71.37	A	M		F	D					F			F															A	F			A						A	F		R	
9H-CC, 9-14	80.83	80.83	A	M		A	D					A																		A	F			A						A		R	F	R
10H-CC, 10-15	91.50	91.50	A	P		A	D								A							R								D	A									F			R	
11H-CC, 9-14	99.16	99.16	A	M			D				A	A			A															D	F						F			A			F	
12H-CC, 9-14	110.05	110.01	A	M			D			A					A															A				A		R		F		A			F	
13H-CC, 11-16	119.05	119.05	A	M		F	D			F	A				A															A	F							F					R	
14H-CC, 12-17	129.11	129.11	A	M	P	A	D	F		A												R	R					A		A													
177-1088C-																																													
1H-CC, 12-17	5.76	5.46	A	G			D						R		R						R						A						A				R			A			F	
2H-CC, 19-24	132.33	130.47	A	M			D			A	A				A								A				F	F	R	A	F			F				A			A			
3H-CC, 10-15	143.35	141.49	A	M		R	D			A	A				R							R								F	F			A									R	
4H-CC, 12-17	152.40	150.54	A	M			A				A				A								R					A		D	F												R	
5H-CC, 12-17	162.13	160.27	A	M			A			A																		D		A	A													
6X-CC, 11-16	165.94	164.08	A	M			A	A																	A			D		F				A									F	
7X-CC, 16-21	171.83	169.97	A	M			F								F								R					A	F	A						R							
8X-CC, 20-25	185.22	185.22	A	M			A			F					A							R						D		A	A													
9X-CC, 15-20	194.06	194.06	A	M			D								A													D		A	A													
10X-CC, 18-23	202.48	202.48	A	M			A			F					A													D			A												F	
11X-CC, 72-77	209.37	209.37	A	M			D					F			A													F		A	A													
12X-CC, 89-94	215.37	215.37	A	M			A			F														A				A															F	
13X-CC, 17-22	233.27	233.27	A	M		F	A	F		F	F				R									A				A		D													

Notes: Abundance abbreviations: D = dominant, A = abundant, C = common, F = few, R = rare, P = present. Preservation abbreviations: G = good, M = moderate, P = poor. For more specific definitions, refer to **"Biostratigraphy,"** p. 10, in the "Explanatory Notes" chapter. This table is also available in ASCII format in the **TABLES** directory.

Table T7. Distribution of benthic foraminifers at Site 1088. (Continued on next page.)

Core, section, interval (cm)	Depth (mbsf)	Depth (mcd)	Abundance	Preservation	*Alabaminella weddelensis*	*Anomalinoides alazanensis*	*Bolivina* spp.	*Bulimina alazanensis*	*Bulimina exilis*	*Bulimina striata*	*Cassidulina laevigata*	*Cassidulina obtusa*	*Cassidulina reniforme*	*Cassidulinoides* spp.	*Chilostomella oolina*	*Cibicidoides mundulus*	*Cibicidoides* spp.	*Cibicidoides wuellerstorfi*	*Dentalina* sp.	*Eggerella bradyi*	*Ehrenbergina* sp.	*Epistominella exigua*	*Fissurina* spp.	*Francesita* sp.	*Globobulimina* sp.	*Globocassidulina subglobosa*	*Gyroidinoides soldanii*	*Gyroidinoides* spp.	*Islandiella* sp.	*Karreriella bradyi*	*Lagena* spp.	*Laticarinina pauperata*	*Lenticulina* sp.	*Martinotiella nodulosa*	*Melonis barleeanum*	*Melonis pompiliodes*	*Nodosaria* spp.	*Nonionella* sp.	*Oolina* spp.	*Oridorsalis* sp.	*Oridorsalis umbonatus*	*Parafissurina* sp.	*Plectofrondicularia* sp.	*Pleurostomella* sp.
177-1088B-																																												
1H-CC, 7-12	5.41	5.41	C	G				1			5		1							2		9	3			2	1	1	3		2									2				
2H-CC, 12-19	14.44	14.44	C	G							6					1		2		4			2			4			2	2				2		2				2				
3H-CC, 14-19	23.97	23.97	C	G			1	1							1								2			2	1	1	3	6	1					6		1		3		1		
4H-CC, 13-18	34.08	34.08	C	G			2									1				2	1	2					2			1		1		1		1								
5H-CC, 12-18	42.92	42.92	C	G			1									6				1	1	1	5				2		4	1	2	2	2			1				1		1	2	
6H-CC, 13-18	52.86	52.86	C	G			4	1															3				6		9		1	1			1		2				3	4	
7H-CC, 23-28	62.47	62.47	C	G			3	3		1						11					1	4	4	8			3	6	10		2									4	1		2	
8H-CC, 10-15	71.47	71.47	C	G			7	3					1			12	1			4			2	1			3	1	12	4	1	3			5		1				4		2	
9H-CC, 9-14	80.83	80.83	C	G			4	2								4	1			2		1					4		8	1	1	6					2		2				2	
10H-CC, 10-15	91.5	91.5	C	M			6	3												2			4				5		1	1	1	4							1				2	
11H-CC, 9-14	99.16	99.16	C	M			5									6	4			2		1	1					2	19	4		4			4					7			1	
12H-CC, 9-14	110.05	110.05	C	M					1											1		1	4		2		1		1			2			1		1	1		1	1			1	
13H-CC, 11-16	119.05	119.05	C	M			1									2	3					3	2	1			2		6	5	1	2			3		2			2			2	
14H-CC, 12-17	129.11	129.11	C	P			4													1		3	3				5		8		1	6			2		1			4			1	
177-1088C-																																												
1H-CC, 12-17	5.76	5.46	F	M	1		1											1		2		1					1		3					1				1						
2H-CC, 19-24	132.33	130.47	F	M			6						1			1						1	7				2		5	1	1	1		1					1				
3H-CC, 10-15	143.35	141.49	F	M			2	1								1						5	3	2			6		1	1		1		1			1					1	
4H-CC, 12-17	152.4	150.54	C	M	10		1							1		6				2		25	1				9		12					12	1		1		1	6			2	
5H-CC, 12-17	162.13	160.27	C	M	6		3									9	5			3		31	5				14		6	1	2	2			5				1	2	1		2	
6X-CC, 11-16	165.94	164.08	C	M	1					1						14	1	1		3		7	3				13		12	3	7	4			6					6			2	
7X-CC, 16-21	171.83	169.97	C	M			1	1				1				33	10			6		2	5				10		25	4		3			5			1	3	7			1	
8X-CC, 20-25	185.22	185.22	C	M		2				10		1		2			1		2	7	1	16	7	2			9		1	7	3			1	9					11			7	
9X-CC, 15-20	194.06	194.06	C	P			2			3				1		9		2		5		14	3				4		4		2		1					1		3				
10X-CC, 18-23	202.48	202.48	C	M			15									14	1	4		4		15	4	2			12		5			3			1					3				5
11X-CC, 72-77	209.37	209.37	C	M			9									38		2		1		5	2	3			13		2	2		1	1		2			1		5				
12X-CC, 89-94	215.37	215.37	C	M			2									6		9		2		2	3	2			6		3	1		1			1					2				
13X-CC, 17-22	233.27	233.27	F	P			22	1					1			15	1			1		4	4				5		2	2													1	

Notes: Abundance abbreviations: C = common, F = few. Preservation abbreviations: G = good, M = moderate, P = poor. For more specific definitions, refer to **"Biostratigraphy,"** p. 10, in the "Explanatory Notes" chapter. This table is also available in ASCII format in the **TABLES** directory.

Table T7 (continued).

Core, section, interval (cm)	Depth (mbsf)	Depth (mcd)	Abundance	Preservation	*Oridorsalis* sp.	*Oridorsalis umbonatus*	*Parafissurina* sp.	*Plectofrondicularia* sp.	*Pleurostomella* sp.	*Polymorphinid* spp.	*Pullenia bulloides*	*Pullenia* cf. *simplex*	*Pullenia quinqueloba*	*Pullenia subcarinata*	*Pyrgo lucernula*	*Pyrgo murrhina*	*Pyrgo* spp.	*Quinqueloculina* sp.	*Rectouvigerina multicostata*	*Sigmoilopsis schlumbergi*	*Siphotextularia* sp.	*Sphaeroidina bulloides*	*Spiroloculina* sp.	*Spirophthalmidium* sp.	*Stainforthia fusiformis*	*Stainforthia* sp.	*Stilostomella lepidula*	*Stilostomella subspinosa*	*Trifarina angulosa*	*Triloculina trihedra*	*Uvigerina hispidicostata*	*Uvigerina peregrina*	*Uvigerina proboscidea*	Indeterminates (agg.)	Indeterminates (calc.)	Sample sum	Number of species	Abundance (specimens/cm^3)
177-1088B-																																						
1H-CC, 7-12	5.41	5.41	C	G		2								1			1												2					1	36	18	203.5
2H-CC, 12-19	14.44	14.44	C	G							4	1		1		4	1			1		1				1	2		1					1	44	21	225.0
3H-CC, 14-19	23.97	23.97	C	G		3		1			8			3		6						1					2				7			1	3	56	24	330.0
4H-CC, 13-18	34.08	34.08	C	G												1	2	1									1				2	2	1	1	2	24	22	109.4
5H-CC, 12-18	42.92	42.92	C	G		1		1	2		5				1	2		2						1			2			1	6		1	3	1	54	32	246.5
6H-CC, 13-18	52.86	52.86	C	G		2		3	4							3		3					1	2			1				6			3	54	23	159.6
7H-CC, 23-28	62.47	62.47	C	G		4	1		2		1		1	2		11		2		3		1					17		8		5	1		1	12	115	33	172.8
8H-CC, 10-15	71.47	71.47	C	G		4			2	1	3		2			2		1				1		5		1	12		3		20			3	10	118	39	157.2
9H-CC, 9-14	80.83	80.83	C	G					2					1	1	1			3	5				2			4	1	2		5			1		65	28	79.2
10H-CC, 10-15	91.5	91.5	C	M		1			2		4									2				2			5				1	2	2		6	48	23	89.1
11H-CC, 9-14	99.16	99.16	C	M		7			1		1					2				3				1			3				4				9	74	25	124.5
12H-CC, 9-14	110.05	110.05	C	M	1	1			1		1													1		1	12	14			2	4			2	54	24	28.0
13H-CC, 11-16	119.05	119.05	C	M		2			2							3		1						4		1	2				2			2	3	50	27	77.0
14H-CC, 12-17	129.11	129.11	C	P		4			1									1			1			3			6				2				3	52	22	22.0
177-1088C-																																						0.0
1H-CC, 12-17	5.76	5.46	F	M		1					2		1	1		1															1	1			1	19	16	80.0
2H-CC, 19-24	132.33	130.47	F	M																				1			3								1	31	20	15.2
3H-CC, 10-15	143.35	141.49	F	M					1		3		1			1		1						1			8	4	3		4			1	2	52	27	20.6
4H-CC, 12-17	152.4	150.54	C	M	1	6			2		3		4														3	1			1	2		1		104	22	15.8
5H-CC, 12-17	162.13	160.27	C	M		2	1		2		2		1	3							1			1	1		21				53			1	9	180	33	57.0
6X-CC, 11-16	165.94	164.08	C	M		6			2		3										2			3			8				1			4	7	101	30	19.6
7X-CC, 16-21	171.83	169.97	C	M		7			1	5	2										2			1			4	4	2		3			1	5	141	34	117.6
8X-CC, 20-25	185.22	185.22	C	M		11			7		5			2								1		2			8		1	1	29					148	30	33.3
9X-CC, 15-20	194.06	194.06	C	P		3					1		3			1								3			7					9			5	78	27	83.0
10X-CC, 18-23	202.48	202.48	C	M		3			5		1										2	1		1			10				6			1		109	24	11.0
11X-CC, 72-77	209.37	209.37	C	M		5					1																20	4			1			3	6	113	26	30.5
12X-CC, 89-94	215.37	215.37	C	M		2					1													2			5	12						4		60	21	48.0
13X-CC, 17-22	233.27	233.27	F	P					1		1		1	3				1						2			3	9				2		2		81	25	41.5

Table T8. Diatom, silicoflagellate, ebridian, *Actiniscus*, sponge spicule, and opaline phytolith occurrence in uncleaned and acid-cleaned smear slides investigated from Site 1088. (**See table note.** Continued on next page.)

Core, section, interval (cm)	Depth (mbsf)	Depth (mcd)	Diatom abundance (uncleaned)	Diatom abundance (acid-cleaned)	Diatom preservation	Silicoflagellate occurrence	Ebridian occurrence	*Actiniscus* occurrence	Sponge spicule occurrence	Opaline phytolith occurrence	*Actinocyclus ingens*	*Actinocyclus ingens* var. *nodus*	*Actinocyclus ingens* var. *ovalis*	*Actinocyclus* aff. *curvatulus*	*Azpeitia nodulifer*	*Azpeitia tabularis*	*Coscinodiscus marginatus*	*Denticulopsis dimorpha*	*Denticulopsis hustedtii*	*Ethmodiscus rex*	*Fragilariopsis barronii*	*Fragilariopsis fossilis*	*Fragilariopsis kerguelensis*	*Fragilariopsis reinholdii*	*Hemidiscus cuneiformis*	*Nitzschia cylindrica*	*Simonseniella barboi*	*Thalassionema nitzschioides*	*Thalassiosira convexa*	*Thalassiosira convexa* var. *aspinosa*	*Thalassiosira insigna*	*Thalassiosira inura*	*Thalassiosira kolbei*	*Thalassiosira leptopus*	*Thalassiosira oliverana* gr.	*Thalassiosira oestrupii*	*Thalassiosira vulnifica*	*Thalassiothrix longissima-antarctica* gr.	*Aulacoseira granulata*	Diatom zone	Diatom age (Ma)
177-1088A-																																							
1H-CC, 15-20	9.89	12.27		T	P	B	B	B	X	B																										X			
177-1088B-																																							
1H-CC, 7-12	5.41	5.41		R	P	X	X	B	X	B						X				X			X																
2H-CC, 12-19	14.44	14.44		T	P	X	B	B	X	B																													
3H-2, 60-60	18.60	17.10	A		G	X	X	X	X	B	X									X	R														R		D			
3H-CC, 14-19	23.97	23.97		C	M	X	B	B	X	B				R	R					X	R			R	R			R	R	F	R	R	R	R		R	F		*T. insigna*	2.6-3.3
4H-CC, 13-18	34.08	34.08		T	P	X	B	B	X	B				X																							X			
5H-CC, 12-18	42.92	42.92		T	P	B	B	B	X	B										X																		X		
6H-CC, 13-18	52.86	52.86		B		B	B	B	X	B																															
7H-CC, 23-28	62.47	62.47		B		B	B	B	X	B	X									X																				
8H-CC, 10-15	71.47	71.37		T	P	B	B	B	X	B																															
9H-5, 23-25	78.25	78.23		T	P	B	B	B	X	B	X									X																				
9H-CC, 9-14	80.83	80.83	B			B	B	B	X	B																															
10H-5, 23-25	87.75	87.73		A	M	X	B	B	X	B	A						R		R	X					R			R									F			
10H-CC, 10-15	91.50	91.50	R	C	M	X	B	X	X	X	R		C			R	R			X		R			R		R								R		F		*F. reinholdii*	5.6-8.1
11H-5, 115-115	98.15	98.15		T	P	B	B	B	X	B										X																				
11H-CC, 9-14	99.16	99.16	B	T	P	B	B	B	X	B																															
12H-CC, 9-14	110.05	110.01	T		P	B	B	B	X	B										X																		X		
13H-5, 76-78	116.78	116.76		T	P	B	B	B	X	B	X									X																				
13H-CC, 11-16	119.05	119.05	T	F	M	B	B	B	X	B							C																					F			
14H-CC, 12-17	129.11	129.11	B			B	B	B	X	B																															
177-1088C-																																								
1H-CC, 12-17	5.76	5.46	B			B	B	B	X	B																															
2H-CC, 19-24	132.33	130.47	R		P	B	B	B	X	B																												X			
3H-CC, 10-15	143.35	141.49	T		P	B	B	B	X	B																												X			
4H-CC, 12-17	152.40	150.54	B			B	B	B	X	B																															
5H-CC, 12-17	162.13	160.27	B			B	B	B	X	B																															
6X-CC, 11-16	165.94	164.08	R		P	B	B	B	X	B						X			X																		X			
7X-CC, 16-21	171.83	169.97	B			B	B	B	X	B																															
8X-5, 10-12	181.72	181.70		F	M	B	B	B	X	B	F							F		X																	F		*D. dimorpha*	10.6-11.7
8X-CC, 20-25	185.22	185.22	T		P	B	B	B	X	B																												X			
9X-4, 70-72	190.42	190.40		F	P	B	B	X	X	B	A									X																				

Table T8 (continued).

Core, section, interval (cm)	Depth (mbsf)	Depth (mcd)	Diatom abundance (uncleaned)	Diatom abundance (acid-cleaned)	Diatom preservation	Silicoflagellate occurrence	Ebridian occurrence	*Actiniscus* occurrence	Sponge spicule occurrence	Opaline phytolith occurrence	*Actinocyclus ingens*	*Actinocyclus ingens* var. *nodus*	*Actinocyclus ingens* var. *ovalis*	*Actinocyclus* aff. *curvatulus*	*Azpeitia nodulifer*	*Azpeitia tabularis*	*Coscinodiscus marginatus*	*Denticulopsis dimorpha*	*Denticulopsis hustedtii*	*Ethmodiscus rex*	*Fragilariopsis barronii*	*Fragilariopsis fossilis*	*Fragilariopsis kerguelensis*	*Fragilariopsis reinholdii*	*Hemidiscus cuneiformis*	*Nitzschia cylindrica*	*Simonseniella barboi*	*Thalassionema nitzschioides*	*Thalassiosira convexa*	*Thalassiosira convexa* var. *aspinosa*	*Thalassiosira insigna*	*Thalassiosira inura*	*Thalassiosira kolbei*	*Thalassiosira leptopus*	*Thalassiosira oliverana* gr.	*Thalassiosira oestrupii*	*Thalassiosira vulnifica*	*Thalassiothrix longissima-antarctica* gr.	*Aulacoseira granulata*	Diatom zone	Diatom age (Ma)
9X-CC, 15-20	194.06	194.06	R		P	B	B	B	X	B																									X			
10X-CC, 18-23	202.48	202.48	B			B	B	B	X	B																												
11X-2, 48-50	206.40	206.38		F	P	B	B	B	X	B	F	F																									*A. ingens* v. *nodus*	14.4-14.2
11X-CC, 72-77	209.37	209.37	B			B	B	B	X	B																												
12X-CC, 89-94	215.37	215.37	B			B	B	B	X	B																												
13X-1, 47-49	224.19	224.17		B		B	B	B	X	B																												
13X-CC, 17-22	233.27	233.27	B			B	B	B	X	B																												

Notes: Abundance abbreviations: D = dominant, A = abundant, C = common, F = few, R = rare, T = trace, X = present, B = barren. Preservation abbreviations: G = good, M = moderate, P = poor. For more specific definitions, refer to **"Biostratigraphy,"** p. 10, in the "Explanatory Notes" chapter. This table is also available in ASCII format in the **TABLES** directory.

Table T9. Distribution of the main components of the radiolarian assemblage in Holes 1088B and 1088C.

Core, section, interval (cm)	Depth (mbsf)	Depth (mcd)	Abundance	Preservation	*Acrosphaera spinosa*	*Actinomma leptodermum*	*Actinomma delicatum*	*Actinomma glownini*	*Antarctissa denticulata*	*Antarctissa longa*	*Antarctissa* sp.	*Anthocyrtidium* spp.	*Axoprunum bispiculum*	*Botryostrobus auritus*	*Botryostrobus* spp.	*Cycladophora cosma*	*Cycladophora davisiana*	*Cycladophora davisiana cornutoides*	*Cycladophora pliocenica*	*Cyrtocapsella japonica*	*Cyrtocapsella tetrapera*	*Diartus hughesi*	*Diartus pettersoni*	*Dictyophimus crisiae*	*Dicymocyrti laticonus*	*Didymocyrtis mammifera*	*Didymocyrtis tetrathalamus*	*Eucyrtidium calvertense*	*Eucyrtidium cienkowskii*	*Eucyrtidium pseudoinflatum*	*Gondwanaria dogieli*	*Haeckeliella inconstance*	*Lamprocyclas aegles*	*Lamprocyrtis heteroporos*	*Lamprocyrtis junonis*	*Lithelius* sp.	*Lithocampe* spp.	*Lychnocanoma grande*	*Phorticium* spp.	*Prunopyle antarctica*	*Pterocanium triloburn*	*Pterocorys* spp.	*Saturnalis circularis*	*Spongoplegma antarcticum*	*Spongotrochus gracilis*	*Spongurus pylomaticus*	*Stichocorys peregrina*	*Stylatractus neptunus* gr.	*Stylatractus universus*	*Stylosphaera timmsi*	*Tetrapyle octacantha*	*Theocorythium vetulum*	*Theocorys redondoensis*	*Thyrsocyrtis clausa*	*Xiphosphaerantha angelina*
177-1088B-																																																						
1H-CC, 7-12	5.41	5.41	C	E		F			F	F		F		F			C						F				F								F		C		F	F		C			F				F						
2H-CC, 12-19	14.44	14.44	C	E	F	F	F				F	F	F	F			C						F				F				F				F		C		F	F		C	F	C				F						F	
3H-CC, 14-19	23.97	23.97	A	E					F		F	F		F					F	C			F				C				F	F		C		F			F		F	C	F	F	C			F						
4H-CC, 13-18	34.08	34.08	C	E															F				F			F	F					F	F	C						F						F				F	F			
5H-CC, 12-18	42.92	42.92	C	G			F					F							F							F	F						F	F									C				C						
6H-CC, 13-18	52.86	52.86	C	G									C						F								F							C	F									F										F
7H-CC, 23-28	62.47	62.47	C	G									F						F								F		F					C													F							
8H-CC, 10-15	71.47	71.37	C	E								F	F		F				F				F			F		F															C	F			F							
9H-CC, 9-14	80.83	80.83	C	G																				C			F	F				C											C						F				
10H-CC, 10-15	91.5	91.5	A	E																		F		C			F					A				F							C										
11H-CC, 9-14	99.16	99.16	C	G									F											F			F									F							C			C							
12H-CC, 9-14	110.05	110.01	C	G																			F	F			F																	F									
13H-CC, 11-16	119.05	119.05	C	G																			F	F			F																	F									
14H-CC, 12-17	129.11	129.11	C	G									F						F					F			F										F							F									
177-1088C-																																																							
1H-CC, 12-17	5.76	5.46	C	G													C																																							
2H-CC, 19-24	132.33	130.47	C	G																			F	F			F	F																	F									
3H-CC, 10-15	143.35	141.49	C	G															F	C					F		F	F																	F									
4H-CC, 12-17	152.4	150.54	C	G																A																																		
5H-CC, 12-17	162.13	160.27	C	G																A																																		
6X-CC, 11-16	165.94	164.08	C	G																A								F																											
7X-CC, 16-21	171.83	169.97	C	G																F								F							F																			
8X-CC, 20-25	185.22	185.22	C	G				R					F			F			F	C								F																											
9X-CC, 15-20	194.06	194.06	C	G									F			F				F	C				F	F			F																											
10X-CC, 18-23	202.48	202.48	C	G									C							F	A					F		F																											
11X-CC, 72-77	209.37	209.37	C	G									F								A																																		
12X-CC, 89-94	215.37	215.37	C	G									C								A																																		
13X-CC, 17-22	233.27	233.27	R	G																	R					R																												

Notes: Abundance abbreviations: A = abundant, C = common, F = few, R = rare. Preservation abbreviations: E = excellent, G = good. For more specific definitions, refer to "**Biostratigraphy,**" p. 10, in the "Explanatory Notes" chapter. This table is also available in ASCII format in the **TABLES** directory.

Table T10. Concentrations of methane, ethane, and propane obtained by the headspace technique at Site 1088.

Core, section, interval (cm)	Depth (mbsf)	C_1 (ppmv)	C_2 (ppmv)	C_3 (ppmv)
177-1088B-				
1H-4, 0-5	4.50	39	2	1
2H-5, 0-5	11.50	11		
3H-5, 0-5	21.00	4		
4H-5, 0-5	30.50	4		
5H-5, 0-5	40.00	4		
6H-5, 0-5	49.50	4		
7H-5, 0-5	59.00	6		
8H-5, 0-5	68.50	5		
9H-5, 0-5	78.00	4		
10H-5, 0-5	87.50	7		
11H-5, 0-5	97.00	9		
13H-5, 0-5	116.00	6		
177-1088C-				
2H-4, 0-5	128.80	6	1	
3H-5, 0-5	139.80	7		
4H-5, 0-5	149.30	7		
5H-5, 0-5	158.80	7		
6X-3, 0-5	165.30	8		
8X-5, 0-5	181.60	7		
10X-5, 0-5	200.80	9		
13X-5, 0-5	229.70	9		

Note: C_1 = methane, C_2 = ethane, C_3 = propane.

Table T11. Interstitial water chemistry from shipboard measurements at Site 1088. (Continued on next page.)

Core, section, interval (cm)	Depth (mbsf)	pH	Method	Alkalinity (mM)	Method	Salinity	Method	Cl (mM)	Method	SO_4 (mM)	Method	Na (mM)	Method	Mg (mM)	Method
177-1088B-															
1H-1, 145-150	1.45	7.90	ISE	2.874	T	35.5	R	558	T	29.3	I	471	CB	56.5	I
1H-2, 145-150	2.95	7.98	ISE	3.371	T	35.5	R	559	T	28.3	I	472	CB	55.8	I
1H-3, 145-150	4.45	8.19	ISE	3.887	T	35.0	R	557	T	28.4	I	472	CB	55.0	I
2H-1, 145-150	6.95	8.06	ISE	2.904	T	35.0	R	559	T	27.7	I	470	CB	55.4	I
2H-2, 145-150	8.45	7.88	ISE	2.911	T	35.0	R	559	T	28.8	I	478	CB	54.0	I
2H-3, 145-150	9.95	7.93	ISE	2.930	T	35.0	R	559	T	27.4	I	474	CB	54.7	I
2H-4, 145-150	11.45	7.95	ISE	3.414	T	35.0	R	559	T	28.5	I	477	CB	54.0	I
2H-5, 145-150	12.95	7.56	ISE	3.072	T	35.0	R	561	T	28.3	I	478	CB	54.8	I
3H-1, 145-150	16.45	7.88	ISE	3.277	T	35.0	R	562	T	28.3	I	476	CB	54.9	I
3H-2, 145-150	17.95	7.85	ISE	2.986	T	35.0	R	562	T	27.9	I	477	CB	53.7	I
3H-3, 145-150	19.45	8.05	ISE	3.090	T	35.0	R	562	T	27.8	I	476	CB	53.9	I
3H-4, 145-150	20.95	7.95	ISE	3.372	T	35.0	R	563	T	28.2	I	478	CB	54.0	I
3H-5, 145-150	22.45	7.97	ISE	2.971	T	35.0	R	562	T	26.7	I	472	CB	54.3	I
4H-1, 145-150	25.95	8.11	ISE	3.058	T	35.0	R	562	T	26.7	I	467	CB	55.5	I
4H-2, 145-150	27.45	8.03	ISE	3.121	T	35.0	R	564	T	26.7	I	471	CB	54.8	I
4H-3, 145-150	28.95	8.17	ISE	3.182	T	35.0	R	565	T	25.3	I	461	CB	57.4	I
4H-4, 145-150	30.45	7.21	ISE	3.207	T	35.0	R	564	T	27.2	I	473	CB	52.2	I
4H-5, 145-150	31.95	8.27	ISE	3.337	T	35.0	R	563	T	27.1	I	477	CB	51.7	I
4H-6, 145-150	33.45	7.63	ISE	2.757	T	35.0	R	563	T	26.5	I	473	CB	52.7	I
5H-1, 140-150	35.45	8.27	ISE	3.216	T	35.0	R	564	T	26.5	I	476	CB	52.3	I
5H-2, 140-150	36.95	7.68	ISE	3.472	T	35.0	R	566	T	24.8	I	475	CB	52.1	I
5H-3, 140-150	38.45	8.25	ISE	3.743	T	35.0	R	565	T	26.3	I	478	CB	51.9	I
5H-4, 140-150	39.95	7.82	ISE	3.342	T	35.0	R	565	T	26.4	I	476	CB	52.3	I
5H-5, 140-150	41.45	8.24	ISE	3.586	T	35.0	R	565	T	25.8	I	479	CB	50.9	I
6H-1, 140-150	44.95	8.27	ISE	3.404	T	35.0	R	564	T	26.0	I	478	CB	50.4	I
6H-2, 140-150	46.45	8.27	ISE	3.272	T	35.0	R	565	T	25.1	I	476	CB	50.7	I
6H-3, 140-150	47.95	8.29	ISE	3.375	T	35.0	R	565	T	26.1	I	479	CB	50.4	I
6H-4, 140-150	49.45	7.63	ISE	3.027	T	35.0	R	565	T	25.0	I	478	CB	50.0	I
6H-5, 140-150	50.95	8.26	ISE	3.163	T	35.0	R	564	T	24.1	I	475	CB	49.9	I
7H-4, 140-150	58.95	7.52	ISE	3.535	T	35.0	R	565	T	23.7	I	477	CB	48.8	I
8H-4, 140-150	68.45	7.73	ISE	3.354	T	35.0	R	567	T	25.1	I	483	CB	48.0	I
9H-4, 140-150	77.95	6.94	ISE	3.175	T	35.0	R	565	T	25.2	I	476	CB	48.5	I
10H-4, 140-150	87.45	7.79	ISE	3.228	T	35.0	R	565	T	24.1	I	475	CB	47.4	I
11H-4, 140-150	96.95	7.49	ISE	3.227	T	35.0	R	566	T	25.4	I	480	CB	46.4	I
13H-4, 140-150	115.95	7.93	ISE	3.249	T	35.0	R	566	T	23.2	I	477	CB	44.9	I
177-1088C-															
2H-3, 140-150	128.75	7.68	ISE	3.335	T	35.0	R	568	T	23.2	I	471	CB	46.4	I
4H-4, 140-150	149.25	7.78	ISE	3.254	T	35.0	R	567	T	22.9	I	477	CB	42.3	I
5H-4, 140-150	158.75	7.94	ISE	3.162	T	35.0	R	568	T	22.3	I	473	CB	43.9	I
6X-2, 140-150	165.25	7.47	ISE	3.099	T	35.0	R	568	T	22.1	I	478	CB	41.9	I
8X-4, 140-150	181.55	7.84	ISE	3.094	T	35.0	R	568	T	20.8	I	477	CB	40.5	I
10X-4, 140-150	200.75	7.50	ISE	2.968	T	35.0	R	570	T	21.7	I	479	CB	39.8	I
13X-4, 140-150	229.65	7.83	ISE	2.866	T	35.0	R	573	T	20.4	I	475	CB	39.9	I

Note: Method abbreviations: ISE = ion selective electrode, T = titration, R = refractometer, I = ion chromatography, CB = charge balance calculation, S = spectrophotometry, AAS = atomic absorption spectrometry, AES = atomic emission spectrometry.

Table T11 (continued).

Core, section, interval (cm)	Ca (mM)	Method	K (mM)	Method	H_4Si0_2 (μM)	Method	NH_4 (μM)	Method	HPO_4 (μM)	Method	Sr (μM)	Method	Li (μM)	Method
177-1088B-														
1H-1, 145-150	11.8	I	13.0	I	392	S	49	S	3.5	S	101	AAS	28.0	AES
1H-2, 145-150	11.9	I	12.2	I	455	S	37	S	2.4	S	114	AAS	28.0	AES
1H-3, 145-150	11.7	I	12.1	I	481	S	41	S	2.1	S	124	AAS	26.1	AES
2H-1, 145-150	12.3	I	12.4	I	520	S	52	S	2.6	S	140	AAS	26.3	AES
2H-2, 145-150	11.2	I	12.0	I	533	S	54	S	2.6	S	149	AAS		AES
2H-3, 145-150	11.4	I	11.4	I	555	S	54	S	3.4	S	154	AAS	24.5	AES
2H-4, 145-150	11.9	I	11.4	I	581	S	69	S	1.9	S	168	AAS	24.6	AES
2H-5, 145-150	11.2	I	11.6	I	595	S	68	S	2.1	S	173	AAS	24.2	AES
3H-1, 145-150	12.2	I	11.9	I	597	S	69	S	2.1	S	214	AAS	22.8	AES
3H-2, 145-150	12.4	I	11.9	I	632	S	75	S	1.9	S	223	AAS	22.9	AES
3H-3, 145-150	12.8	I	11.4	I	664	S	80	S	1.9	S	234	AAS	22.4	AES
3H-4, 145-150	12.5	I	12.0	I	686	S	87	S	2.1	S	249	AAS	22.2	AES
3H-5, 145-150	12.7	I	12.4	I	706	S	114	S	1.8	S	254	AAS	21.6	AES
4H-1, 145-150	14.2	I	12.3	I	673	S	89	S	1.5	S	276	AAS	21.7	AES
4H-2, 145-150	14.3	I	12.1	I	669	S	89	S	3.5	S	267	AAS	21.1	AES
4H-3, 145-150	15.4	I	12.4	I	682	S	95	S	1.5	S	295	AAS	20.8	AES
4H-4, 145-150	15.9	I	12.7	I	684	S	92	S	1.6	S	304	AAS	20.3	AES
4H-5, 145-150	14.5	I	11.8	I	682	S	119	S	1.2	S	318	AAS	20.0	AES
4H-6, 145-150	14.3	I	12.2	I	669	S	116	S	1.2	S	326	AAS	20.3	AES
5H-1, 140-150	14.5	I	11.3	I	653	S	109	S	1.3	S	350	AAS	19.0	AES
5H-2, 140-150	14.4	I	11.4	I	634	S	113	S	1.3	S	350	AAS	19.4	AES
5H-3, 140-150	14.0	I	11.6	I	651	S	113	S	1.3	S	371	AAS		AES
5H-4, 140-150	14.4	I	11.6	I	643	S	141	S	1.0	S	380	AAS	18.7	AES
5H-5, 140-150	14.4	I	10.8	I	627	S	112	S	1.3	S	390	AAS	18.8	AES
6H-1, 140-150	14.6	I	11.1	I	625	S	123	S	1.2	S	420	AAS	17.3	AES
6H-2, 140-150	14.6	I	11.3	I	636	S	121	S	1.2	S	427	AAS	18.4	AES
6H-3, 140-150	14.8	I	11.3	I	632	S	114	S	1.2	S	444	AAS	18.0	AES
6H-4, 140-150	14.7	I	11.2	I	664	S	112	S	1.2	S	448	AAS	16.9	AES
6H-5, 140-150	14.5	I	10.9	I	632	S	121	S	1.2	S	443	AAS	16.6	AES
7H-4, 140-150	15.1	I	11.0	I	647	S	138	S	1.2	S	508	AAS	15.9	AES
8H-4, 140-150	15.3	I	10.7	I	701	S	136	S	1.2	S	562	AAS	14.9	AES
9H-4, 140-150	16.9	I	11.4	I	767	S	152	S	1.9	S	608	AAS	13.8	AES
10H-4, 140-150	17.8	I	10.7	I	813	S	157	S	1.8	S	657	AAS	13.3	AES
11H-4, 140-150	18.0	I	10.5	I		S	174	S	1.9	S	700	AAS	12.7	AES
13H-4, 140-150	19.3	I	10.4	I	874	S	174	S	2.1	S	758	AAS	12.0	AES
177-1088C-														
2H-3, 140-150	21.5	I	10.7	I	904	S	201	S	2.1	S	805	AAS	11.8	AES
4H-4, 140-150	22.1	I	10.2	I	874	S	215	S	2.4	S	835	AAS	12.3	AES
5H-4, 140-150	22.3	I	10.3	I	885	S	212	S	2.6	S	819	AAS	13.4	AES
6X-2, 140-150	21.8	I	9.5	I	891	S	215	S	2.6	S	809	AAS	13.5	AES
8X-4, 140-150	22.2	I	9.6	I	928	S	227	S	2.4	S	850	AAS	13.6	AES
10X-4, 140-150	24.0	I	9.3	I	900	S	250	S	2.4	S	864	AAS	13.0	AES
13X-4, 140-150	26.0	I	9.3	I		S	256	S	2.3	S	886	AAS	16.0	AES

Table T12. Concentrations of inorganic carbon and calculated calcium carbonate at Site 1088. (Continued on next two pages.)

Core, section, interval (cm)	Depth (mbsf)	IC (wt%)	$CaCO_3$ (wt%)
177-1088B-			
1H-1, 74-75	0.74	10.6	88.0
1H-2, 74-75	2.24	10.7	88.9
1H-3, 25-25	3.25	10.8	89.7
1H-4, 70-71	5.20	11.0	91.2
2H-1, 44-45	5.94	10.6	88.2
2H-2, 20-21	7.20	10.2	84.6
2H-4, 44-45	10.44	10.6	88.7
2H-6, 43-44	13.43	10.4	86.2
3H-1, 63-64	15.63	10.5	87.5
3H-2, 65-66	17.15	10.3	85.5
3H-3, 22-23	18.22	10.4	86.6
3H-4, 17-18	19.67	10.6	88.1
3H-5, 51-52	21.51	10.4	86.8
3H-6, 24-25	22.74	10.5	87.1
4H-1, 67-68	25.17	10.5	87.4
4H-2, 37-38	26.37	10.0	83.6
4H-3, 23-24	27.73	10.5	87.2
4H-4, 24-25	29.24	10.8	90.0
4H-5, 23-24	30.73	10.7	89.4
4H-6, 26-27	32.26	10.8	90.0
4H-7, 27-28	33.77	10.7	88.9
5H-1, 117-118	35.17	10.8	89.6
5H-2, 62-63	36.12	10.9	90.8
5H-3, 119-120	38.19	10.7	88.9
5H-4, 114-115	39.64	11.0	92.0
5H-5, 77-78	40.77	10.9	91.0
5H-6, 118-119	42.68	11.0	91.8
6H-1, 75-76	44.25	10.9	90.4
6H-2, 71-72	45.71	11.0	91.8
6H-3, 70-71	47.20	10.9	91.1
6H-4, 60-61	48.60	11.1	92.7
6H-5, 26-27	49.76	11.1	92.3
6H-6, 81-82	51.81	11.2	93.6
7H-1, 80-81	53.80	10.9	90.7
7H-2, 64-65	55.14	11.0	91.6
7H-3, 91-92	56.91	10.6	88.7
7H-4, 61-62	58.11	11.0	92.0
7H-5, 65-66	59.65	11.1	92.2
7H-6, 40-41	60.90	11.0	91.8
8H-1, 70-71	63.20	10.8	89.9
8H-2, 74-75	64.74	11.0	91.9
8H-3, 20-21	65.70	10.7	89.1
8H-4, 21-22	67.21	11.1	92.2
8H-5, 24-25	68.74	11.0	92.0
8H-6, 19-20	70.19	11.1	92.8
9H-1, 65-66	72.65	11.0	91.6
9H-2, 22-23	73.72	10.9	91.2
9H-3, 22-23	75.22	11.1	92.5
9H-4, 65-66	77.15	11.1	92.8
9H-5, 132-133	79.32	11.1	92.8
9H-6, 22-23	79.72	11.1	92.7
10H-2, 22-23	83.22	11.1	92.8
10H-3, 26-27	84.76	11.3	94.1
10H-4, 20-21	86.20	11.2	93.2
10H-5, 22-23	87.72	10.9	91.0
10H-6, 76-77	89.76	10.4	86.9
10H-7, 22-23	90.72	10.7	89.2
11H-1, 124-125	92.24	10.6	88.3
11H-2, 124-125	93.74	10.9	90.8
11H-3, 124-125	95.24	10.6	88.3
11H-4, 124-125	96.74	10.8	90.2
11H-5, 124-125	98.24	10.3	86.0
12H-1, 120-121	101.70	10.9	90.9
12H-2, 75-76	102.75	11.2	93.3
12H-4,120-121	106.20	10.6	88.5

Table T12 (continued).

Core, section, interval (cm)	Depth (mbsf)	IC (wt%)	$CaCO_3$ (wt%)
12H-5, 72-73	107.22	10.5	87.1
12H-6, 74-75	108.74	10.8	90.4
12H-7, 20-21	109.70	10.8	90.3
13H-1, 75-76	110.75	10.8	89.6
13H-2, 75-76	112.25	11.0	91.5
13H-3, 75-76	113.75	10.8	89.7
13H-4, 120-121	115.70	11.3	94.4
13H-5, 75-76	116.75	10.9	90.8
13H-6, 75-76	118.25	11.4	94.9
14H-1, 120-121	120.70	10.7	89.0
14H-2, 100-101	122.00	11.2	93.2
14H-3, 79-80	123.29	10.8	89.8
14H-4, 119-120	125.19	10.9	90.9
14H-5, 68-69	126.18	10.9	90.9
14H-6, 43-44	127.43	11.3	94.4
177-1088C-			
2H-1, 75-76	125.05	10.8	89.9
2H-2, 71-72	126.51	10.2	85.2
2H-3, 67-68	127.97	11.2	93.4
2H-4, 70-71	129.50	11.3	94.2
2H-5, 44-45	130.74	11.2	93.0
3H-1, 70-71	134.50	10.9	90.9
3H-2, 70-71	136.00	11.2	93.6
3H-3, 71-72	137.51	11.1	92.1
3H-4, 23-24	138.53	11.1	92.2
3H-4, 96-97	139.26	11.0	91.7
3H-5, 121-122	141.01	11.1	92.6
3H-6, 116-117	142.46	11.3	93.9
4H-1, 22-23	143.52	10.9	91.0
4H-2, 122-123	146.02	11.0	92.1
4H-3, 22-23	146.52	10.8	90.4
4H-4, 119-120	148.99	11.0	91.2
4H-5, 22-23	149.52	11.0	91.4
4H-6, 19-21	150.99	11.2	93.0
5H-1, 122-123	154.02	11.3	94.4
5H-2, 23-24	154.53	11.2	92.9
5H-3, 76-77	156.56	11.2	93.3
5H-4, 26-27	157.56	11.2	93.4
5H-5, 76-77	159.56	11.0	92.0
6X-1, 54-55	162.84	11.1	92.2
6X-2, 53-54	164.33	11.3	94.1
6X-3, 36-37	165.66	11.2	93.7
7X-1, 31-32	166.31	11.1	92.7
7X-2, 31-32	167.48	11.3	94.1
7X-3, 31-32	168.98	11.2	93.2
7X-4, 31-32	170.48	11.3	93.8
8X-1, 20-21	175.80	11.1	92.4
8X-2, 20-21	177.30	11.5	95.6
8X-3, 20-21	178.80	11.3	93.8
8X-4, 20-21	180.30	11.3	93.8
8X-5, 20-21	181.80	11.1	92.2
8X-6, 20-21	183.30	11.2	93.3
8X-7, 20-21	184.80	11.0	91.8
9X-1, 70-71	185.90	11.2	92.9
9X-2, 70-71	187.40	11.4	94.9
9X-3, 70-71	188.90	11.2	93.2
9X-4, 70-71	190.40	11.0	92.1
9X-5, 70-71	191.90	10.9	90.6
9X-6, 70-71	193.40	11.2	93.2
10X-1, 36-37	195.16	11.5	95.7
10X-2, 36-37	196.66	11.3	93.8
10X-3, 36-37	198.16	11.1	92.2
10X-4, 36-37	199.66	11.3	94.3
10X-5, 36-37	201.16	11.2	93.2
11X-1, 37-38	204.77	11.3	94.3
11X-2, 49-50	206.39	11.1	92.3
11X-3, 54-55	207.41	11.1	92.3
11X-4, 10-11	208.47	11.2	93.1
12X-1, 2-3	214.12	11.3	94.4

Table T12 (continued).

Core, section, interval (cm)	Depth (mbsf)	IC (wt%)	$CaCO_3$ (wt%)
13X-1, 49-50	224.19	11.4	95.2
13X-2, 49-50	225.69	11.2	93.1
13X-3, 49-50	227.19	11.4	94.7
13X-4, 49-50	228.69	11.3	93.9
13X-5, 49-50	230.19	11.0	91.6
13X-6, 49-50	231.69	11.1	92.8
13X-7, 10-11	232.80	11.3	94.3

Note: IC = inorganic carbon, $CaCO_3$ = calcium carbonate.

Table T13. Summary of physical properties measurements conducted at Site 1088.

Measurement	Core 177-1088A-	Core 177-1088B-	Core 177-1088C-
GRA sample spacing	1H: 2 cm	1H-14H: 2 cm	1H-13X: 2 cm
MS sample spacing	1H: 2 cm	1H-14H: 2 cm	1H-13X: 2 cm
NGR sample spacing	1H: 2 cm	1H-14H: 2 cm	1H-13X: 2 cm
PWL sample spacing	1H: 2 cm	1H-14H: 2 cm	1H-5H: 2 cm
OSU-SCAT sample spacing	1H: 4 cm	1H-14H: 4 cm	1H-5H, 10X: 4 cm
CM-2002 sample spacing	—	—	—
PWS3	*N* = 16	*N* = 227	*N* = 64
MAD		*N* = 163	*N* = 33
TC	*N* = 1	*N* = 11	*N* = 11

Notes: GRA = gamma-ray attenuation, MS = magnetic susceptibility, NGR = natural gamma radiation, PWL = *P*-wave logger, OSU-SCAT = Oregon State University Split Core Analysis Track, CM-2002 = Minolta spectrophotometer, PWS3 = *P*-wave velocity sensor 3 for split cores, MAD = moisture and density, TC = thermal conductivity.

Table T14. Thermal conductivity measurements at Site 1088.

Core, section, interval (cm)	Depth (mbsf)	Depth (mcd)	TC (W/[m·K])	Start (s)	Length (s)	End (s)
177-1088A-						
1H-1, 50	0.50	2.88	0.831	83.0	25.0	108.0
1H-1, 50	0.50	2.88	0.825	94.5	25.5	120.0
177-1088B-						
4H-1, 75	25.25	25.25	1.000	111.0	25.0	136.0
5H-3, 75	37.75	37.75	1.102	78.0	26.0	104.0
5H-3, 75	37.75	37.75	1.144	27.0	26.5	53.5
6H-3, 75	47.25	47.25	1.070	94.5	25.5	120.0
7H-3, 75	56.75	56.75	1.162	102.0	25.0	127.0
7H-3, 75	56.75	56.75	1.147	124.0	25.5	149.5
8H-3, 75	66.25	66.25	1.176	51.5	25.0	76.5
8H-3, 75	66.25	66.25	1.155	61.0	26.5	87.5
9H-3, 75	75.75	75.75	1.094	110.5	26.5	137.0
9H-3, 75	75.75	75.75	1.115	91.0	25.0	116.0
10H-3, 75	85.25	85.25	1.119	74.0	25.0	99.0
10H-3, 75	85.25	85.25	1.119	116.5	28.5	145.0
11H-3, 75	94.75	94.75	1.156	79.5	30.5	110.0
11H-3, 75	94.75	94.75	1.172	49.5	25.0	74.5
12H-3, 75	104.25	104.25	1.209	121.0	25.0	146.0
12H-3, 75	104.25	104.25	1.148	77.5	40.0	117.5
13H-3, 75	113.75	113.75	1.159	95.0	25.0	120.0
13H-3, 75	113.75	113.75	1.206	25.0	28.0	53.0
14H-3, 75	123.25	123.25	1.161	111.5	25.5	137.0
14H-3, 75	123.25	123.25	1.180	68.5	26.5	95.0
14H-3, 75	123.25	123.25	1.133	114.0	25.0	139.0
177-1088C-						
2H-3, 75	128.05	126.19	1.169	107.0	25.0	132.0
2H-3, 75	128.05	126.19	1.214	53.0	29.5	82.5
3H-3, 75	137.55	135.69	1.143	120.5	28.5	149.0
3H-3, 75	137.55	135.69	1.172	67.0	25.0	92.0
4H-3, 75	147.05	145.19	1.114	79.0	26.0	105.0
4H-3, 75	147.05	145.19	1.098	73.0	25.0	98.0
5H-3, 75	156.55	154.69	1.141	100.0	25.0	125.0
5H-3, 75	156.55	154.69	1.170	56.0	25.0	81.0
6X-2, 75	164.55	162.69	1.095	101.5	25.5	127.0
6X-2, 75	164.55	162.69	1.120	67.0	25.0	92.0
7X-3, 75	169.42	167.56	1.168	97.0	25.0	122.0
7X-3, 75	169.42	167.56	1.204	50.0	25.0	75.0
8X-3, 75	179.35	179.35	1.226	43.5	28.5	72.0
8X-3, 75	179.35	179.35	1.156	87.5	25.0	112.5
9X-3, 75	188.95	188.95	1.092	41.5	25.0	66.5
9X-3, 75	188.95	188.95	1.104	65.5	25.0	90.5
10X-3, 75	198.55	198.55	1.149	59.5	28.5	88.0
10X-3, 75	198.55	198.55	1.104	121.5	26.5	148.0
11X-3, 75	207.62	207.62	1.078	59.0	25.0	84.0
11X-3, 75	207.62	207.62	1.035	113.0	25.0	138.0
13X-3, 75	227.45	227.45	1.187	77.0	25.0	102.0
13X-3, 75	227.45	227.45	1.201	36.0	25.0	61.0

Notes: TC = thermal conductivity. Start, Length, and End refer to the interval of the time-temperature series used for the determination of thermal conductivity. This table is also available in ASCII format in the **TABLES** directory.

Table T15. Temperature measurement attempts at Site 1088.

Core, section	Depth (mbsf)	Comments
177-1088A-		
1H	Bottom water	Noisy data
177-1088B-		
4H	34.0	Noisy data
7H	62.5	Noisy data
11H	100.5	Electronics failure
14H	129.0	Noisy data